Sivan Dalshad Mohammed

Effects of bromodomain or androgen-receptor inhibitors in combination with radiopharmaceuticals in castration-resistant prostate cancer cell monolayers and multicellular spheroids

Master's Thesis in Biomedicine

Oslo Metropolitan University Faculty of Health Sciences

OSLO METROPOLITAN UNIVERSITY
STORBYUNIVERSITETET

Oslo universitetssykehus

ACKNOWLEDGEMENTS

I want to start by thanking God for blessing me and allowing me to get to know and work on this master's project with the most wonderful and great people at the Department of Radiation Biology, Institute for Cancer Research.

Now I would like to thank my main supervisor in the project Asta Juzeniene sincerely. I'm grateful for your constant professional guidance and invaluable support and encouragement throughout the whole process. Without you sacrificing your time and the effort you put in teaching me, this work indeed would not have been possible.

To my co-supervisor Alfonso Urbanucci, thank you for your support, and concerned input into the project and my well-being. To my other co-supervisor, Nikolai Engedal, thank you for being available when I needed your help and always greeting me with a smile on your face no matter how busy you were. I'm fortunate to have such dedicated and outstanding supervisors.

A special gratitude to Dr. Li-Wei Ma, for the constant help in the lab from the very beginning. You were always available when I needed your help and always very patient and generous.

I wish to thank Vilde Stenberg for her support, encouraging words and taking the time to check this thesis, in addition to providing me with PSMA labeled radiopharmaceuticals. I will like to thank Dr. Petras Juzenas, who sacrificed his time tirelessly to offer me help with flow cytometry analysis and helping with technical issues in the lab. The effort you put in is so much appreciated. I also wish to thank Mantas Grigalavicius for his help regarding any technical issues I faced in the lab.

Further, I wish to acknowledge Anna Julie Tornes for her constant encouragement and great writing tips at the start of my writing process. Thank you to Professor Øyvind S.Bruland, for his encouragement and asking and caring for my well-being.

Thank you to Mona-Elisabeth Revheim at Nuclear Medicine department (OUH) for providing us with high-quality Xofigo (Radium-223).

Not least, I'm hugely grateful for my supportive family for supporting me throughout this whole process, and to all my friends, thank you for the support and all your wonderful and encouraging words.

Oslo, May 2021

Sivan Dalshad Mohammed

ABSTRACT

Background: Prostate cancer not responding to androgen deprivation therapy is known as castration-resistant prostate cancer (CRPC). Despite rapid increase of treatment options, the disease remains incurable, when metastases appear, which might be due to the diverse mechanisms and the heterogeneity and multifocal nature of the disease. For this reason, novel and highly effective therapy approaches against metastatic CRPC (mCRPC) are required. Exploring combination therapy using existing and novel agents provide better response than treatments with single agents. The progression of treated-naïve- prostate cancer is shown to be driven by androgen-receptor (AR), along with bromodomain and extra terminal domain (BET) proteins. Thus, inhibition of such proteins is an alternative, promising anticancer therapy. Treatments of mCRPC with BET inhibitors, JQ1, AZD5153 or AR inhibitor, Enzalutamide (ENZA) in combination with radiopharmaceuticals, are not being investigated. **Aim:** Evaluating the preclinical therapeutic efficacy of combining BET or AR inhibitors with radiopharmaceuticals, α-emitting ^{223}Ra targeting bone metastases or ß-emitting ^{177}Lu-PSMA-617 in the prostate cancer C4-2 cells grown in cell monolayers (2D) and multicellular spheroids (3D).

Methods: Prostate cancer C4-2 cells growing 2D and 3D culture models were treated with selected concentrations of JQ1, AZD5153 or ENZA in combination with various activities of ^{223}Ra. In 2D model, the treatment effects were assessed by counting colonies after 10-14 days and assessing cell survival fraction curves. Growth rates of the spheroids after treatments were evaluated by following the morphological changes and measurement of the cross-sectional area of the spheroids. Flow cytometry analysis was used to study cell apoptosis/necrosis, DNA damage and cell cycle distribution 72 h after combination treatment. In addition, C4-2 spheroids were treated with a combination of a selected concentration of AZD5153 and various activities of ^{177}Lu-PSMA-617).

Results: The studied BET inhibitors, JQ1, AZD5153 had antiproliferative effects as mono-treatment in C4-2 monolayer cells and decreased C4-2 spheroid growth in a dose and time-dependent manner. ENZA did not inhibit C4-2 cell survival in a dose-dependent manner. The combination of AZD5153, JQ1 or ENZA with ^{223}Ra showed the synergistic decrease in C4-2 spheroid growth. The combination treatments reduced the percentage of C4-2 cells in S and M phases of the cell cycle. However, the reduction was not statistically significant. However, the combination treatments had no proapoptotic activity. Additionally, the combination of AZD5153 with ^{177}Lu-PSMA-617, synergistically decreased C4-2 spheroid growth. **Conclusion:** The combination treatments of JQ1, AZD5153 or ENZA and ^{223}Ra or AZD5153 and^{177}Lu-PSMA-617 induced synergistic inhibition of C4-2 spheroids growth. These preclinical combination therapies provide rational for clinical evaluation of these combinations for treatment of mCRPC patients.

SAMMENDRAG

Bakgrunn: Prostata kreft, er en av de hyppigste formene for kreft hos menn (etter lungekreft). Denne sykdommen utvikler seg i prostata kjertelen. Når prostata kreft utvikler seg til et stadie, hvor hormon behandling (androgensuppressiv terapi, også kalt androgen deprivation therapy,ADT) ikke gir tilfredsstillende effekt, er den ikke helbredelig, siden det finnes ingen andre effektive behandlingsformer. Derfor er helt nye måter for å helbrede denne sykdommen på nødvendige for pasienter som lever med denne sykdommen. Kombinasjonsbehandling kan være en måte å bekjempe denne sykdommen på. Kombinasjonen av to eller tre behandlingsformer kan øke overlevelse og bedre livs kvaliteten for pasienter. Studier har vist at utviklingen av prostata kreft fra ikke-aggressive typer til denne aggressive typen er drevet frem av androgen reseptor, i lag med Bromodomain og extra terminal domain proteiner. Dette indikerer på at hemming av slike proteiner, virker som en lovende anti-kreft terapi. Med tanke på dette ble BET hemmereneAZD5153 og JQ1 benyttet i kombinasjon av radiofarmasøytisk som Radium-223 for behandling av kastrasjonsresistent prostatakreft, noe som ikke har blitt undersøkt tidligere som et behandlingsalternativ i vår kunnskap. **Mål:** Å utforske effekten av BET-bromodomain protein hemmere AZD515 og JQ1 eller androgen-reseptor hemmeren Enzalutamide (ENZA) i kombinasjon med radiofarmasøytisk ^{223}Ra eller ^{177}Lu-PSMA-617.

Metoder: In vitro kombinasjonsbehandling av prostatakreft C4-2 celler ble utført ved å kombinere bestemte konsentrasjoner (basert på MTT, CellTiter Glo og klonogenisk celle levedyktighet assayer) av AZD5153, JQ1 eller ENZA med varierende aktiviteter av Radium-223 (Xofigo) i både 2-dimensjonell -og 3-dimensjonell (multicellulære sferoider) kultur modeller. Effekten av kombinsjonsbehandling ble evaluert ved å tele kolonier 10-14 dager etter behandling og overlevelse kurver ble laget. Effekten av kombinasjonsbehandlingen i sferoider ble evaluert 7 og 14 dager etter initiert behandling ved å studere morfologiske endringer og måling av tverrsnittsareal av sferoider. Flow cytometery analyse for deteksjon av apoptose (programmert celledød), DNA skade-og cellesyklus distribusjon ble gjort 72 timer etter kombinasjonsbehandling. I tillegg ble kombinasjonsbehandling med en bestemt konsentrasjon av AZD5153 og varierende aktiviteter av radiofarmasøytisk ß-emitter^{177}Lu-PSMA-617 utført i C4-2 sferoider.

Resultat: BET protein hemmerene JQ1 og AZD5153, viste antiporoliferativ aktivitet som monoterapy i C4-2 celle monolayer og reduserte sferoid vekst på dose-og tidsavhengig måte. Celldyktihget ble ikke redusert av ENZA på en dose-avhengig måte. Kombinasjonsbehandling av C4-2 sferoider med JQ1, AZD5153 eller ENZA og Radium-223 viste synergistisk reduksjon i spheorid vekst, i tillegg ble reduksjon av celler i S og M faser av cellesyklusen observert, dessuten var denne reduksjonen ikke statsistisk signifikant.Videre, førte kombinasjonsbehandling til økning i DNA skade og ingen signifikant propapotisk aktivitet ble observert. Videre, resulterte kombinasjonsbehandling av C4-2 sferoider med AZD5153 og ^{177}Lu-PSMA-617 i synergistisk effekt og reduserte sfeorid vekst. **Konklusjon:** Kombinasjonsbehandling med JQ1, AZD5153 eller ENZA og ^{223}Ra eller AZD5153 og ^{177}Lu-PSMA-617 induserte synergistisk hemming av C4-2 sferoid vekst. Disse prekliniske resultatene gir en rasjonal for klinisk evaluering av disse kombinasjonene for spredt kastrasjonsresistent prostata kreft pasienter.

ABBREVIATIONS

α	Alpha
AR	Androgen Receptor
ARSI	AR signaling inhibitors
ADT	Androgen deprivation therapy
ATP	Adenosine-triphosphate
ANOVA	Analysis of variance
DNA	Deoxyribonucleic acid
DHT	5α-dihydrotestosterone
DSB	Double-strand breaks
DMSO	Dimethyl sulfoxide
ß	Beta
Bq	Becquerel
BET	Bromodomain and Extra-Terminal
BRD	Bromodomain
BSA	Bovine serum albumin
CRPC	Castration-resistance prostate cancer
CDK	Cyclin-dependent kinase
CT	Computed tomography
CellTiter	CellTiter-Glo®Luminescent cell viability assay
CI	Combination index
EBRT	External beam radiation therapy
ET domain	Extra-terminal domain
FBS	Fetal bovine serum
FDA	Fluorescein diacetate
γ	Gamma
GS	Gleason Score
HAT	Histone acetyltransferase
HDAC	Histone deacetylase
HR	Homologous recombination
LNCaP	Lymph node carcinoma of the prostate
Lu-177	Lutetium-177
LET	Linear energy transfer

LD	Lethal dose
mCRPC	Metastatic castration-resistance prostate cancer
MCS	Multicellular spheroid
MTT	3-(4, 5-Dimethyl thiazol-2-yl)-2, 5-diphenyl tetrazolium bromide
NHEJ	Non-homologous end joining
PARP	poly ADP-ribose polymerase
PSA	Prostate-specific antigen
PTEN	Phosphatase and tensin homolog
PS	Penicillin/Streptomycin
PE	Plating efficiency
PI	Propidium iodide
PBS	Phosphate-buffered saline
RNA	Ribonucleic acid
RNase	Ribonuclease
RNA pol II	RNA polymerase II
RPMI	Roswell Park Memorial Institute Medium
SSB	Single-strand breaks
SF	Survival fraction
$T_{1/2}$	Half-life
TRT	Targeted radionuclide therapy

TABLE OF CONTENTS

1 Introduction

1.1 Prostate cancer

Prostate cancer is a heterogeneous disease resulting from mutations in the genome and dysregulation of the transcriptional machinery, which leads to dynamic alterations of gene expression, uncontrolled and abnormal cell growth (1, 2). Prostate cancer cells have the potential to invade surrounding tissues and further spread to other organs. Benign prostate cells transform into cancer cells through a multistep process, generally starting from a pre-cancerous lesion which leads to a malignant tumor (1) Alterations that lead to this transformation a normal prostate cell to a cancer cell are known as classical cancer hallmarks and known as sustaining proliferative signaling, evasion of growth suppressors, replicative immortalization, cell death resistance, inducing angiogenesis, activating invasion and metastasis, genome instability and mutation, metabolic reprograming, avoidance of immune destruction (1). Androgen-receptor (AR) mediated signaling, androgen independence and castration resistance, are prostate cancer specific hallmarks.

1.1.2 Epidemiology of prostate cancer

Prostate cancer is the second most frequent cancer in men, and the fifth leading cause of cancer death in men worldwide (3). In 2019, 4877 new cases and 952 death cases were registered in Norway (4). In 2020, 1414259 new cases and 375304 death cases were registered worldwide (5). Aging, familial and genetic factors, ethnicity, environmental factors, metabolism, diet, physical activity, hormonal factors (androgens and insulin-like growth factor-1) and lifestyle (smoking, alcohol) are involved in prostate cancer development (6, 7). The incidence and mortality rates for prostate cancer correlate with increasing age, and the average age of diagnosis is 66 years (3, 7). Hereditary prostate cancer accounts for about 5-15% of all prostate cancer cases (8).

1.1.3 Anatomy and histology of the prostate

The prostate is a walnut-sized muscular gland and a part of the male reproductive anatomy. The prostate is located beneath the urinary bladder and surrounds the so-called prostatic urethra (the first part of the urethra canal). The size of the prostate enlarges with age, known as benign prostatic hyperplasia (9). Anatomically, the prostate is divided into the following zones: the peripheral zone, transition zone and central zone. The peripheral zone makes up about 70% of glandular tissue, the central zone consists of 25% of glandular tissue and the transition zone constitutes 5% of the prostate. The rest of the prostate consists of anterior fibromuscular stroma, and contains no glandular tissue (9). The peripheral zone is the origin of almost all prostate cancers (about 70-85%). The incidence rates of prostate cancer are 24% in the transition zone, and 5% arising in the central zone (9, 10). Cancer that arises in the central zone is thought to be of a more aggressive type and more likely to invade the seminal vesicles (10). The different zones are easily

distinguishable by image-guided interventional procedures of the prostate gland, commonly used in prostate biopsy (9).

The prostate gland acinar tissue is mainly deputed to the secretion of prostatic fluid, which is mixed with the seminal fluid, protecting spermatozoa. Three histologically differentiated cell types are found in the glandular epithelium including; luminal secretory cells (deputed to the production of the prostatic fluid), basal cells, and neuroendocrine cells. The stromal cell types surrounding the prostatic acini are made of smooth muscle cells and fibroblasts. Stem cells in the prostate gland are thought to reside in the basal layer, giving rise to the epithelial cell types of the prostate (11). Interestingly these cells are also found to have regenerative potential upon treatment with androgen deprivation therapy (ADT) (12).

1.1.4 Carcinogenesis of prostate

The initiating step of the malignant transformation is prostatic intraepithelial neoplasia, which involves an abnormal non-invasive neoplastic transformation of the lining of the epithelial tissue along prostatic ducts and acini (13). Prostatic intraepithelial neoplasia lesions are normally found in the peripheral zone, and its prevalence is high despite its underreported diagnosis since the only method of detection is biopsy. These types of lesions are classified into 2 groups: low grade and high-grade prostatic intraepithelial neoplasia, based on the immediate precursory of early invasiveness (14). Prostatic intraepithelial neoplasia lesions progress to locally advanced prostate cancer, which is a locally invasive carcinoma, characterized by degraded basal cell layer and thus cancer cells are able to invade through the basal lamina (14). The disease metastasizes at first to lymph nodes, and then to other distant organs, such as bones, lungs and liver (14). More than 60% of patients with advanced prostate cancer will develop bone metastases, the most common site for prostate cancer metastases (15). Bone metastases are the leading cause of death in prostate cancer patients (15).

1.1.5 Androgen and AR

Androgens are male sex hormones with characteristic roles under differentiation and development of the male reproductive system and secondary sexual characteristics (16**).** Testosterone is the primary form of androgens, making up about 90% of circulating androgens (17). The luteinizing hormone regulates the testosterone production by Leydig cells in the testicles. Its release from the pituitary gland is regulated by luteinizing hormone-releasing hormone secretion from the hypothalamus (Fig.1.1) (17). Less than 4% of testosterone circulates free (not bound to protein), while the major part of testosterone circulates bound to serum sex hormone-binding globulin and albumin. Only the free form enters prostate cells (18). Intracellularly, testosterone is converted into a biologically active 5α-reduced metabolite of testosterone, 5α-dihydrotestosterone (DHT), catalyzed by the 5α-reductase enzyme. Testosterone and DHT mediate their biological activity through binding to the AR and inducing AR transcriptional activity (Fig. 1.1) (19). Androgen signaling through AR is critical for the normal development of the prostate gland (20). The AR has three functional domains: the ligand-binding domain, deoxyribonucleic acid (DNA)binding domain (acting as a transcription factor) and the NH2-terminal transactivation domain. The DNA binding domain is

linked to the ligand-binding domain by a hinge region (20). In the absence of ligand (testosterone or DHT), the AR is cytoplasmic, associated with heat-shock and other chaperone proteins (20). AR transcriptional activity upon binding DHT is modulated by its interaction with several androgen co-regulatory proteins (ARA) in the nucleus, mediating transcription and activation of many AR-targeted genes.
Some coactivators bind the AR predominantly at DNA regulatory regions called enhancers and promoters. These coregulatory proteins are classified into coactivators and corepressors (21). The best-studied AR coactivators are p300/CREB-binding protein and the p160/steroid receptor coactivator proteins. These coregulatory proteins have been shown to be overexpressed in prostate cancer (22), and regulated by androgens (23). There is however a number of other AR coregulators that are deputed to chromatin remodeling and that have been found to have multiple functions in both AR-mediated transcription and in DNA repair, one such protein is bromodomain-containing protein 4 (BRD4) (24, 25).
AR target genes encode proteins that exhibit important functions in various cellular pathways, control proliferation, differentiation, and anti-apoptotic pathways (19). In normal prostate cells, the activation of these pathways is tightly regulated. In prostate cancer cells, there is an imbalance between cell proliferation and apoptosis, caused by an abnormality in AR signaling. The AR can be aberrantly activated for several reasons, which include amplification of the AR gene, leading to an overexpression of the AR protein, mutations of the AR ligand-domain, and consequent promiscuous activation by multiple ligands including growth factors, and cytokines (26). Finally, the aberrant activity of AR coregulatory proteins can also induce AR aberrant activity.

ARs are found in benign prostatic hyperplasia and in all histological types and clinical stage of the prostate cancer (27). The AR activity has a significant role in sustaining the development of prostate cancer, androgen-dependent prostate cancer and its progression to castration-resistance prostate cancer (CRPC) (28)

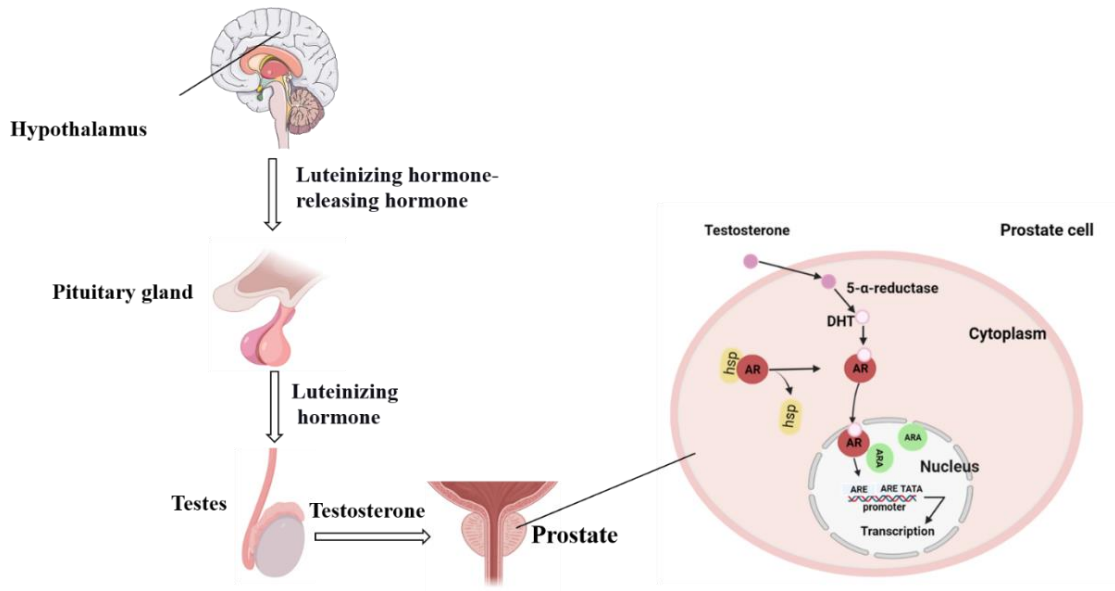

Figure 1.1. Production of testosterone and activation of AR signaling pathway. Synthesized testosterone is transported to target tissue such as the prostate, enters a cell and is converted to 5α-dihydrotestosterone (DHT) by 5-α-reductase enzyme. DHT binds to AR and promotes the dissociation of heat-shock proteins (hsp) from the AR. The AR then translocate into the nucleus, where it binds to androgen receptor coregulators (ARA) that enhance its transcriptional activity and binds to the androgen response element (ARE) in the promoter region to mediate transcription of AR targeted genes. The figure is modified with permission from(29) and (30), and created using illustrations from Biorender (https://biorender.com) and smart SERVIER MEDICAL ART(https://smart.servier.com)

1.2 Diagnosis and classification of prostate cancer

Diagnosis of prostate cancer and its different disease stages are determined by using different examination tools. The primary care setting is a digital rectal examination of the prostate and a serum prostate-specific antigen (PSA) blood test. This is followed by a transrectal ultrasound imaging and ultrasound guided needle biopsy of the prostate (31, 32). If prostate cancer cells are detected during the investigation by the pathologist, the presence of eventual metastases is determined by magnetic resonance imaging, computed tomography (CT) or positron emission tomography (PET) (31). The staging and extra-prostatic extension of the cancer are determining factors in the disease prognosis estimation process and choice of treatment for the patient (31, 32).

The prostate cancer clinical staging is assessed by a classification called TNM (T- tumor volume, N – involvement of lymph nodes, M –metastasis classification) (33).

Prostate cancer aggressiveness is determined by the Gleason Score (GS), a prostate-specific score system based on characteristics of the histological arrangement pattern of prostate cancer cells obtained from a needle biopsy (34). The scoring system ranges from 1-5, where score 1 is highly differentiated and resembles

the prostate tissue of origin, and score 5, constitutes a significant difference from normal glandular tissue (34, 35). Because prostate cancers are highly morphological heterogeneous (36), two different patterns in a biopsy sample are assigned; a primary predominant pattern and a second most prevalent pattern. The sum of these two patterns obtains the total GS, for example, 3+4= 7, where the primary score is 3 (most predominant pattern) and the secondary is 4 (second most predominant pattern) (37). The GS is used together with PSA level test to determine disease prognosis and treatment options.

1.2.1 Prostate-specific antigen

PSA is a proteolytic serine protease enzyme produced by the epithelial cells of the prostate glandular structures (prostatic acini). PSA protease activity liquefies the gel-formed semen, into smaller polypeptides, making motility of sperm possible. PSA is encoded by the kallikrein-related peptidase 3, which is a well-known AR target gene (38).

Production of PSA occurs in both normal prostate cells and cancerous prostate tissue. In normal prostate gland, PSA is confined to the gland, thus only small amount leaks into the blood circulation, while in pathological conditions of the prostate such as beningn prostatic hypertrophy, infection, prostatitis and prostate cancer, PSA enters the blood circulation, therefore elevated levels of PSA can be detected. The PSA level in a blood test is reported as nanograms of PSA per milliliter (ng/ml) of blood, and a 4.0 ng/ml is considered normal level (39). The PSA values of greater than 4.0 ng/ml is the consensus standard at which further evaluation for prostate cancer should occur(40). However, an elevated level of PSA is not a specific marker for prostate cancer, since the elevated PSA in the blood also can be detected in other pathological condition. For this reason, age and other risk factors must be taken into consideration upon diagnosing a patient with an increased level of serum PSA (23, 39).

PSA tests are the most widely used noninvasive diagnostic tests for prostate cancer. PSA is also widely used in the management of patients with diagnosed prostate cancer such as in surveillance following diagnosis, monitoring response to therapy and in combination with both clinical and histological criteria in risk stratification for recurrence. Serum PSA values greater than 20 ng/ml has a positive predictive value of 65% for metastatic skeletal involvement (40).

1.3 Treatment for prostate cancer

1.3.1 Treatment options and strategy for localized prostate cancer

Choice of treatment strategy among different treatment options for prostate cancer depends on the staging of the disease progression, diagnostic results (e.g. PSA levels and the GS), a patients age and general health conditions (41)**.** Specific clinical guidelines (evidence-based recommendations) are presented by the European Association of Urology, which can be used for evidence-based treatment of different prostate cancer scenarios. It is, however, not a replacement for clinical expertise in the treatment-making decision process for each case since individual values, preferences, or circumstances also must be taken into account in the treatment process (42).

For localized prostate cancer (defined as no identifiable nearby tissue or distant metastases), there are three treatment options available; active surveillance, surgery (radical prostatectomy), and radiation therapy (43) .

1.3.1.1 Active surveillance

Active surveillance is a viable treatment option for prostate cancer patients with clinically low-risk (T1/T2a, PSA<10, GS ≤6 or group 1)and limited intermediate-risk (T2, PSA of 10-20 ng/ml and GS 2 (Gleason 3+4)) (44). It involves close surveillance of patients intending to avoid unnecessary treatments. Then, patients are followed up regularly through structured surveillance programs, including PSA testing, clinical examination, and repeated prostate biopsies (42).

1.3.1.2 Surgery

The second treatment option for localized prostate cancer is radical prostatectomy, which is an assisted surgical approach used as a means of definitive treatment of localized prostate cancer. The procedure involves the removal of the entire prostate gland and seminal vesicles (45), and results in a drastic reduction of PSA levels. Thus, prostate cancer recurrence after surgery is easily detectable clinically by the rise of serum PSA levels. A biochemical recurrence is considered if the PSA is rising above 0.2 ng/ml in three consecutive tests with 1 week apart, which can signify emergence of castration resistance (46). Although radical prostatectomy is a curative treatment in many patients, some patients experience increased biochemical recurrence (47). Prostate cancer recurrence after definitive therapy of radical prostatectomy is usually treated with radiotherapy (RT) (48), defined salvage RT radical prostatectomy.

1.3.1.3 Radiotherapy

Approximately 25% of all prostate cancer patients receive radiotherapy (external beam (EB), brachytherapy and targeted radionuclide therapy (TRT)) as definitive treatment (49). Radiotherapy is used as a first treatment option in primary localized prostate, alone and in combination with other therapies depending on the cancer stage and risk factors (50).

In EB radiation therapy (EBRT), radiation is delivered to localized tumors from an X-ray radiation source outside the body. High X-ray radiation beams leave a linear accelerator (source of electronic induced irradiation) from a collimator built in a gantry (51). Commonly, the entire prostate gland is irradiated by EBRT because of the multifocal nature of prostate cancer, as well as the inability to target localized malignant foci by imaging (52). Irradiation of the entire prostate by EBRT means it harms the targeted tumor and surrounding tissues. Thus, EBRT cannot be used for patients with multiple cancer metastasis. However, EBRT is an effective option in the treatment of localized prostate cancer (53).

Brachytherapy is internal radiotherapy, and includes implantation of permanent or temporary radioactive seeds/capsules into the prostate tumor site and can be used for low-risk disease and selective intermediate-risk prostate cancer (54). The implanted radioactive seeds irradiate the prostate at the site of the tumor. There are two types of brachytherapy in clinical use, depending on whether the radioactive source is implanted

permanently (low dose rate brachytherapy) or temporary (high dose rate brachytherapy). Both of these types can be used alone or in combination with EBRT (51).

Radical prostatectomy and RT for localized prostate cancer are in many instances highly curative. However, about 20% to 30% of the patients eventually relapse (55). The treatment options for recurrent localized prostate cancer following radiation therapy include: salvage surgery, salvage cryoablation of the prostate, and hormone therapy (56). In high-risk localized or metastatic prostate cancer cases, accounting for approximately 15% of prostate cancer diagnosis (T2c, PSA> 20 ng/ml, GS ≥8 or 2), treatment options used are typically EBRT without or in combination with ADT (57).

1.3.2 Androgen deprivation therapy (hormone therapy)

The initial and gold standard treatment for hormone-sensitive metastatic prostate cancer is ADT, either surgical or chemical castration. Surgical castration is done by bilateral orchiectomy. Medical castration is castration via administration of gonadotropin-releasing hormone (agonists or antagonists), suppressing testicular androgen synthesis, induces disease regression, and prolongs survival until the tumor cells acquire selective mechanisms allowing for growth in androgen-depleted conditions (58).

Advanced metastatic prostate cancer disease (metastases to, e.g., bones) are usually treated with ADT, despite its ability to prolong overall survival and alleviate bone pain and disease progression(59).

1.3.3 Molecular and cellular mechanisms of castration resistant prostate cancer

Progression of prostate cancer to CRPC despite regression of the disease by ADT or surgical castration occurs eventually in most patients within 2 to 3 years (60).

CRPC is defined as cancer progressing while the patient is on ADT, despite castrate levels of serum testosterone. Eventually, CRPC emerges after initial ADT, with an expected survival period of only 16-18 months, and only 5-10% of patients with the disease live ten years after initiating ADT (61). CRPC is the most challenging prostate cancer form because hormone-depriving therapy that once was effective no longer has any therapeutic effect on CRPC patients. Thus, treatment options are limited (62).

Several molecular mechanisms are proposed to be involved in CRPC, the disease remain sensitive to low level of hormones in circulation and still relies on the AR signaling pathways (63, 64). In fact, despite tumor cell adaptation to androgen-depleted conditions in CRPC, the disease remains dependent on androgen and still relies on the AR signaling pathway (60, 64).

CRPC AR-dependent resistance mechanisms include AR gene amplification and AR overexpression, AR mutation, AR co-factor activity imbalance, AR variants and intra-tumoral steroid hormone synthesis.(60, 63). A summary of these mechanisms and AR-independent resistance mechanisms is described below.

AR amplification and AR mutations

Overexpression of AR is found in 80% of CRPC cases (65)**.** In the microenvironment of a tumor with low levels of AR despite androgen blockade by ADT, a subpopulation of cells develop sensitivity to the low level

of androgen conditions through upregulation of the AR gene. The gene becomes overexpressed for several reasons. The most well-known is the AR gene locus amplification(66). AR overexpression results in hypersensitivity of prostate cancer cells to residual androgens in circulation (60).

Several point mutations of the AR gene can lead to in increased AR activity in androgen-depleted conditions (63). For instance mutations of the AR ligand binding domain, resulting in activation by other molecules other than androgen activation of the AR mechanisms (60).

Mutations found in the AR gene, especially in the AR ligand-binding domain, are commonly point mutations. An example of such mutation is widely studied T877A (67) , first found in the ligand binding domain of AR in LNCaP cell lines. This mutation results in change in the steroid binding specificity of AR, resulting in activation of AR by other steroid hormones other than testosterone and provides insensitivity to anti-androgens (67).

AR variants

The resistance mechanisms mentioned above are dependent on androgen, while recently identified splice variants of AR (AR-Vs) in CRPC lack the C-terminal ligand binding domain (caused by a deletion), thus binding of ligand are no longer required for the translocation of AR to the nucleus, which further promotes transcription of target genes (60). Examples of such splice variants of AR lacking ligand binding domain are ARV_7 and ARV_{567} (60) . Translocation of AR and AR-V7 to the nucleus requires dimerization. Recent studies have shown that these receptors translocate to the nucleus together by heterodimerization, which is significant since dimerization cannot occur due to the lack of ligand binding domain in the AR-V7. Consequently, translocation to the nucleus of the receptors in castrated conditions must occur in other ways, such as heterodimerization (63).Additionally, the ligand-independent variants of AR, are also associated with resistance to current anti-androgen agents such as ENZA and Abiraterone (60).

Co-factors activity imbalance

The transcriptional activity of AR is mediated by several other transcriptional cofactors, known as co-activators or co-repressors; many of them are enzymes (60) . The cofactors may be involved in the transcriptional activation or repression of specific targets of AR by modifying proteins in the coregulatory complex through mechanisms such as phosphorylation, acetylation, methylation or ubiquitylation, as well as working as chaperones, ribonucleic acid (RNA) splicing regulators, and recruiters of transcriptional machinery (60).

Changes in these cofactors have shown to affect AR's transcriptional activity, allowing AR activity even in androgen-depleted conditions, leading to CRPC development (63). Inhibition of the co-activators p300/CREB-binding protein and GATA binding protein 2 decreases AR expression and prostate cancer growth. On the other hand, steroid receptor coactivator proteins, a family composed of steroid receptor coactivator proteins -1,-2, and -3 (68), influence AR regulation by formatting promoter/enhancer complexes

at the transcriptional start site of AR target genes (63). An upregulation of co-activators, including FK506-bidning protein 51

and steroid receptor coactivator proteins, are observed in CRPC compared to localized prostate cancer (63). Additionally, co-repressors are usually downregulated in CRPC, suggesting that cofactors affect the function of AR and allowing for AR activity in CRPC, despite the low androgen levels present (63).

Intra-tumoral steroid hormone synthesis

Another AR-dependent resistance mechanism that plays a role in AR reactivation after ADT of primary prostate cancer is intratumorally steroid hormone synthesis (69). Increased androgen synthesis (testosterone and DHT), by the tumor cells themselves is an important mechanism in the reactivation of AR in castrate serum androgen levels (69). The production of androgens intra-tumoral occurs by three different mechanisms. One significant mechanism is converting weak adrenal androgens (androstenedione, DHEA) to testosterone and DHT. The second mechanism intra-tumoral cells use is *de novo* to become independent of serum androgen, that occurs through cholesterol conversion. Several key transcripts encoding enzymes, including CYP11A1 and CYP17A1, are upregulated in prostate cancer cell line. Finally, the third mechanism is synthesis of androgens *de novo* by converting acetic acid to DHT (63, 69).

Research has also shown that an elevated level of circulating insulin in CRPC is associated with ADT, and increased steroidogenesis in prostate cancer cell lines, is associated with an elevated serum insulin level (70).

The AR-independent resistance mechanisms that do not involve AR singling pathways include the PI3K (phosphatidylinositol 3-kinase) pathway (71). Alteration of the phosphatase PTEN (loss of function), a tumor suppressor protein normally down regulating the PI3K pathway, results in the activation of the PI3K pathway. PTEN has lost its function in several of primary prostate cancers. Further, loss of PTEN is associated with prostate cancer's progression to aggressive metastatic prostate cancer and CRPC development (71).

1.3.4 Targeted treatment with AR signaling inhibitors (ARSIs) for castration-resistant prostate cancer

Given the dependence of CRPC on AR signaling, AR signaling inhibitors (ARSI) are used in the locally recurrent setting and also in the metastatic CRPC (mCRPC) (72). Enzalutamide (ENZA), abiraterone and apalutamide that target and block the AR-signaling pathways, have been clinically tested and approved by the FDA for the treatment of CRPC in the past years because of their contribution in increased lifespan of many patients as well as extension of metastasis-free OS (73, 74).

ENZA (MDV3100, the clinical formulation) is an AR antagonist that FDA approved in 2012. ENZA inhibits AR signaling by a three-fold mechanism of action; it blocks androgens from binding to the AR, blocks nuclear translocation of activated AR, and inhibits binding to chromosomal DNA and signaling co-activators (Fig.1.2) (75, 76).

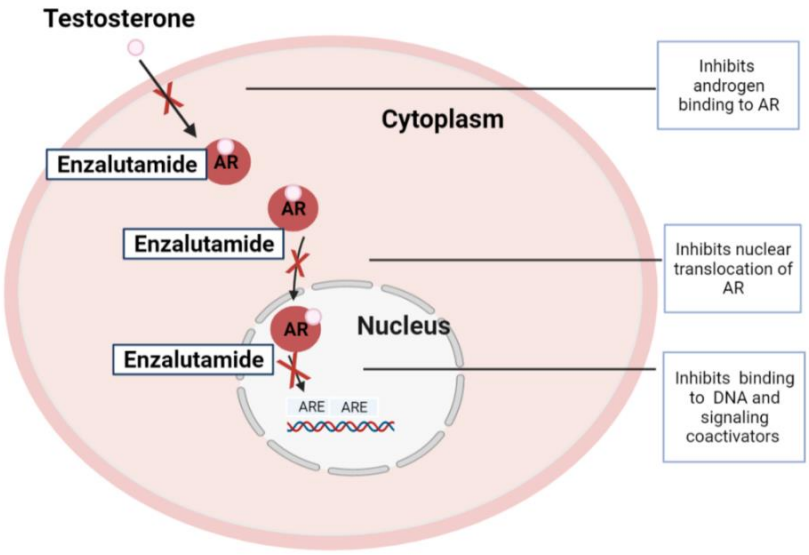

Figure 1.2. Enzalutamide mechanism of action.T, testosterone, ARE, Androgen-receptor elements. The figure is adapted by permission from (77) and created using illustrations from Biorender (https://biorender.com).

1.3.5 Treatment for metastatic castrate-resistant prostate cancer

The treatment for mCRPC has been expanding in the last ten years, and includes chemotherapy, oral targeted therapies with ARSIs, immunotherapies, radiopharmaceutical therapy and poly ADP-ribose polymerase (PARP) inhibitors, which have demonstrated some improvements in overall survival (Table 1.3) (78). However, secondary resistance to these advanced treatment agents arise in approximately 20-40% of mCRPC patients. Therefore, medical improvements for mCRPC are highly relevant. New approaches in fighting mCRPC are in clinical trials and under development (74, 79). The aim is to target non-AR-driven pathways involved in the pathogenesis and progression of mCRPC (80).

Table 1.3. Therapeutic agents with an overall survival benefit that have been approved for treatment of metastatic CRPC (78). OS, overall survival, PARP, poly (ADP-ribose) polymerase, FDA, Food and Drug Administration, EMA, European Medicines Agency.

Drug and therapy	Mechanism of action	OS benefit (months)	Approved	
			FDA	EMA
Cabazitaxel, Taxane chemotherapy	Microtubule inhibitor	2.4[81]	2010	2011
Docetaxel, Taxane chemotherapy	Microtubule inhibitor	2.4[82]	2004	2007
Sipuleucel-T, Immunotherapy	T-cell activation	4.1[83]	2010	2013
Abiraterone acetate, pregnenolone analogue	CYP17 inhibitor	4.6[84]	2011	2011
ENZA, receptor signaling pathway inhibitor	Targeted AR inhibitor	4.8[85]	2012	2013
Olaparib,	PARP inhibitor	3.4[86]	2020	-
Xofigo, α-emitting radionuclide therapy	Bone targeting	3.6[87]	2013	2013
Rucaparib	PARP inhibitor	Not available	2020	-

1.3.5.1 Chemotherapy

The first chemotherapeutic agent associated with a prolonging survival benefit in patients with mCRPC, was Docetaxel, first approved in 2004. Docetaxel induces apoptosis through activation of the intrinsic death pathway (Bcl2- phosphorylation), along with inducing cell cycle arrest by interaction with β-tubulin and stabilizes microtubule and blocking its activity during cell cycle division (G2/M phase cell cycle-arrest) (88-90). Several therapeutic agents for CRPC, following docetaxel, have been approved, which has shown survival improvement for CRPC patients, such as Cabazitaxel (approved in 2010), which was first approved for mCRPC patient's post-docetaxel setting by the FDA (91).

1.3.5.2 Targeted radionuclide therapy

TRT is a growing treatment approach for mCRPC because of its ability to deliver a highly concentrated radiation dose selectively targeted tumor cells while minimizing damage to surrounding tissues (92). TRT comes under the internal radiation category and involves the administration of radioisotopes or radiolabeled molecules that either naturally accumulates in metastatic bone tumors (such $^{223}RaCl_2$ (Xofigo), $89SrCl_2$

(Metastron)) or are designed to target and deliver radiation to tumors (^{153}Sa-EDTMP (Quadramet), ^{177}Lu or ^{225}Ac labelled small molecule ligands targeting prostate-specific membrane antigen (PSMA) (92). In this way, ionizing radiation is delivered selectively to targeted areas.

1.3.5.2.1 Radiation biology

Radiobiology refers to the biological response of cells to ionizing radiation(93). That is classified into electromagnetic and particulate radiation (94). X- and γ-rays (no charge) are electromagnetic radiation, with low linear energy transfer (LET), while protons, neutrons and α-particles are particulate radiation with high-LET (94). LET is a particle's average energy lost over a certain distance; expressed as keV/µm. Furthermore, LET of a particle is dependent on the energy of the particle (95). Ionizing radiation damage to the cell can be caused through either direct or indirect ionization of the DNA molecule. Direct damage of DNA occurs when ionizing radiation interacts directly with the DNA molecule, disrupting the molecular structure and further leading to cell damage and might result in cell death. The indirect damage of DNA occurs by ionization of, for example, a water molecule (H_2O) in the cell, thereby producing free radicals such as hydroxyl radical (OH•) (94). Ionizing radiation induces various DNA lesions in cells, including single-strand breaks (SSBs) and double-strand breaks (DSBs). A SSB is break in the sugar-phosphate backbone of a single strand of DNA that can be efficiently repaired using the undamaged complementary strand as a template (94).

However, in DSBs lesions both DNA-strands are broken, and thus, there is no undamaged template available. Consequently, this type of DNA lesion is complex for the cell to repair and is considered the most lethal among the wide range of DNA lesions(94, 95). Despite the lack of a complimentary template, cells try to repair DSBs by two central repair mechanisms, known as non-homologous end joining (NHEJ) and homologous recombination (HR). DNA repair by NHEJ occurs by joining DNA ends without any template. Therefore, the original DNA sequence is not restored. Still, this pathway is the most common pathway that cells use in DSBs repair and plays an essential role in DSBs repair during all cell cycle phases (95, 96). The homologous recombination mechanism plays a major role in the repair of DSBs during S-and G_2-phases, since homologous sister chromatids are used as repair templates (95).

Radionuclides with high LET radiation (e.g., α-particles) induce more cell death by producing DSBs that are difficult to repair than radionuclides emitting low LET radiation (such as ß-particles). Therefore, high LET radionuclide particle emitters are preferred in radionuclide therapy (93).

α-particles are positively charged and relatively large particles, generally emitted by the decay of heavy radioactive nuclides, such as uranium, radium, and actinium. α-particles can travel relatively short distances because of the heavy weight and size of the helium nucli, and thus is stopped by a thin layer of paper or the human skin, and presenting no external radiation danger to humans. In the decay of an unstable heavy parent radioactive atom, emission of α-particle occurs, resulting in a daughter nuclide with two fewer protons and two fewer neutrons than the parent nuclide (Fig.1.4) (97, 98).

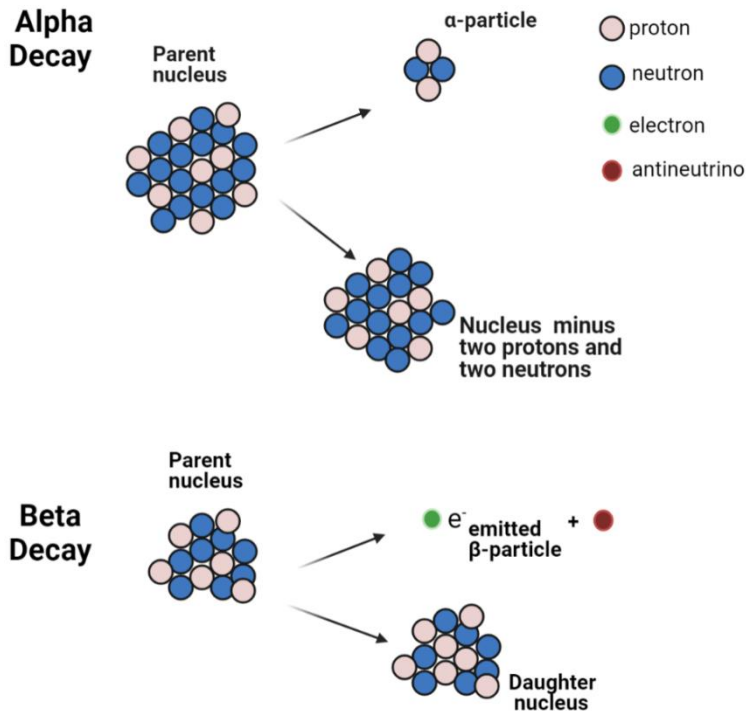

Figure 1.4 Decay of an α and β -particle. The figure is inspired by the references (97, 98), created using illustrations from Biorender (https://biorender.com).

ß-particle occurs when the neutron to proton ratio in an atom is too high. These particles can travel further in the air but can easily be stopped by a piece of clothing or this ß-sheet like aluminum (97, 98). ß-particles can also penetrate the protective layer of skin, thus are somewhat of external danger, but as α-particles, overall, they constitute an internal hazard (97). β-radiation is commonly emitted from particles including ^{14}C and ^{90}Sr (97, 98). ß-decay is either (ß-) decay or (ß+) decay, also known as positron decay. When the proton and neutron ratio of a particle is too high, it decays by ß-particle emission, in which a neutron is transformed to a proton by emission of an electron along with an antineutrino (Fig.1.4). The antineutrino is an almost massless and charge less particle that conserves energy released in the decay. When a proton and neutron ratio of a radioactive nuclide is too low, the unstable radionuclide decays by ß+-decay. In ß+-decay, emission of a positively charged beta particle (a positron) and a neutrino occur, which is resulted from the conversion of a proton in the nucleus into a neutron. In case of contact between a positron and a free electron, the positron combines with the electron and is annihilated, which gives rise to two 511 keV γ -rays in the opposite direction. ß-particles, compared to α-particles, are more penetrating but have low LET, thus cause minor damage due to their ionization being less localized and deliver energy to a large area (97, 98). Table 1.5 gives a summary of the physical and biological differences between ß, α and γ rays.

Table 1.5. Summary of physical and biological differences between α, β and γ radiation (92, 97). DBS; double-strand breaks, SSB; single-strand breaks.

Properties	Radiation sources		
	α-particle	**ß-particle**	**γ ray**
Identity	^{4}He nucleus	Electron	Photon
Charge	2+	1-	Chargeless
Mass	4	0.0005	Massless
Penetrative power	Low	Medium	High
Linear energy transfer	50-230 keV/µm	0.1-1.0 keV/µm	0.2 keV/µm
Range in tissue	0.04-01 mm	0.05-12 mm	Centimeters
Ionizing ability	High	Medium	Low
DNA damage	DSB	SSB	SSB
Irradiation field	Whole body	Whole body	Limited area
Bystander effect	Yes	Yes	Yes
Cross-fire effect	Yes	Yes	Yes

1.3.5.2.2 Radioactivity

A radioactive nucleus may decay through spontaneous fission, α-particle, β-particle, photon emission (γ -ray emission) or electron capture to become more stable (98).The decay process of a radionuclide is a random spontaneous process. The disintegration rate (A) for a radionuclide is defined as the number of disintegrations per unit time (generally seconds) and is proportional to the number of radioactive atoms present (N) and the disintegration constant (λ). The disintegration constant is defined as the probability of disintegration per unit time for a specific radioactive nuclide. The disintegration rate (A) is given by the equation:

$$A = \lambda N \qquad \textit{(Eqn.1)}$$

A is radioactivity, and its SI-unit is Becquerel (Bq), 1 Bq equals 1 disintegration per second (98).

The time it takes for a certain radionuclide to reduce its original activity to one half, in the process of becoming more stable, is called the half-life ($T_{1/2}$) (98). The half-life for all radionuclides is unique and varies among different radionuclides, and it is also related to the disintegration constant. The equation is given by:

$$\lambda = \frac{\ln(2)}{T_{1/2}} \qquad \textit{(Eqn. 2)}$$

1.3.5.2.3 Cross fire and bystander effect

The crossfire effect describes a situation in which a radiopharmaceutical affects not only directly targeted cells but also the cells which are surrounding the targeted cells (99). The radiation path length in biological tissue of a radiopharmaceutical is a deciding factor in inducing such a crossfire effect. This means ß-particles are more efficient in inducing crossfire irradiation effect than α-particles due to their longer range in

tissue (100). The cells that are not directly bound to the radiopharmaceutical are in the crossfire of the radiation (Fig 1.6). The crossfire effect can be particularly beneficial for large and highly heterogeneous tumors since not all tumor cells can be reached by a radiopharmaceutical directly. The α-particle's highly energetic (5-9 MeV) and short path length (50-100 µm) features make it a suitable candidate for bone marrow malignancies and small solid tumors (93).

An irradiated cell can release chemical and cytotoxic signals, causing biological effects in non-irradiated cells. The effect is called the bystander effect (Fig.1.6). This effect is smaller for cell monolayers than for cells that are in gap-junction with the directly radiated cells, due to the distance separating monolayer cells from each other (101).

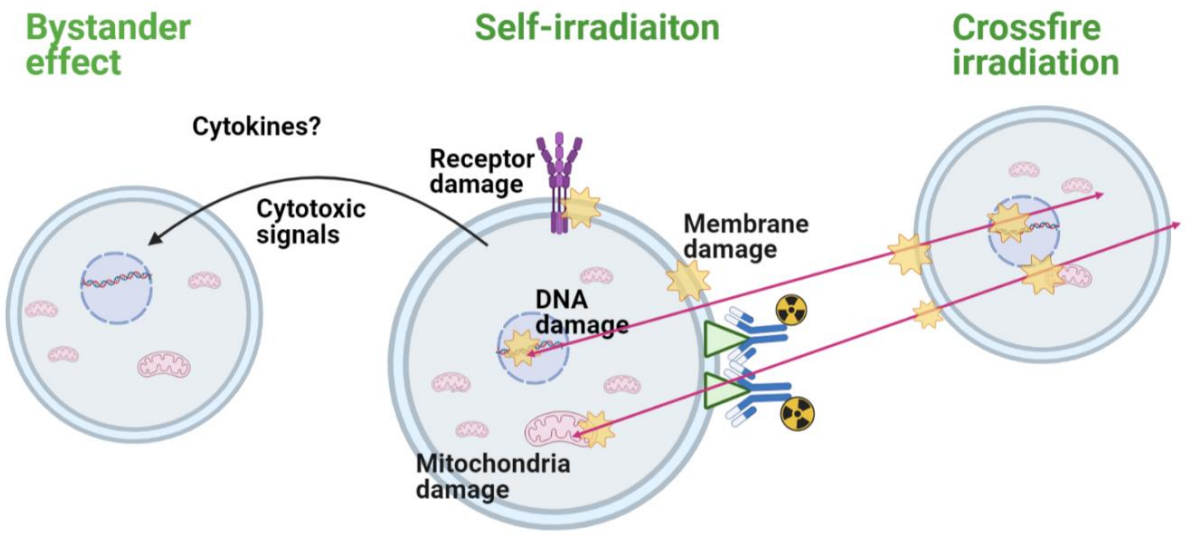

Figure 1.6. Illustration of targeted cell irradiation by radiopharmaceutical agents, and producing crossfire irradiation and bystander effect in non-targeted cells. The figure is adapted with permission from (102), and created using illustrations from Biorender (https://biorender.com)

1.3.5.2.4 Radium-223

The natural bone-targeting ^{223}Ra with the half-life of 11.4 days, is the first and only α-particle emitting radiopharmaceutical approved by the FDA for the treatment of mCRPC patients with symptomatic bone metastases and no known extra skeletal metastatic disease. Ra-223 therapy with its overall survival benefit (Table 1.2) has revolutionized the field of TRT. It decays via a chain of five short-lived daughter radionuclides to stable ^{207}Pb, emitting four α particles and two β^- particles (Fig.1.7). α-particle emitting radionuclides are particularly effective in killing cancer cells by breaking DBSs in cell nucleus, because they can deliver a high amount of energy at short range without damaging surrounding healthy tissue. The approved single dose activity of ^{223}Ra is 50 or 55 kBq/kg of body weight (103). This alpha-emitter holds great promise and has potential in treating bone mCRPC, additionally combinational treatments with other therapeutic agents for mCRPC is under investigation (103). Because of the bone-seeking characteristics of ^{223}Ra, its clinical use is

limited to prostate cancer patients with osteoblastic metastases. Chelate complex formation is essential to treat extraskeletal cancer metastases Ra-223, like other alkaline earth metals, forms very weak complexes (92).

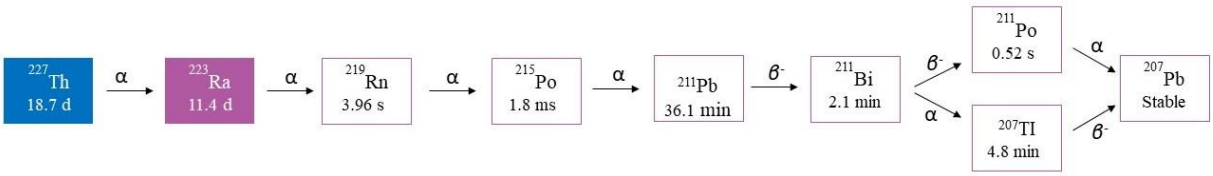

Figure 1.7. Simplified decay chains of ^{223}Ra into a stable isotope of lead ^{207} Pb. Alpha particle (α), Beta-particle (β$^-$-electron). Figure is inspired by (92).

1.3.5.2.5 Lutetium-177-PSMA-617

PSMA is a transmembrane glycoprotein, that consists of 750 amino acids. PSMA is overexpressed in prostate cancer cells, which makes it an excellent molecular target for both diagnostic imaging and TRT. Various PSMA-targeting ligands and antibodies labeled have been developed, labeled with β-emitters including ^{177}Lu,^{161}Tb, ^{67}Cu and ^{47}Sc and studied in preclinical and clinicals (92, 104).The most frequently used β-emitting radionuclide in clinical PSMA targeting therapy is ^{177}Lu with a half-life of 6.7-day. Lu-177-PSMA is administered intravenously, followed by the binding to PSMA on prostate cancer , internalzation into the cell in which it emits β-particle radiation and remains over the 6.7-day half-life of ^{177}Lu (Fig. 1.8). The short path length of ^{177}Lu results in minimal radiation to non-targeted normal tissue, and its maximal tissue penetration of 2 mm, results in a cross-fire effect in which cells that may express lower PSMA are also been targeted. These characteristic features of ^{177}Lu makes it favorable for TRT (105). The β- particles emitted by ^{177}Lu have a mean range of 670 µm and energies of 0, 1-2, 2 MeV, making it an ideal radionuclide for treating metastases (104, 106).

Studies have shown that treatment of mCRPC patients with the small molecule radioligand ^{177}Lu-PSMA-617 gives a better therapeutic effect and causes fewer adverse effects than third-line treatments (107). The soon expected approval of ^{177}Lu-PSMA-617 for patients with mCRPC will shift TRT into the mainstream of cancer treatment. Despite β-emitting ^{177}Lu-PSMA-617 therapy, mCRPC still remains incurable. This may partly be explained by that around 30% patients are ^{177}Lu-PSMA resistant, and that inter- and intra-patient tumoural PSMA heterogeneity exist (108). There is a need for optimized targeted (α-emitting TRT) or combinational therapies for these patients. Further, ^{177}Lu-PSMA in combination with other therapies is in development (105, 107).

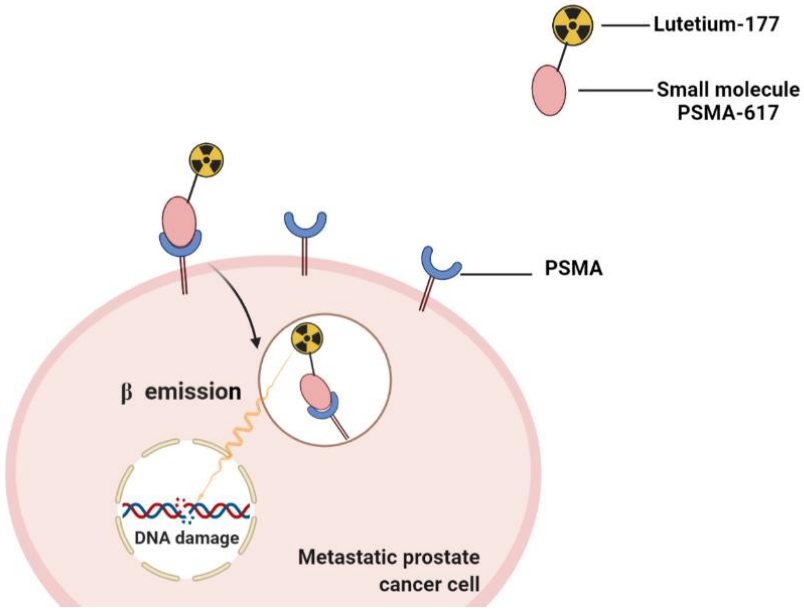

Figure 1.8. Radioligand (^{177}Lu-PSMA-617) therapies for mCRPC. A PSMA targeting small molecule (PSMA-617) radiolabelled with ^{177}Lu, binds to PSMA on prostate cancer cells, and cause direct and indirect damage. The figure is adapted from (105), and created using illustrations from Biorender (https://biorender.com)

1.3.6 Combinational therapies

Most patients with mCRPC initially respond to therapies with ARSIs, taxane-based chemotherapies, immunotherapy or ^{223}Ra, but each of these therapies provides only limited 2-4 months overall survival benefit (OS) for the patients (Table 1.3). Hence, combination regimens are being explored for its potential clinical outcomes, by targeting multiple oncogenic pathways simultaneously; while potentially minimize the risk for the development of resistance to treatment (109, 110). For instance, several agents have been studied in combination with Docetaxel, including abiraterone acetate, DN-101 and lenalidomide (109, 111). In addition, an ongoing sequential treatment for mCRPC with ^{223}Ra and Docetaxel are currently in phase II clinical trial (112). Additionally, treatment of mCRPC patients with ^{223}Ra in combination with other agents, including ENZA is being used in real world settings (113).

1.3.7 Targeting Bromodomain-containing proteins in prostate cancer

Epigenetics can be defined as heritable modifications in gene function that do not entail changes in genomic DNA sequence, leading to change of phenotype (114). Epigenetic mechanisms comprising DNA methylation, histone modifications, and noncoding RNAs affect chromatin structure and regulate gene expression (115). Several histone modification patterns can occur on histones, including histone acetylation, which is linked to regions of open chromatin accessibility to DNA and RNA polymerases (114). Dysregulation of acetylation levels on histones are deregulated in cancers, caused by changes in activity or expression of the two enzymes catalyzing acetylation, acetyltransferase (HATs) and deacetylases (HDACs) (114). In many cancer types, deregulation of HDACs changes the expression of oncogenes, tumors

suppressors and miRNAs. Therefore, oncological agents targeting HDACs are being developed (116). Another way to disrupt pro-tumorigenic transcription is targeting epigenetic readers, such as Bromodomain containing proteins (BRD) (114).

BRDs is a large class of proteins that generally include a bromodomain and other domain explicating the typical function of the protein. The human genome encodes for 61 bromodomains in 46 diverse proteins, variations in the amino acid residues around the acetyl-lysine binding site impart ligand specificity (117, 118). Bromodomain and extra-terminal domain (BET) proteins are a subclass of bromodomain containing proteins. BET proteins are mainly epigenetic readers that have an important role in transcription regulation and cell proliferation. This sub-family consists of four proteins BRD2, BRD3, BRD4, and the testis-specific restricted BRDT. They are characterized by two tandem N-terminal bromodomains, an extra-terminal (ET) domain, and a C-terminal domain. These proteins contribute in transcription regulation by binding to acetylated lysine residues on histone tails, through their hydrophobic cavity, recruiting other transcription factors to the chromatin and influence gene expression (119). The bromodomain motif consists of approximately 110 amino acids, which are conserved in several genes. The C-terminal domain interacts with the positive transcription elongation factor b cyclin T1/CDK9 complex (P-TEFb) to activate RNA polymerase II (Fig. 1.9) (120). P-TEFb is dependent on BRD4, for its localization to sites of active transcription of growth-promoting genes, including *MYC*, where it's phosphorylated and further increases the processivity of RNA polymerase II (120, 121). Additionally, BRD4 interacts with the Mediator complex, which is a transcription co-activator protein complex of the RNA polymerase II. It is important to note that BRD4 are not the only BET member that has this functional interaction with polymerases, since the other BRDs members (BRD2 and BRD3) also facilitate RNA polymerase II elongation through binding to hyper acetylated chromatin. Finally, the ET domain of BET proteins, also take part in transcription regulation by interacting with other key proteins (122). Therefore, BETs have an important role in facilitating transcription activation by directly interaction with promoters and gene sequences (119). However, BET proteins also play an important role in cell cycle regulation, BRD4 functions as mitotic bookmark and cell cycle gatekeeper. For instance, BRD4 particularly binds to acylated H3 and H4, bookmarks genes for transcription in late mitosis and early G1 phase. BRD4 is also needed for cell cycle progression (122), and is also involved in DNA repair.(25).

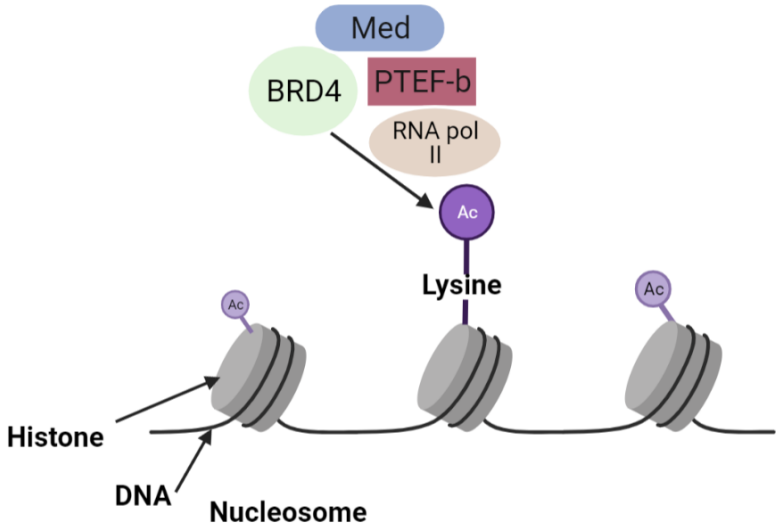

Figure 1.9. BET proteins function. Regulation of transcription activation through binding to acylated histones on nucleosomes. Med, Mediator, RNA pol II, RNA polymerase II, Ac, Acetyl, P-TEFb, positive transcription elongation factor b. The illustration is adapted and modified with permission from (122) and created using illustrations from Biorender (https://biorender.com)

Several preclinical studies have reported the association of BET proteins with human cancer (123-125). For instance, BRD2 is overexpressed in B-cell lymphoma, and BRD3 and BRD4 directly drive Nut midline carcinomas, which is an aggressive form of undifferentiated squamous cell carcinoma (121, 124). BET proteins are overexpressed in CRPC and depend on AR signaling for their expression in prostate cancer (126). Clinical trials are ongoing with BET inhibitors to prove the efficacy of many compounds also in CRPC settings (127, 128).

Based on these studies, targeting BET proteins as a strategy for the development of novel anticancer drugs that inhibits the binding of BET to acylated histones have gained a lot of attention as of recently (Fig.1.10) (121, 124). The regulation of one of the well-known cancer oncogenes *MYC* are shown to be implicated in BET protein function. Thus, by inhibition of BET proteins, down regulation of *MYC* oncogene expression (overexpressed in solid tumors) is achieved, which again results in decreased cell proliferation (122). In addition, interaction between BRD4 with the N-terminal domain of AR has also been identified. Given that BRD4 interact with AR raises the prospect of using BET inhibitors as an alternative strategy for targeting the AR-driven cancers, including CRPC (114, 129).

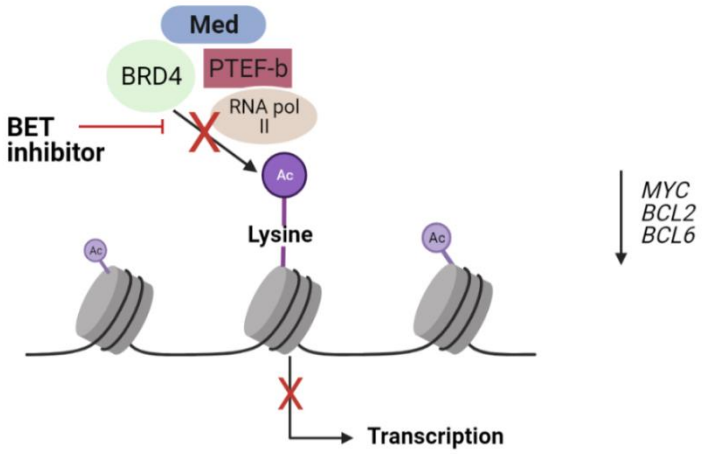

Figure 1.10. BET inhibitor mechanism of action. Prevents transcription of certain genes like *Myc*, *bcl2* and *bcl6*, leading to decreased cell proliferation and increased apoptosis. Med, mediator, RNA pol II, RNA polymerase II, Ac, Acetyl and P-TEFb, positive transcription elongation factor b. The figure is adapted with permission from (122). and created using illustrations from Biorender (Biorender.com).

Several BET inhibitors with different antitumor activity have been developed and investigated in prostate cancer. The first two BET inhibitors resulting in displacement of BET proteins from chromatin are I-BET (a benzodiazepine derivative) and JQ1(122). A study published in Nature by Asangani and colleague investigated JQ1 and I-BET (122, 130). In addition, interaction between BRD4 with the N-terminal domain of AR has also been identified. The authors reported that BRD4 interacts with the N-terminal domain of AR and contribute in prostate cancer progression to CRPC Given that BRD4 interact with AR raises the prospect of using BET inhibitors as an alternative strategy for targeting the AR-driven cancers, including CRPC (114, 130, 131). In the same study it was also showed that AR signaling-competent human CRPC cell lines are sensitive to inhibition of BET. Furthermore, JQ1 have shown to induce G1 cell cycle arrest, apoptosis, and repressing the expression of anti-apoptotic factors in AR positive PC-cell lines, while disruption of AR recruitment to target gene, result in down regulation of AR-target genes (114, 130, 131).

However, BET inhibition by JQ1 reduces levels of the constitutively active AR variant 7, an AR splice variant that do not express the AR ligand-binding domain. Since BET inhibitors efficacy as single agents seems to be limited based on preclinical studies, combination therapy with other agents have been explored as a new possibility to potentiate the anticancer effect (124). For instance, combination of JQ1 with the androgen antagonist ENZA, shown to display enhanced efficacy in vivo (114, 132).

Since the development of the first BET inhibitor, JQ1, several other BET inhibitors with different degree of antitumor activity have been developed (122, 133). One of the BET inhibitors is AZD5153, which is a novel, selective and bioavailable BET inhibitor. Unlike the other BET inhibitors, like JQ1 and I-BET762 which bind monovalent with one molecule to each BRD, AZD5153 targets two bromodomains in BRD4 simultaneously, thus it is a bivalent BET inhibitor (122, 134). This bivalent binding mode of AZD5153,

allows the displacement of BRD4 from chromatin at a lower drug concentration (134). An in vitro study utilizing AZD5153 BET inhibitor on PC-3 and primary prostate cancer cells, reported downregulation of BRD4 targets, *CCND1*, *MYC*, *Bcl2*, FOSL1 and CDK4 (135).

2 Aims

The focus of this thesis is to combine BET, AZD5153 and JQ1, or AR, ENZA, inhibitors with radiopharmaceuticals for the treatment of CRPC. The radiopharmaceuticals chosen for this thesis are the α-emitter ^{223}Ra (Xofigo®) and ß-emitter ^{177}Lu-PSMA-617, both used in the treatment of mCRPC Most patients with mCRPC intially response to taxane-based chemotherapies, immunotherapy or ^{223}Ra treatment, each of these therapies provide a limited 2–4 months overall survival benefit (Table 1.3) (136). Epigenetic alterations have shown to be involved in the evolution of prostate cancer (137). In particular ,overexpression of BET proteins such as BRD4 and other BRDs in CRPC have been associated with chromatin re-configuration and relaxation (126). In addition, BRD4, the main target for most of the BET inhibitors, has been shown to have a role in DNA repair and AR mediated transcription (131). More than 50% of primary and metastatic prostate tumors have genomic alterations in bromodomain (BRD) containing proteins (138, 139). The combination of RT with anti-androgen agents such as ENZA has been partially explored in the clinic (140). Both combinations of BET inhibitors or ENZA with radiopharmaceuticals are attractive treatment approaches for mCRPC due to the non-overlapping mechanisms of actions.

The hypothesis of this study is that combining BET or AR inhibitors with radiopharmaceuticals will result in synergistic therapeutic effects.

The overall aim of this thesis is to evaluate the preclinical therapeutic efficacy of combining BET, JQ1 and AZD5153, or AR, ENZA inhibitors with radiopharmaceuticals, ^{223}Ra or ^{177}Lu-PSMA-617 in CRPC C4-2 cell line. In this regard, the research objectives are:

To explore the combination of different inhibitors with radiopharmaceuticals;

To assess combination effects in a cell monolayer model;

To study combination effects in an advanced multicellular tumor spheroid model;

To identify mechanisms in the interaction between inhibitors and radiopharmaceuticals;

To propose recommendations for further preclinical studies.

3 Materials & Methods

3.1 Cell lines and culture conditions

All experimental segments of this master's thesis were carried out *in vitro*, by using the methods and materials described below. All materials used in this thesis are presented in Appendix A.

3.1.1 Cell lines

The human prostate cancer cell line C4-2, a derivate from LNCaP cell line, was used in this thesis. (141). The LNCaP cell line was obtained from a lymph node metastatic lesion of a 50-year-old male with prostatic adenocarcinoma in 1980 (142). Many androgen-sensitive sublines have been established from the LNCaP cell line, including; C4-2 and C4-2B sublines (142). The C4-2 subline was established by introducing the LNCaP and MS (a bone stromal cell line) cells into castrated nude mice (androgen depleted hosts) (141). Upon cellular interaction with stromal cells, following the mice castration the androgen-dependent LNCaP cells progressed to an androgen-independent phenotype, giving rise to the C4-2 subline (142).

This subline shares the same genetic background with LNCaP cells and mimics both the phenotypic and genotypic changes often observed in clinical human CRPC (143). The characteristics of C4-2 cell line (and its parental LNCaP cell line) are shown in Table 3.1.

Table 3.1. Characteristics of prostate cancer C4-2 subline utilized in this thesis and its parental LNCaP cell line (142, 144).

Characteristics	**Cell line**	
	LNCaP	**C4-2**
Derivate from	Metastatic lesion from male human	LNCaP cells, grown in castrated nude mice
Cell type	Epithelial	Epithelial-like
Culture properties	Adherent, single cells and loosely attached clusters	Adherent
Androgen dependency	Dependent	Sensitive/independent
Androgen receptor	Positive	Positive
PSA	Positive	Positive

3.1.2 Culture conditions

The C4-2 cell line (ATCC® CRL3314™, Manassas, Virginia) was grown in RPMI 1640 medium with L-glutamine and sodium bicarbonate (Sigma-Aldrich) supplemented with 10% heat-inactivated fetal bovine serum (FBS, Thermo Fisher Scientific) 100 units/ml penicillin and 100 µg/ml streptomycin (PS,Thermo Fisher Scientific) at 37°C with 5% CO_2 level.

Once cell confluency (percentage of the surface area of a culture flask covered by cells) was 75-85 %, the cells were subcultured into new culture flasks; cells were rinsed with sterile Dulbecco's phosphate buffered saline without Ca^{2+} and Mg^{2+} (PBS, Sigma Aldrich) and detaching with Trypsin (Sigma-Aldrich), a protease that inhibits the attachment of cells to surfaces. Detached cells were further supplied with the complete growth medium for the inactivation of trypsin by media containing FBS. To maintain exponential growth subculturing was performed twice per week. Since C4-2 cells have a high growth rate, a splitting ratio of 1:5 was followed.

Further, cell counting was performed by mixing 50 µl of cell suspension with 50 µl Trypan blue (Thermo Fisher Scientific) and analyzed using CountessTM II Automated cell Counter (AMQX1000, Thermo Fisher Scientific). To new culture flasks, cells were seeded at a cell concentration of 3.5 million cells in 175 cm^2 or 1, 5 million cells in 75 cm^2 flasks, and maintained in an incubator (Forma Scientific) at 37°C with 5% CO2-saturation to regulate the physiochemical environment such as pH, osmotic pressure and temperature.

3.1.3 Freezing cells

To maintain the viability of cells, when cells not in use cryopreservation (freezing down cells) was applied. When cells in a 175 cm^2 cell culture flask, were approximately 80% confluent (80% of the surface of the flask covered by cell monolayer), they were trypsinized and transferred to a 50 ml tube, centrifuged and the supernatant was removed. The following two solutions were prepared beforehand, the solution I: a mix of RPMI- medium and FBS with a 1:1 ratio. Solution II: a mix of RPMI-medium and 20% dimethyl sulfoxide (DMSO, Sigma Aldrich) in a 4:1 ratio.

A volume of 2.5 ml of solution I, was added to the cell pellet, right after 5 ml of the other solution II was slowly added. The cell solution was aliquot in sterile cryovials (1.8 ml put in each cryovial). Finally, cells were immediately placed in the freezer with a temperature of -80°C, and next day to a nitrogen tank.

3.2 Cell culture models

Two-dimensional (2D, cellular monolayer cultures) and three-dimensional (3D, multicellular spheroids) culture models were applied. Although the traditional 2D culture model is widely used in cancer and biomedical research, this model has some disadvantages, such as reduced interactions between the cellular and extracellular environment and reduced ability to mimic the *in vivo* conditions (145, 146). In addition, cells grown in 2D culture model, differ than those in vivo as they are more flat and stretched, such abnormal cell morphology influence various cellular process such as cell proliferation, differentiation, apoptosis, gene and protein expression (147). The 3D cell culture model has attracted significant attention as an effective tool in evaluating therapeutic invention efficacy, particularly in cancer research treatment, for their resemblances to tissue structure and functional properties in living organisms (148). In 3D culture model cells grow in all directions creating an *in vitro* environment similar to how cells are growing in the *in vivo* environment, which creates a more accurate in vitro model for research, including drug discovery application (147).

3.2.1 Three-dimensional (3D, multicellular spheroid model)

There are different 3D culturing techniques applied in tumor biology including; cell culturing in aggregates (spheroids), cells embedded in gels or other artificial and natural extracellular matrix compounds or cells growing on 3D scaffold materials (148). The multicellular spheroid model (MCS) applied in this study, is a widely used 3D-culturing technique.

Several different methods are available for spheroid generations, including; scaffold-based and scaffold-free. The choice of method depends on the preferred number and size of spheroids. To produce a larger number of spheroids, the method of choice is a spinner flask system. However, when the aim is to produce spheroids of a consistent size and shape, the common methods are pellet culture, the liquid overlay technique, or a hanging drop array (spheroid array). Recent methods use micro-fluidic techniques and nano-printed culture plates to produce spheroids. Nevertheless, all these methods share the same aim: increasing cell interactions with neighboring cells and extracellular matrix (149).
To generate MCS, the liquid overlay technique was used in this study. This simple method allows for the generation of a single spheroid in multi-well plates. The principle of the method is that each well of a multi-well plate is coated with artificial matrices (non-adhesive polymers such as agarose, hyaluronic acid, or a mixture of non-adhesive polymer with other biomaterials) before the addition of cell suspension. The use of non-adhesive polymer is crucial for the formation of spheroids since it provides a non-adhesive surface and increases cell-to-cell contact, resulting in cellular aggregation (150).

3.2.2 Preparation and individual spheroid formation in 96-well plates

The1.5% agarose (Sigma Aldrich) was prepared in PBS with Ca^{2+} and Mg^{2+} (Sigma Aldrich) and boiled for 10 minutes at 200 °C. Fifty µl of the gel mixture was added to each well of a transparent 96-well flat bottom plate (Nunclon™ Delta Surface, Thermo Scientific), under sterile conditions using a manual precision dispenser. The agarose mixture was kept at a temperature of 120°C the whole time to prevent the agarose from early gelation during pipetting. Plates with agarose were left to cool down to room temperature for 60 minutes. Additionally, 200 µL of PBS supplemented with penicillin/streptomycin was added to the outer walls of the 96-well plate to create an evaporation barrier.

The C4-2 cells from a 175 cm^2 or a 75 cm^2 flask were harvested by trypsinization during their exponential growth phase (70-80% confluence). The cells were counted and resuspended in fresh medium to a concentration of 500 cells per 100 µl, i.e., 5000 cells/ml. The number of cells seeded in an individual well was 500 cells.

Hundred µl of cell suspension was added to each well, and the plates were centrifuged for 15 min at 1691 rpm (470 g) before incubation (37 °C, 5% CO_2) for five days to allow spheroids to form (Fig. 3.2). The cells within the multicellular spheroid are characterized by an external layer of viable cells (called proliferating zone), an internal layer of quiescent cells (caused by the gradient of nutrient and oxygen diffusion) and an

inner layer of necrotic cells (called necrotic core), mimicking the cellular heterogeneity observed in solid tumors (151).

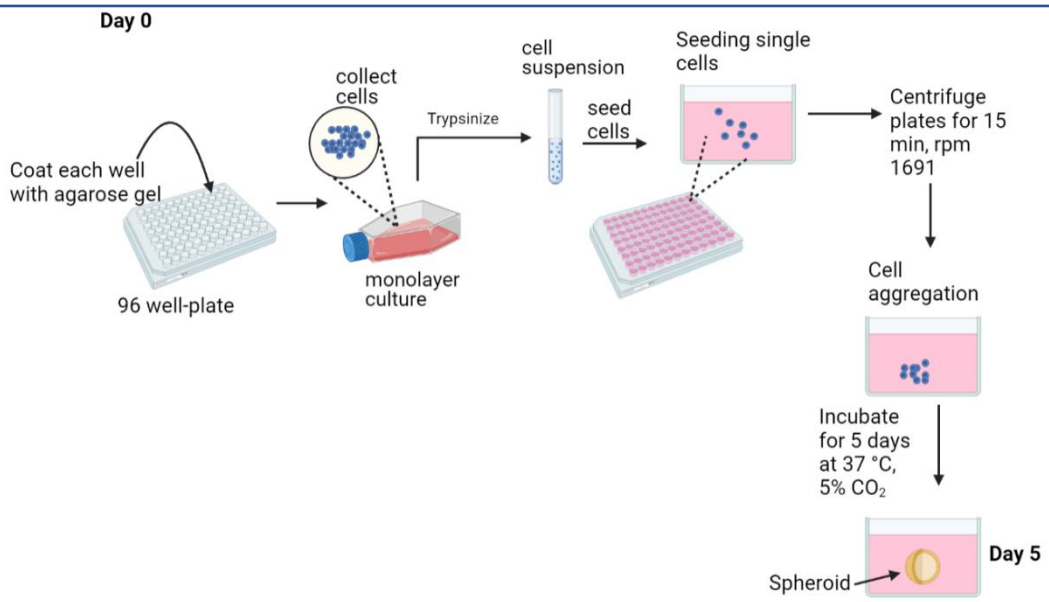

Figure 3.2. Schematic presentation of the preparation and formation of multicellular spheroids using the liquid overlay technique. C4-2 cells (500 cells/well) were seeded in an agarose-coated 96-well plate and then incubated for 5 days for spheroids to form. The figure is inspired by (152), and created using illustrations from Biorender (https://biorender.com).

3.3 Cell viability assays

The 3-(4, 5-Dimethyl thiazol-2-yl)-2, 5-diphenyl tetrazolium bromide (MTT), CellTiter-Glo®Luminescent cell viability (CellTiter) and clonogenic assays were performed to examine the effect of JQ1, AZD5153 or ENZA on C4-2 cells in monolayer (2D), and to determine drug concentrations to use in further combination experiments. Additionally, fluorescence-based live-dead fluorescein diacetate (FDA, Sigma Aldrich)/propidium iodide (PI, Sigma Aldrich) assay was performed to determine the effect of the BET or AR inhibitor on C4-2 cell viability within C4-2 spheroids.

3.3.1 MTT assay

The MTT assay was applied to evaluate the viability of C4-2 cells after treatment with different concentrations of DMSO, JQ1, AZD5153 or ENZA MTT assay was applied. This assay is based on the reduction of 3-(4, 5-Dimethyl thiazol-2-yl)-2, 5-diphenyl tetrazolium bromide and produce formazan a purple-colored product, which is quantified by using a spectrophotometer. This product cannot be produced by dead cells, due to the lack of NAD(P) H-dependent cellular oxidoreductase enzymes responsible for this reaction (153).

C4-2 cells (1000, 2500 or 5000 cells/well) were seeded in transparent 96-well flat bottom plates and allowed to adhere overnight, and then the cells were treated with various concentrations of DMSO, BET inhibitors or ENZA for 2-7 days. Each day after treatment the media from one treated group (7 wells in the same group)

was replaced with fresh media. Afterwards, the plates were taken out of the incubator, the media was discarded and cell viability were determined by adding 100 µl MTT 0.25 mg/ml (Sigma Aldrich) (stock solution was 5 mg/ml dissolved in PBS solution) into each well and incubated for 2-3 h in the incubator. Then, the MTT solution was discarded from each well and replaced with 50 µl DMSO, to solubilize the formazan crystals. Finally, the intensity of the dissolved formazan crystals (purple color) was read at absorbance 570 nm using multimode microplate reader (Spark® Multimode Microplate Reader, Tecan Austria GmbH). DMSO was used to obtain a value for background absorbance.

3.3.2 CellTiter-Glo Luminescent Cell Viability Assay

CellTiter (Promega, Madison, Wisconsin United States) is based on luminescent detection of adenosine triphosphate (ATP). Viable cells are metabolically active and produce adenosine triphosphate (ATP). The amount of ATP detected by the luciferase reaction mirrors the number of viable cells in the sample. The addition of the CellTiter-Glo reagent to a cell sample results in lysis of the cell membrane and ATP release from viable cells present. The reagent also contains the luciferin and luciferase enzymes that generate a luminescent signal proportional to the amount of ATP present in the presence of O_2 and Mg^{2+}. C4-2 cells (1000 cells/well) were seeded in 96 well-plates (transparent flat-bottomed) and treated with different concentrations of the AZD5153, JQ1 or ENZA and incubated at 37 ºC for 7 days. Afterwards, media was removed from wells and 20 µl CellTiter-Glo reagent (Promega) was added (Fig. 3.3). The cell solution was transferred to a white 96-well plate (Corning ®COSTAR), and the luminescent signal was recorded using Spark multimode reader microplate reader(154). DMSO was used as control to obtain a value for background luminescence.

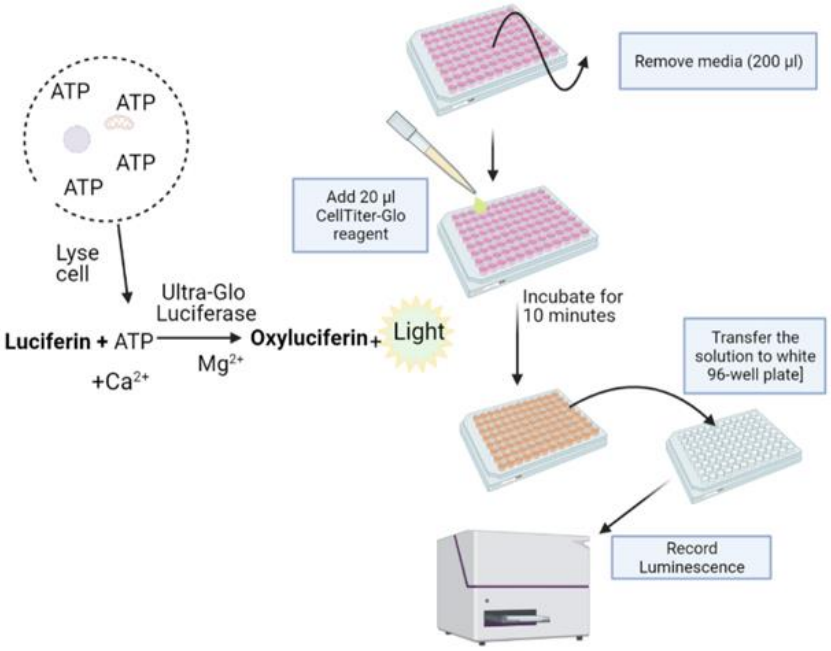

Figure 3.3. Summary of CellTiter-Glo®Luminescent Cell viability assay. The Luciferin reaction shown is inspired by Cell-Titer-Glo®2.0 Assay Technical Manual, Promeega, Inc (155), and figure is created using Biorender (https://biorender.com).

3.3.3 Clonogenic assay

The clonogenic assay is considered as the "gold standard", and is widely used to test reproductive cell survival *in vivo*. First described in the 1950s in the field of radiobiology (94). A single cell that survives, while also able to divide unlimited and produce colonies, is said to have retained its reproductive integrity and is being clonogenic (94). Formed colonies, must consist of ≥50 cells for it to be considered a colony and counted as such.

By performing a clonogenic assay, a cell survival curve is generated, which describes the relation between a given dose of a drug used to cause cell damage and the fraction of cells that have retained their productive integrity, despite being exposed to such drugs (94).
The surviving fraction is given by the following formula:

$$Survival\ fraction = \frac{Colonies\ counted}{Cells\ seeded \times \frac{PE}{100}} \qquad (Eqn.\ 3)$$

The plating efficiency (PE) indicates the percentage of cells that are seeded and forms colonies.
In clonogenic assay, 1000 cells per 25cm^2 flasks (2-3 flasks per treatment group) were plated, after 24 hour the medium from each flask were removed and 5 ml of prepared working solution of DMSO, JQ1, AZD5153 or ENZA (Table3.3) was added.
Further, the flasks were incubated for 10-14 days. The colonies were then fixated with 100% ethanol (Antibac AS, Norway) and stained with 0.4 % methylene blue (Thermo Fisher Scientific). The colonies were counted and PE and survival fraction (SF) were calculated using the equations 2-3.

Table 3.4. The different concentrations of JQ1, AZD5153 and ENZA, used to determine the concentration to use for further combination treatment experiments.

Drug name / Concentrations			
JQ1 (nM)	**AZD5153 (nM)**	**ENZA (µM)**	**DMSO (%)**
10	2	0.5	0.001
25	5	1	0.005
50	10	2.5	0.01
75	25	5	0.05
100	50	10	0.1
250	75	25	0.5
500	100	50	1
1000	250	75	5
2000	500	100	10

3.3.4 Florescence live-dead (FDA-PI) based assay

FDA-PI assay were performed to determine cell viability within C4-2 spheroids after treatment with various concentrations of DMSO, JQ1, AZD5153 or ENZA. FDA is a non-fluorescent molecule which is hydrolysed to fluorescent fluorescein in viable cells. It is a viability probe that measures both enzymatic activity, which is required to activate its fluorescence, and cell-membrane integrity, which is required for intracellular retention of their fluorescent product. PI is an intercalating fluorescent agent that binds between the bases of DNA. PI is membrane impermeant, which prevents DNA binding in viable cells, allowing identification of dead cells in a population (156, 157).

In brief, C4-2 spheroids were prepared as described and shown above (Fig. 3.2). Bright field microscopy images of spheroids before treatment (day 0) were taken using Axiovert 200m Inverted Fluorescence Motorized Microscope (Carl Zeiss, GERMANY) with AxioVision Rel.4.8 software (Carl Zeiss). The following parameters were used: 4x objective, 5.6 voltage, contrast method bright field, N.A 0.55, exposure time for bright field images was 1 ms. Then, the spheroids were treated with different concentrations of the BET or AR-inhibitors (Table 3.4). The growth of spheroids was evaluated at day 3,7,14 and 21 after treatment by taking bright field images. The cross-sectional area of each spheroid was measured and spheroid growth graph curves were obtained. Additionally, the measured cross-sectional area (mm^2) of spheroid at day (X) was normalized to the control at day X after subtracting baseline areas for all spheroids (day 0) using the following equation:

$$Normalized\ cross-sectional\ area = \frac{Sn\ (Day\ X) - Sn\ (Day\ 0)}{Scontrol\ (Day\ X) - Scontrol\ (Day\ 0)} \qquad (Eqn.4)$$

Where:

S is a cross-sectional area (mm^2), n is a spheroid treated with a drug, radiopharmaceutical or both, the control is a spheroid treated with DMSO, X –day after treatment.

Finally, at day 14 or 24, fluorescence live-dead-based (FDA-PI) assays were performed on a few spheroids per group using fluorescence microscope (Carl Zeiss Axiovert 200m Inverted Fluorescence Motorized Microscope, GERMANY). The FDA and PI mixed solution was prepared by mixing 8 µl FDA, 50 µl PI, and 2.5 ml PBS with Ca^{2+} and Mg^{2+}. The spheroids were washed three times with 100 µl of PBS with Ca^{2+} and Mg^{2+}, then incubated with 100 µl staining solution at room temperature for 5 min in the dark. Finally, the spheroids were washed with PBS with Ca^{2+} and Mg^{2+} (100 µl in/out, three times), and 100 µl PBS were added to spheroid before analyzing with microscope. The following parameters were used: 4x objective, 5.6 voltage, contrast method bright field, N.A 0.55, exposure time for bright field images was 1 ms, 60 ms for FDA and 1.8 s for PI.

3.4 Seeding cell number

In clonogenic assay, cell number optimization is important since too many-seeded cells lead to the overlapping of colonies, while a low number of cells lead to the formation of too few colonies. We decided to use 1000 cells per 25cm^2, based on an experiment in which 2000 cells per 25cm^2 flask were used resulting in over 400 colonies. Too many colonies in the control group, resulted in merging of colonies, and making it difficult to count the colonies accurately.

For spheroid formation, the initial cell number affects the size and morphology of the spheroids. A high cell number leads to the formation of a too-large weak spheroid that causes disintegration and survival issues (necrotic core), while a low cell number gives a non-favorable spheroid size. The optimal seeding cell number for the formation of spheroids was determined in the previous experiments to be 500 C4-2 cells/well in the laboratory (Department of Radiation Biology, OUH). Initial cell numbers of 250, 500, and 1000, 2000, and 2500 cells/well were seeded and cultured for 6 days, and bright field microscopy images were taken and evaluated.

3.5 Activity of ^{223}Ra

The activity (kBq/ml) of ^{223}Ra to use in all experiments was based on previous experience of the group in the laboratory (Department of Radiation Biology, OUS). The activity to use in combination treatment of cell monolayer (2D) followed by flow cytometry analysis, in which a great number of cells were used (described in Chapter 3.6), was determined by seeding 1000 cells/well in 96-well plates incubated for 24 h and treated with 250 nM JQ1, 50 nM AZD5153 or 10 µM ENZA incubated for 2 h, further the cells were treated with different ^{223}Ra activities for 1 h, followed by removal of the media in each well to remove the ^{223}Ra. Afterwards,100 µl of fresh drug-containing medium was added to each well and incubated for 7 days. Each day after treatment the media from one treated group (6 wells in the same group) was replaced with fresh media. Finally, at day 7 the MTT assay was performed as described above (Chapter 3.3.1).

3.6 Combination treatments

Combinational experiments utilizing BET or AR-inhibitors with ^{223}Ra were carried out in both 2D monolayer and 3D spheroid culture models. In addition, combination experiment utilizing AZD5151 with ^{177}-Lu-PSMA-617 was carried out in spheroids. Non-lethal concentration of each drug selected based on the above-mentioned cell viability assays, selected concentrations were used as a pilot for designing combination treatment experiments in both monolayer (2D) and spheroids (3D).

3.6.1 Combination treatment in 2D monolayer culture model

The effect of JQ1, AZD5153 or ENZA in combination with ^{223}Ra were examined by seeding 1000 cells per 5 ml in 25cm^2 flasks. Two 25cm^2 culture flasks were used per treatment group. The cells were incubated overnight for adhesion to the plastic surface (Fig.3.5). The activity of ^{223}Ra was measured by Cobra II Auto-Gamma (Packard) using a CPM/kBq factor of 27 (counting window from 50-300 keV). Before treatment, the media was removed from the flasks. Then 1 ml of prepared 0.1% DMSO (control), 25 or 50 nM JQ1, 6.25,

10 or 25 nM AZD5153 or 1.25 or 10 µM ENZA were added to its respective flasks and incubated for 2-3 hours. Then the cells were incubated together with 2.5, 5 or 10 kBq/ml ^{223}Ra for 1 hour at 37°C in a humidified atmosphere of 5% CO_2. Afterwards, the media was removed and replaced with 5 ml of freshly prepared drug-containing media and further incubated for 10-14 days. At the experimental-endpoint, colonies were washed with 0.9% NaCl (B Braun), fixed with 95% ethanol (Antibac As), and stained with 3-4 ml 0.4% methylene blue for 20 minutes at room temperature. Excess stain was gently removed with cold water and the flasks were left to dry. Stained colonies were counted and SFs curves were obtained.

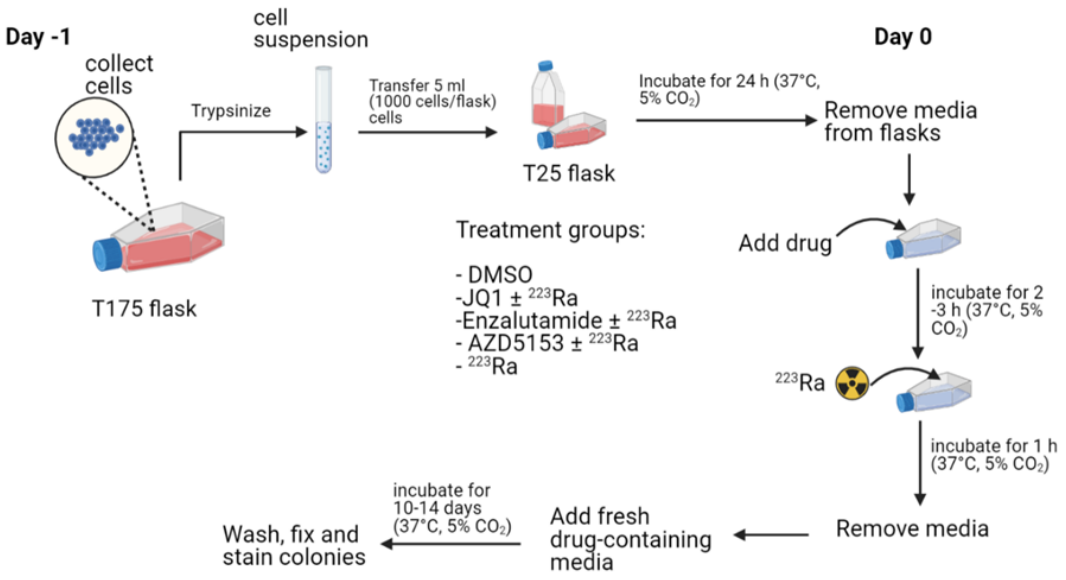

Figur.3.5. Schematic summary of the clonogenic assay. C4-2 cells seeded in 25cm^2 flasks, treated with selected concentrations of JQ1, AZD5153, or ENZA alone and in combination with 2.5, 5 or 10 kBq/ml ^{223}Ra, and clonogenicity were assessed. and figure is created using Biorender (https://biorender.com).

3.6.2 Combination treatment in multicellular spheroids (3D)

Combination treatment of BET inhibitors or ENZA with ^{223}Ra on C4-2 spheroids was performed. Preparation and formation of spheroids were performed as shown above (Fig. 3.2).

The spheroids were prepared as described above (Fig.3.2). The 96-well plates containing formed spheroids were taken out from the incubator and images of the spheroids were taken using microscopy before treatment (day 0) (Fig.3.6). Then the spheroids were incubated with the final concentration of 0.1% DMSO (control), 50 nM JQ1, 25 nM AZD5153 or 10 µM ENZA for 2-3 hours (Fig 3.6). Further, the C4-2 spheroids were co-incubated with 2.5, 5 or 10 kBq/ml ^{223}Ra for 1 hour. Ra-223 was removed by washing each well six times with fresh medium. Finally, 200 µl of fresh prepared drug-containing media were added to the respective wells. From day 7 after the treatment, the media from each well was replaced twice a week with fresh media. Spheroid growth after the treatment was evaluated at day 7 and 14 by measuring the cross-sectional area of each spheroid.

Similarly, the effect of AZD5153 in combination with ^{177}Lu-PSMA-617 was examined in C4-2 spheroids following the same flowchart shown below (Fig.3.6). The radiolabeling of PSMA with ^{177}Lu were done by Vilde Stenberg at OUH by using $^{177}LuCl_3$ dissolved in diluted HCl (ITG,Garching, Germany). The PSMA-617 ligand was obtained from MedKoo (Morrisville, North Carolina). It was dissolved in 0.5 M ammonium acetate in 0.1 M hydrogen chloride. For radiolabelling, $^{177}Lu\ Cl_3$ was added to a pre-heated mixture of PSMA-617 in 0.5 M ammonium acetate in 0.1 M hydrogen chloride, and pH were adjusted to 5-6. The solution was incubated for 30 min on the thermomixer at 90°C and 450 rpm. The radiochemical purity of the radioligand was measured by thin layer chromatography using instant thin layer chromatography strips (Tec-control, Biodex, New York).

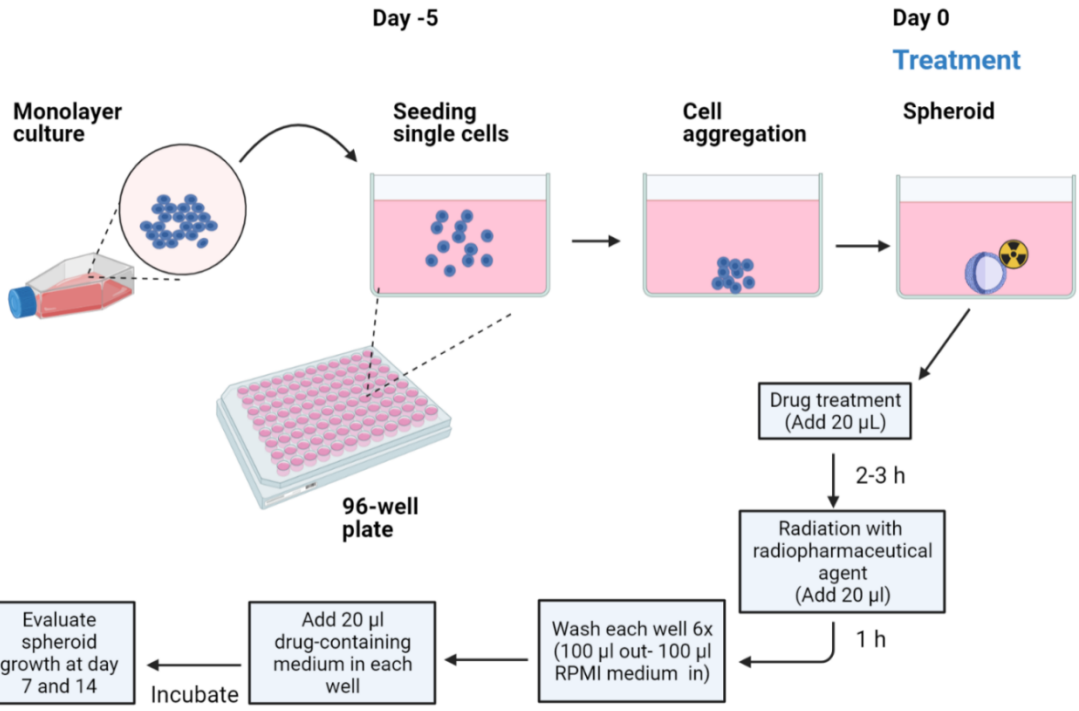

Figure 3.6. Schematic presentation of treatment of C4-2 spheroids with 25 nM AZD5153, 100 nM JQ1 or 10µM ENZA in combination with 2.5, 5 or 10 kBq/ml] of ^{223}Ra for 1 hr. The figure is created using Biorender (https://biorender.com).

3.7 Flow cytometry

Flow cytometry was used to detect apoptosis, DNA damage and cell cycle analysis of C4-2 cells, followed by the combination treatment of ^{223}Ra and BET inhibitors or ENZA.

Flow cytometry is a cell analyzing method used to study various cell properties such as cell size and DNA content. Analyzing cell properties in a flow cytometer system is based on the detection of light scattering and fluorescence emissions induced by lasers (light source).

Visible light scattering provides information about the phenotype and morphology of the cell and is measured in two different directions; forward scatter (gives information about cell size) and side scatter (giving information about cell granularity and complexity). Fluorescence emission, independent of light

scatter, indirectly gives information about the cell or cellular content by measuring the amount of expressed fluorescent proteins, fluorescent dye (e.g., propidium iodide), or fluorescently conjugated antibodies (e.g., FITC) in cells (158).

A flow cytometer consists of the following main components; fluidics, optics (excitation and detection), detectors, and a computer (electronics).

The fluidic system consists of sheath fluid (e.g., a buffered saline solution). Upon analyzing a cell-containing solution, the solution is pressurized and delivered to a laser intercept point, where the sample is being hydrodynamically focused and exposed to laser light and analyzed. The optical system includes a light source (laser) and detection optics (photodiodes and photomultiplier), collecting visible and fluorescent light signals used to analyze cells, further directed to optical detectors by a series of filters. The detectors sense the two types of light signals mentioned above; forward scatter and side scatter. Finally, the detectors are connected to the electronic system (computer), which converts the detected scatters into voltage, and a computer can read data (158).

C4-2 cells (0.5×10^6 or 1×10^6) were seeded in $25cm^2$ flasks for 24 hours, followed by treatment with 250 nM JQ1, 50 nM AZD5153, or 10 µM ENZA for 2 hours, then co-incubated with 2.5, 5 or 10 kBq/ml ^{223}Ra for 1 hour. The media was removed and replaced with new fresh drug-containing medium added to its respective flasks. The cells were further incubated for 72 hours.

To perform flow cytometry analysis, floating and adherent treated C4-2 cells were harvested from each sample. The collected cells were washed twice with 1 ml PBS (without Ca^{2+}/Mg^{2+}) and collected by centrifugation at 1200 rpm for 5 min, and further re-suspended in 2 ml PBS. Then 1 ml of the solution transferred into a 1.5 ml Eppendorf tubes for apoptosis detection, the rest cells were used for DNA analysis.

For apoptosis detection (Fig.3.7), a 2 ml 0,9% NaCl with 10 mM HEPES, 2,5 mM Ca^{2+} and 1 mM Mg^{2+} was used as annexin V-binding buffer, where 100 µl Annexin V-FITC (ImmunoTools) and 2 µl (1 mg/ml) PI were added and mixed. Annexin-V binds to phosphatidylserine (PS) on apoptotic cell surfaces in the presence of Ca^{2+}, but it can also bind to PS in the interior of dead cells (necrotic cells), by passing through their membrane, thus PI is used as a counterstain for Annexin V-FITC. Further, each sample was incubated with 100 µl of the Annexin V-FITC/PI solution for 15 minutes. After staining the samples were kept on ice before measurements. Flow cytometry analysis was performed with CytoFlex S instrument (Beckman Coulter). FITC fluorescence was excited with a 488 nm laser and detected using a bandpass filter 525/40 nm. PI fluorescence was excited with a 561 nm laser and detected using a bandpass filter 585/42 nm. Flow cytometry data were analyzed using a FlowJo software (FlowJo LLC, a subsidiary of Becton Dickinson).

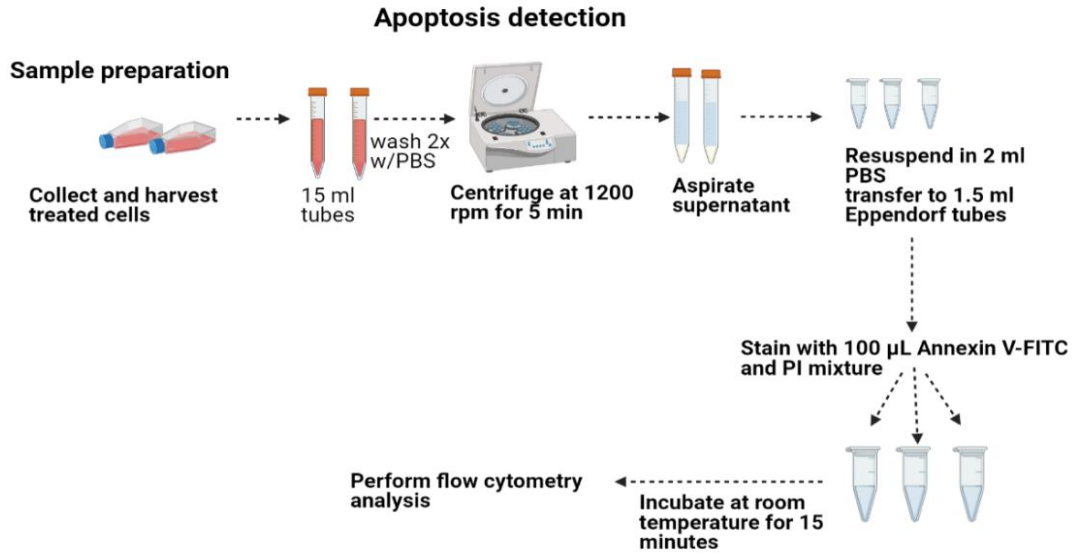

Figure 3.7. Process diagram for apoptosis detection using flow cytometry. The figure is created using illustrations from Biorender (https://biorender.com).

Further, for the detection of DNA damage and cell cycle analysis, the remaining collected cells were treated with 100 µl of eFluor 450 to stain dead cells (Thermo Fisher Scientific) for 30 min at room temperature (Fig. 3.8). Afterwards, the cells were washed and fixated in 1 ml ice-cold 100% methanol and placed at -20°C. Labelling of cells with antibodies for cell cycle analysis, DNA damage and mitotic cells was performed immediately before flow analysis.

Methanol fixated cells were washed with 2 ml of PBS with 0.2% Tween-20 (Sigma Aldrich) and collected by centrifugation. Finally, the cells were incubated with 150 µl solution containing primary antibodies, rabbit anti-phospho Ser10 Histone H3 (anti-H3S10p, binds to phosphorylated histone H3, Merck) and Anti-phospho-Histone γH2A.X (Ser139) antibody (Merck) for 60 minutes at room temperature under occasional agitation during incubation. Additionally, to the antibody solution 5 µl of RNase enzyme cocktail (Thermo Fisher Scientific) was added to degrade RNA thus hindering RNA from interfering with the DNA staining.

Afterwards, each cell sample was washed with 2 ml PBST and centrifuged. Further, the cells were incubated with 100 µl solution containing secondary antibodies Alexa Fluor™ 647 donkey anti-rabbit IgG (H+l) (Thermo Fisher Scientific) and polyclonal goat anti-mouse Immunoglobulins/FITC Goat $F(ab')_2$ (Dako) for 30 minutes at room temperature. The cells were washed with 5 ml PBST, and each sample was stained with 150 µl solution containing fluorochrome PI (binds to DNA in non-viable cells) in PBST with 2% bovine serum albumin (BSA) for 30 minutes. Finally, flow cytometry analysis was performed.

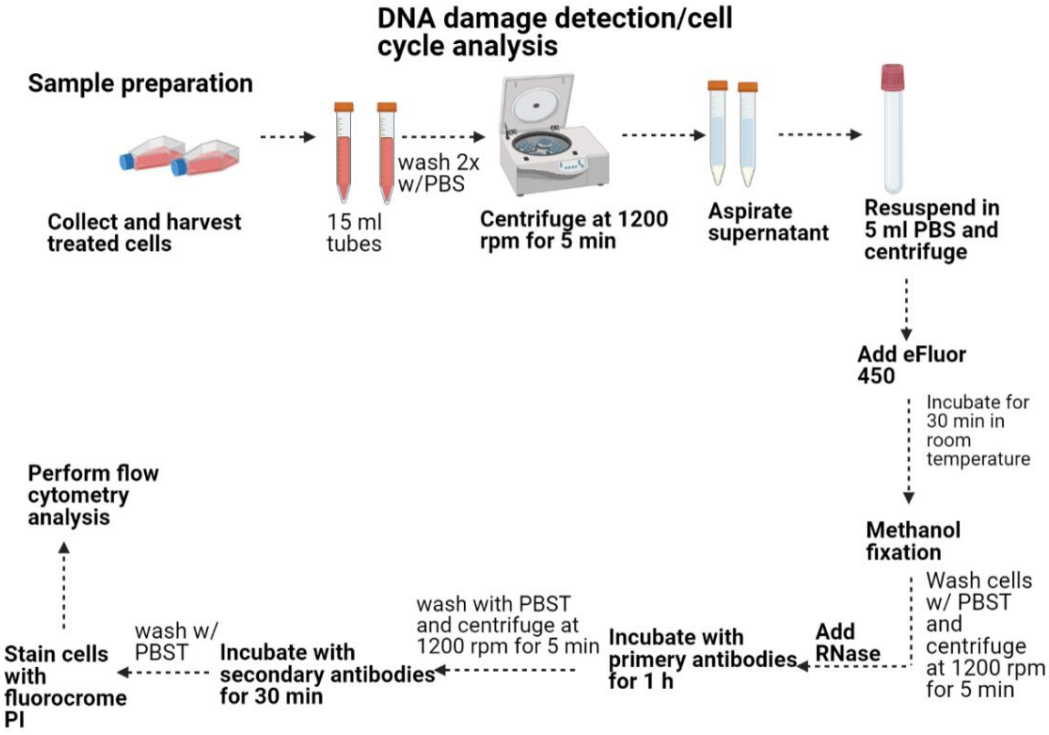

Figure 3.8. Process diagram for detection of mitotic cells and DNA damage using flow cytometry. The figure is created using illustration from Biorender (https://biorender.com).

3.8 Statistical analysis

For statistical analysis and graph presentation, Sigma Plot software 14.0 (Systat, USA) was used. Normality test and equality of variance were evaluated before choosing a statistical test. If the assumption of the equality of variance were not fulfilled upon comparisons of two groups (mono-treatment vs combination therapy), Student t-test, specifically Welch's t-test (assuming an unequal population of variances within two groups), was applied to calculate statistical significance ($p < 0,05$) for triplicate independent experiments in both 2D and 3D culture model. For group comparisons from flow cytometry analysis, the One-way analysis of variance (ANOVA) was carried out (statistically significant $p<0, 05$).

Bliss independence model was applied to determine the BET inhibitors or ENZA interactions in combination with radiopharmaceuticals. The model is based on the assumption that two drugs exhibit their effects independently and compares the effect of combination response observed with the expected combination response (expected additive), which is calculated based on each drug used alone independently (Fig.4.9 and Eqn.4). Further, the combination index (CI), were used along with statistical Welch's t-test (a p-value of 0, 05, was defined as statistical significance) to claim synergy when drugs interaction is independent, the CI is defined as: CI< 1 is synergy, CI=1 is additive and CI> 1 antagonism (159).

$$A = A_1 + A_2 - A_1 \times A_2 \qquad \textit{(Eqn.4)}$$

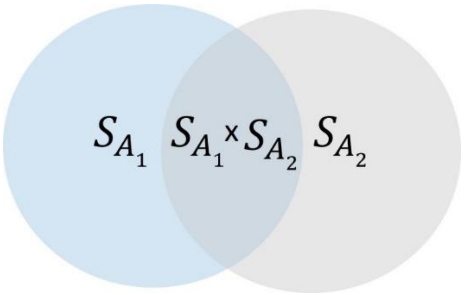

Figure 4.9. Illustration of drug independence based on Bliss independence, S, survival. The circles represent the survival fraction of cells upon mono-treatment utilizing drug A_1 or drug A_2, denoted as S_{A1} and S_{A2}. When the cells are treated with a combination of the two drugs, drug A_1 affects only the cells that survived drug A_2 and vice versa. Two drugs that exhibit their effects independently, the survival fraction of cells upon combination of the drugs equal to: $S_{A1}xS_{A2}$. Illustration is adapted from (159). From the equation:

A_1 is the mono-treatment of JQ1, AZD5153 or ENZA

A_2 is the mono-treatment of radiopharmaceutical ^{223}Ra or ^{177}Lu-PSMA-617. .

In addition, in spheroids the effects of the treatment between BET or androgen receptor inhibitors with and without radiopharmaceutical were evaluated separately at each dose of used drug for each spheroid measurement day. Interaction value and standard deviation (SD) was calculated by:

$$Interaction\ value = \frac{A_{1\times2}}{A_{1\times}A_2} \qquad \textit{(Eqn.5)}$$

A_1 is the mono-treatment of JQ1, AZD5153 or ENZA

A_2 is the mono-treatment of radiopharmaceutical (^{223}Ra or ^{177}Lu-PSMA-617).

A_{1x2} is the combination of JQ1, AZD5153 or ENZA and ^{223}Ra or ^{177}Lu-PSMA-617.

$$SD = \frac{A_{1\times2}}{(A_1\times A_2)} \times \sqrt{\frac{\Delta A_1}{A_1})^2 + (\frac{\Delta A_2}{A_2})^2 + (\frac{\Delta A_{1\times2}}{A_{1\times2}})^2} \qquad \textit{(Eqn.6)}$$

4 RESULTS

To examine the effect of BET or AR inhibitor in combination with radiopharmaceuticals in CRPC C4-2 cells growing in monolayer and multicellular spheroids various experiments were performed. The results from the experiments obtained from mono-treatment and combination therapy utilizing the various drugs in combination with radiopharmaceuticals are presented in this chapter. Further, results from flow cytometry analysis (apoptosis, necrosis, DNA damage and cell cycle distribution) upon exposure to combination therapy between BET inhibitors or ENZA and different activities of ^{223}Ra or ^{177}Lu-PSMA-617, are also detailed in this chapter.

4.1 Effect of JQ1, AZD5153, and ENZA on C4-2 cells growing in monolayers

The effect of various concentrations of JQ1, AZD5153 and ENZA was evaluated using the MTT, CellTiter and clonogenic assays in AR-positive, hormone-independent C4-2 cell line (Fig. 4.1). The clonogenic, MTT and CellTiter assays demonstrated that JQ1 and AZD5313 dose dependently inhibited C4-2 cells survival (Fig. 4.1 A-H and L). Only a 10-20% growth inhibition of C4-2 cells treated with ENZA was observed using CellTiter assay. ENZA did not inhibit C4-2 cell survival in a dose-dependent manner. These data suggest that C4-2 cells were resistant to ENZA. DMSO inhibited C4-2 cell survival in a dose-dependent manner (Fig. 4.1 G and H). DMSO concentrations 5 and 10% were lethal.

A time-dependent decrease in cell survival was observed after treatment with AZD5153 and JQ1 (Fig.4.1 I-J), while ENZA did not lead to inhibition of C4-2 cell survival in a time dependent manner (Fig.4.1 K). A statistically significant decrease in cell survival was observed with 250 nM JQ1 and 100 nM AZD5153 after 3 days (Figs.4.1 J and I). Based on these results we decided to use this time (3 days) in our later combination experiments for flow cytometry analysis.

The lethal doses of BET or AR inhibitors obtained from MTT, CellTiter assays or clonogenic cell survival differed greatly (Table 4.2), because these methods assess cell viability differently. Based on the survival curves (Fig.4.1) obtained from MTT, CellTiter and clonogenic assay a dose of each drug were selected for further combination experiments in 2D model. A concentration of 0.1% of DMSO (control) was chosen for all combination treatments going forward, since it is insufficient in causing cell death (Fig. 4.1 G and H). For the BET inhibitors and ENZA the selection of drug concentration for further experiments were at first chosen based on the MTT and CellTiter-Glo cell viability assays (Fig.4.1 A-F), 50 nM JQ1, 25 nM AZD5153 and 10 µM ENZA were selected. For another experiment a concentration of 25 nM JQ1, 6.25 nM AZD5153 and 1.25 µM ENZA were selected, and for a third combination experiment a concentration of 50 nM JQ1, 10 nM AZD5153 and 10 µM ENZA were chosen.

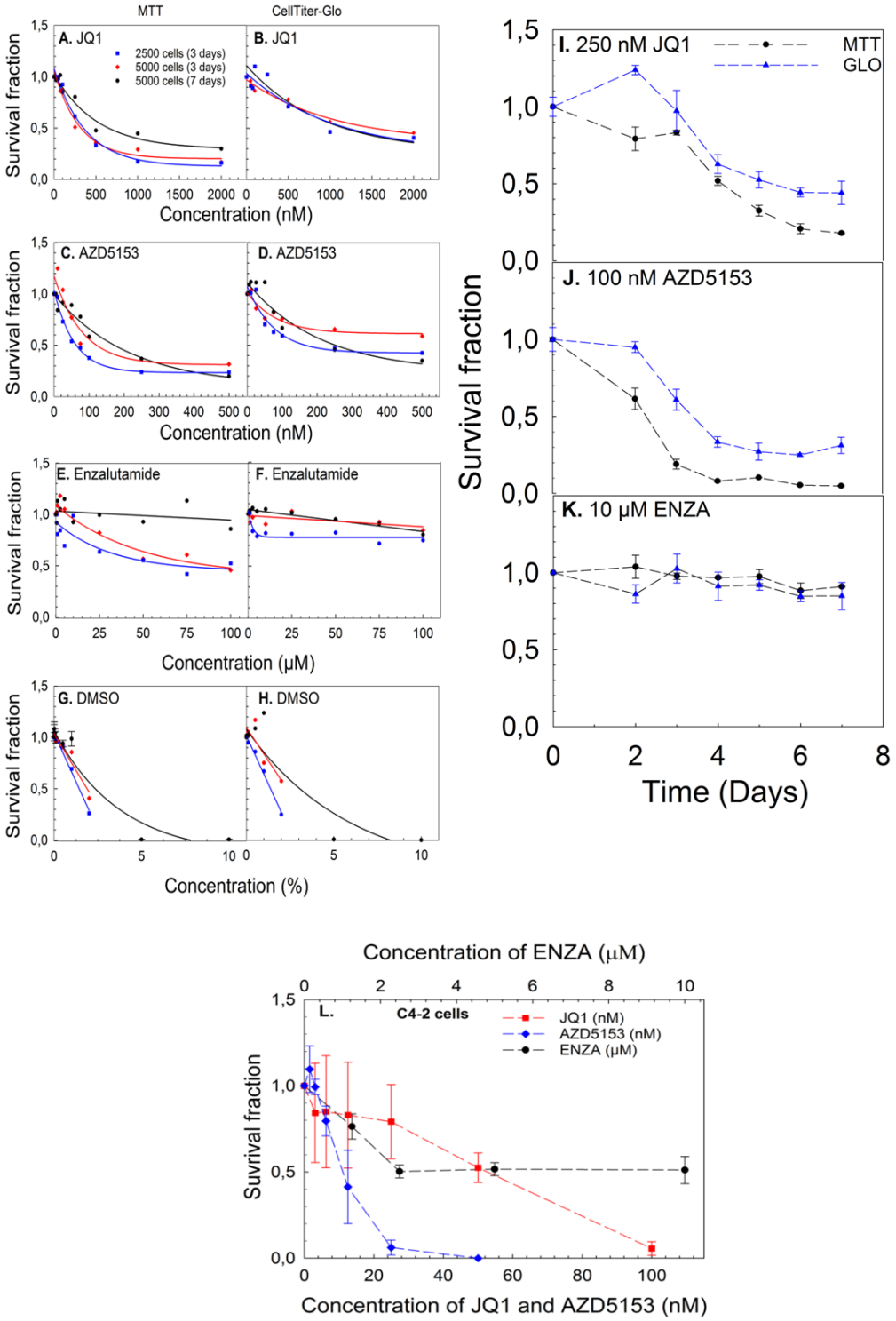

Figure 4.1. Cell survival curves as measured by MTT assay, Cell Titer Glo cell viability assay and clonogenic assay for C4-2 cells upon treatment with various concentrations of BET inhibitors, ENZA or DMSO. A number of 2500 or 5000 cells/well were plated in 96 well plates and were treated with different concentration of JQ1, AZD5153, ENZA or DMSO, incubated for 3 days (blue and red line) or 7 days (black line) **(A-H)**, cell viability was assessed by MTT and CellTiter-Glo Luminescence assay and analyzed by approximate regression. Data are from three independent experiments. **(I, J and K)** Cell survival as a function of time (Days). A number of 1000 cells/well were seeded in 96-well plates and incubated overnight, then the C4-2 cells were treated with 250 nM JQ1, 100 nM AZD5153 or 10 nM ENZA and incubated for 7 days, cell viability was assessed by MTT and CellTiter-Glo cell viability assay at day 7, error bars show ±SD of three technical replicates of one independent experiment. **(L)** Clonogenic cell survival curves normalized to control (0, 1 % DMSO) for JQ1, AZD5153 and ENZA on C4-2 cells**.** Thousand cells were plated into 25cm^2 flasks

(three parallels per treatment group) incubated for 24 h, followed by replacing of culture medium with drug-containing media to each representative flask of AZD5153, JQ1 or ENZA until formation of colonies. Data is presented as mean ±SD of three independent experiments.

Table 4.2. Summary of various lethal doses (LD) of the BET or AR inhibitors on C4-2 cell survival in clonogenic, MTT and CellTiter assays. NA; not achieved.

LD	Concentration of drugs								
	JQ1 (nM)			AZD5153 (nM)			ENZA (µM)		
	Clono-genic	MTT	CellTiter	Clono-genic	MTT	CellTiter	Clono-genic	MTT	CellTiter
10	4	78	195	4	10	23	0.3	2	2
25	24	156	477	6	25	53	1.4	14	74
50	54	352	1211	12	63	166	4	70	NA
75	81	766	NA	18	245	NA	NA	NA	NA
90	96	NA	NA	23	NA	NA	NA	NA	NA

4.2 Activity of BET and AR inhibitors on multicellular C4-2 spheroids

To determine the activity or inhibitory effects of various concentrations of DMSO, BET and AR inhibitors in multicellular C4-2 spheroids, microscopy images of these spheroids were taken before treatment (day 0) and after treatment at day 3, 7, 14 and 21 (Fig.4.3 A-D and Appendix B). Growth rate of the spheroids after treatment were evaluated by following the morphological changes and measurement of the cross-sectional area of each spheroid until day 21 (Fig.4.4) and until day 14 for DMSO treated spheroids. The concentrations of JQ1 and AZD5153 below 100 and 25 nM, respectively, were non-toxic. The average starting size for the spheroids in the control group was 0.109 mm^2 on day 0 (before treatment) and 0.656 mm^2 on day 21 (Fig.4.3). The doubling times increased from 9 days (control) to 11 days (250 nM JQ1), 45 days (2000 nM JQ1), 10 days (50 nM AZD5153), 15 days (500 AZD5153), 11 days (10 µM ENZA) and 10 days (100 µM ENZA) showing that the cell growth rate was slowing down (Fig.4.4 G). The doubling times of the C4-2 spheroids treated with increased concentration of JQ1 and AZD5153 increased, while the doubling time of the spheroids treated with ENZA was around 10-12 days at increasing concentrations (Fig.4.4 G).

To further explore the effect of the BET or AR inhibitors on C4-2 cell viability within the spheroids, C4-2 cell viability within the spheroids were monitored at day 14 for the control group, DMSO, and at day 24 for the BET or AR inhibitors treated spheroids, using the FDA-PI assay. Cell viability in DMSO treated spheroids demonstrated that DMSO effects viability in a dose-dependent manner, and a 5% was toxic, and no viable C4-2 cells were observed in the spheroids (Fig. 4.3 E). However, the spheroids are observed and present in the bright field microscopy images (Fig.4.3 A). This means that the cells are dead, and DNA is degraded, and PI cannot bind to DNA. The spheroids treated with lower concentrations of DMSO started to disintegrate when reached a diameter of around 1.5 mm, due to this the results only presented after 14 days. For further experiments 0.1 % DMSO was chosen. The majority of C4-2 cells within the spheroids treated with the BET inhibitors remained viable, despite increasing drug concentrations (Fig. 4.3 F and G).

Non-toxic concentrations of JQ1 (100 nM JQ1) and AZD5153 (25 nM) were chosen for further combination experiments (Fig 4.3 B and C). Higher doses of ENZA showed to result in a significant cell death within spheroids (Fig. 4.3 H). Nevertheless, complete cell death was not achieved with the various concentrations of ENZA that were tested. Based on the results (Fig. 4.3 D and H) a concentration of 10 µM ENZA, were selected for further combination experiments, since a higher concentration of the drug, do not inhibit spheroid growth significantly. The spheroid cross-sectional area growth declines in a dose dependent manner in C4-2 spheroids treated with various concentrations of BET or AR inhibitors (Fig. 4.4 A-F). While the cross-sectional area does not expand over time of the spheroids treated with ENZA (Fig. 4.4 F).

In addition, fold-change in average of the spheroid cross-sectional area from baseline (day 0) treated with various concentrations of the BET inhibitors or ENZA were calculated at day 3, 7, 14 and 21 to determine for how long to follow and evaluate the spheroid growth in further combination treatment experiments (Fig. 4.4 D-F). Based on these experiments, day 7 and 14 were selected to evaluate spheroid growth in further treatments combination experiments, since the growth of the spheroids followed a similar trend in growth after 3, 7, 14 and 21 days. The selected time points represent a trade-off to appreciate the treatment effect whilst preventing the spheroid to become too big and disintegrated, which would render challenging the measurement of spheroid cross-sectional area. The majority of spheroids started to disintegrate when they reached a diameter bigger than 1.5 mm.

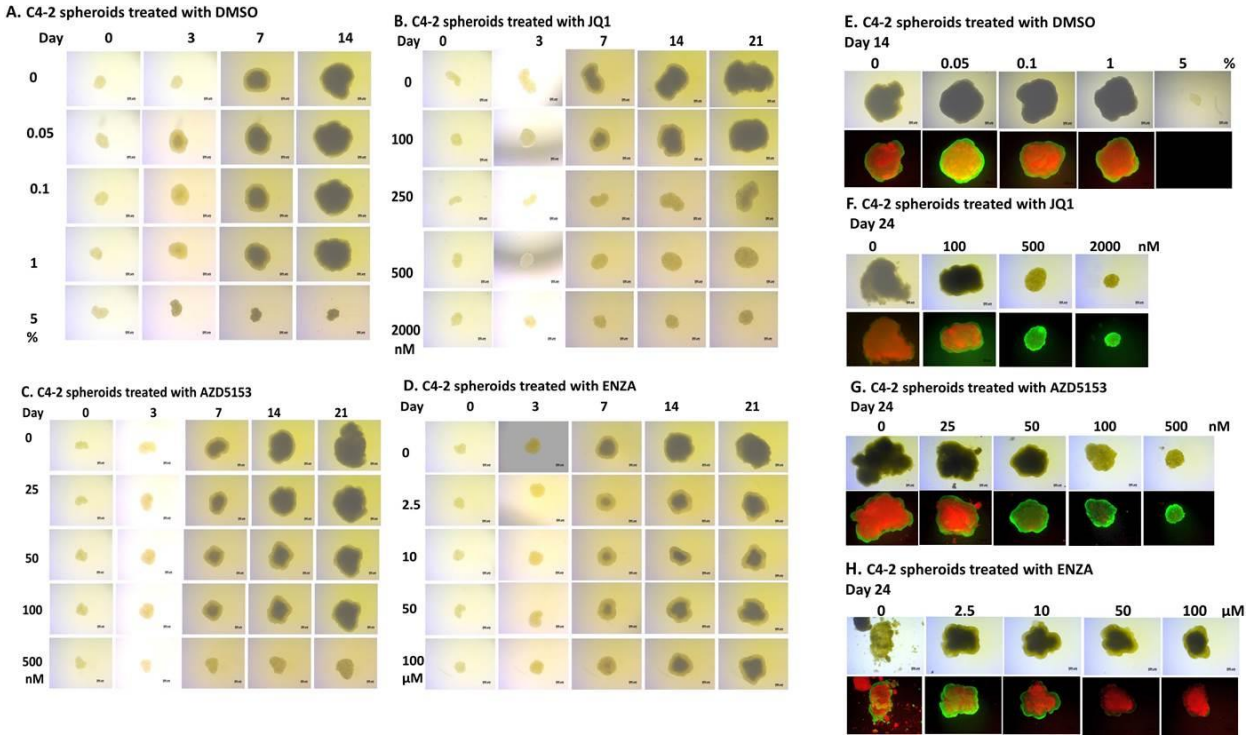

Figure 4.3. The growth and viability of C4-2 spheroids after the treatment with DMSO, BET or AR inhibitors. (A-D) Time-lapse representative bright-field microscopy images of C4-2 spheroids after treated with DMSO **(A)**, JQ1 **(B)**, AZD5153 **(C)** or ENZA **(D)** in increasing concentrations. Five hundred cells per well were seeded in 96 well plates and incubated for 5 days for spheroids to form. Further images (4x objective) of spheroids were taken at day 0 before the treatment, and spheroids were incubated with varying concentrations of DMSO, JQ1, AZD5153 or ENZA for 21 days. After 7 days the media were replaced with fresh media twice per week. Followed treatment spheroid images were taken of the same spheroid at day 3, 7,

14 and 21. The scale bar is 200 µm. N is one independent experiment. The representative FDA/PI fluorescent images of spheroids treated with DMSO **(E)**, JQ1 **(F)**, AZD5153 **(G)** or ENZA **(H)**. The images represent stained spheroids 14 or 24 days after initial treatment with the various drugs. Representative bright field and merged FDA and PI images are presented. Viable cells appear as green, while dead cells appear as red. Scale bars, 200 µm. N=1.The representative image was chosen from 6 images in the same group.

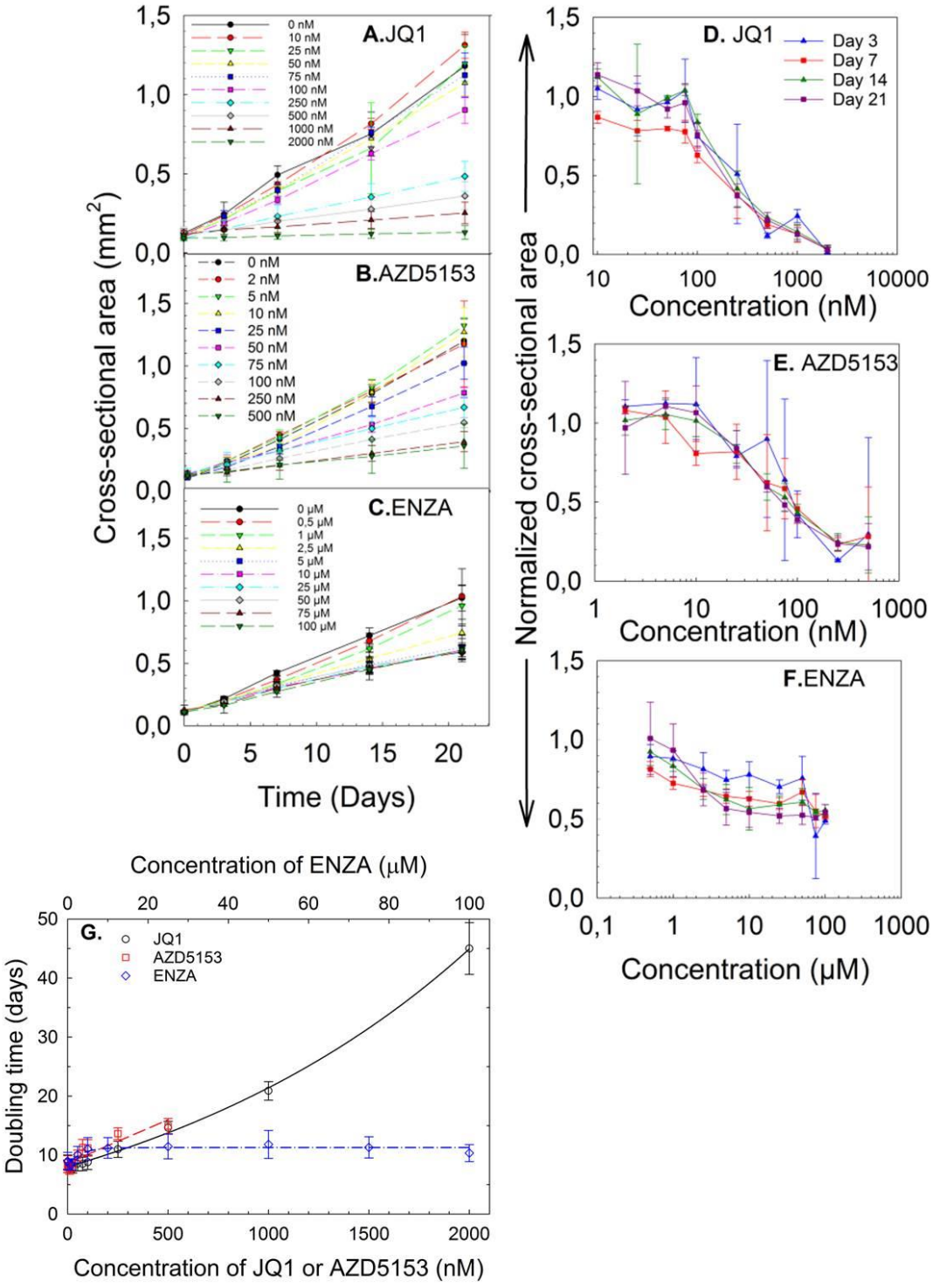

Figure 4.4. Growth curves of C4-2 spheroids after treatment with JQ1 (A, D), AZD5153 (B, E) or ENZA (C, F). (**A-C**) Measured cross-sectional area (mm^2) of spheroids as function of time (Days). **(D-F)** Measured cross-sectional area (mm^2) of spheroids normalized to the control (Day 0,) versus various concentrations of each drug. Error bars show ±SD for 6 technical replicates and correspond to one independent experiment. **(G)** Doubling time (days) of C4-2 spheroids treated with various concentration of JQ1, AZD5153 or ENZA. Error bars show ± SD for 6 technical replicates and correspond to one independent experiment.

Table 4.5. Summary of the drug concentrations selected for further combination experiments.

Drug name	Selected drug concentration		
	Clonogenic assay	Multicellular spheroids	Flowcytometry
DMSO	0.1%	0.1%	0.1%
JQ1	25 and 50 nM	100 nM	250 nM
AZD5153	6.25, 10 and 25 nM	25 nM	50 nM
ENZA	1.2 and 10 nM	10 µM	10 µM

4.2 BET or AR inhibitors and radiopharmaceuticals in combination

The effects of BET or AR inhibitors in combination with ^{223}Ra were studied in C4-2 cells in 2D and 3D models. In addition, the effects of AZD5153 and ^{177}Lu-PSMA-617 was investigated in C4-2 spheroids. The combined action of each BET or AR inhibitor with radiopharmaceuticals was assessed based on Bliss independence model and interaction indexes were calculated (described in Chapter 3.8 statistical analysis).

4.2.1 Response of C4-2 cells to BET or AR inhibitors in combination with ^{223}Ra

Combination treatment of C4-2 cells with JQ1, AZD5153 or ENZA with ^{223}Ra was performed in three independent experiments using different concentrations of the drugs. Theoretical SFs were calculated if drugs acted additively according to Bliss, and the obtained SFs were compared with the theoretical ones. If drugs in combination acted synergistically, the theoretical SFs were significantly higher than measured ones. The combination of 50 nM JQ1 and 1 or 2.5 kBq/ml ^{223}Ra were statistically synergistic only in one of the three experiments (CI<1 and p<0.05, Table 4.7).

A concentration of 10 or 25 nM AZD5153 and 1 kBq/ml ^{223}Ra were statistically synergistic in two of the experiments (CI<1, p<0, 05), while additive in one of the experiments. The combination of 25 nM AZD5153 and 2.5 kBq/ml ^{223}Ra was statistically synergistic in only one experiment (CI<1 and p< 0.05), and 6. 25 nM or10 nM AZD5153 and 2.5 kBq/ml were additive (CI=1) in the two other independent experiments (Table 4.7).

The combined effect of 10 µM ENZA, but not of 1.25 µM ENZA, and 1 kBq/ml or 2.5 kBq/ml ^{223}Ra, was statistically synergistic in all experiments, (Table 4.7). The interaction values are presented for only 1 kBq/ml and 2.5 kBq/ml of ^{223}Ra (Fig. 4.6 D-F), because the combination of BET or AR inhibitors with 5 or10 kBq/ml ^{223}Ra were not synergistic (Fig. 4.6)

Importantly, it was noticed that C4-2 cells treated in combination with JQ1, AZD5153 and ^{223}Ra were not strongly attached to the plastic bottom of the flasks compared to C4-2 cells treated with one drug, which might

explain the observed variations in SFs in the different experiments. Number of colonies counted in each of the three experiments is presented Appendix C).

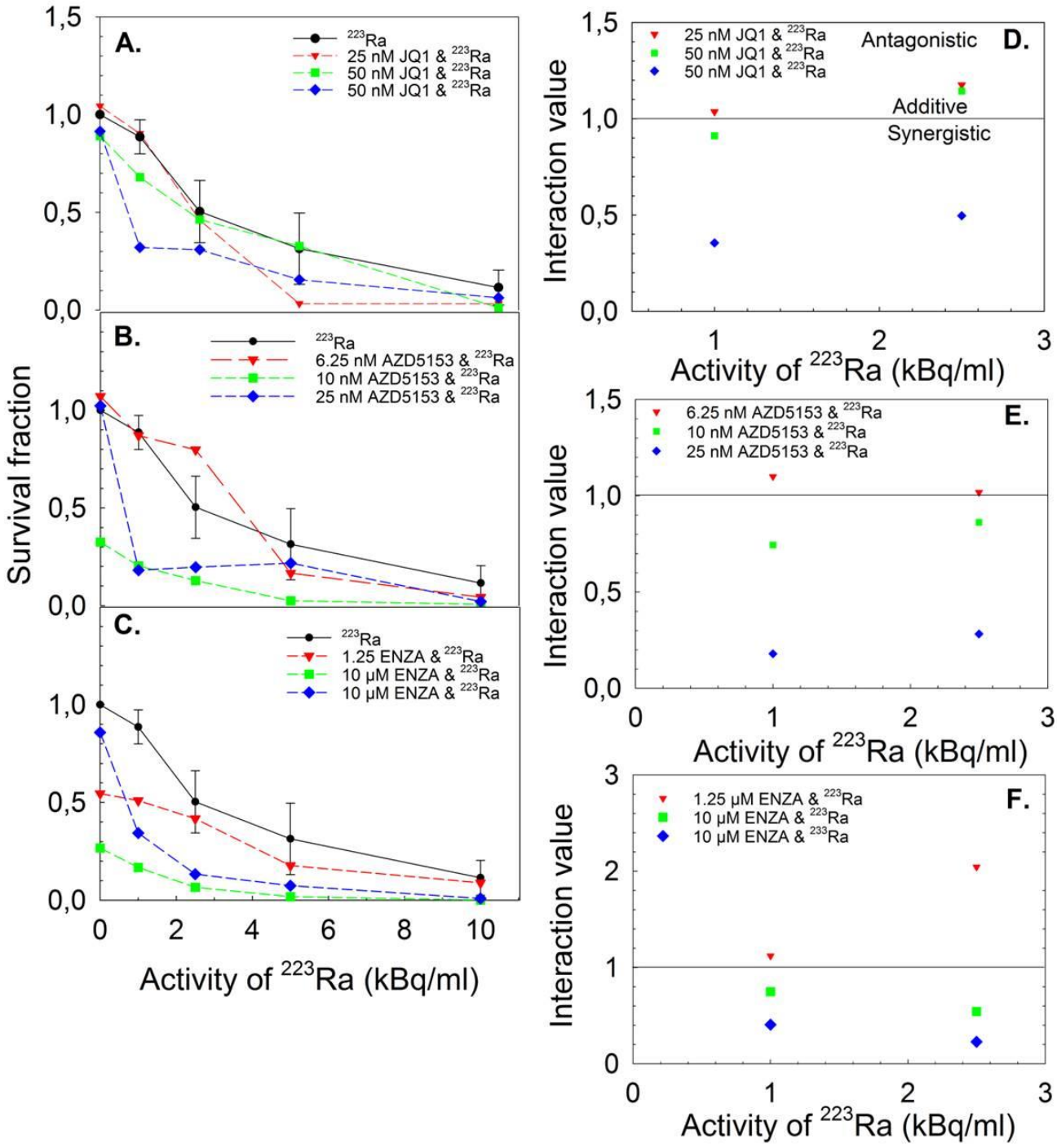

Figure 4.6. Survival fraction curves and interaction values of C4-2 cells treated with different concentrations of BET or AR inhibitors in combination with different activities (kBq/ml) ^{223}Ra. Thousand cells per 5 ml were subcultered in 25cm^2 flasks (2 technical replicates per group). After 24 h incubation, the media in each flask was replaced with 5 ml drug-containing media. The cells were treated with 25 or 50 nM JQ1, or 6.25, 10 or 25 nM AZD5153, or 1.25 or 10 µM ENZA, for 2 h, followed by 1 h co-treatment with different activity of ^{223}Ra. Further, the media were replaced with fresh drug-containing media and incubated for 10-14 days. **(A-C)** Survival fraction curves are normalized to the average plating efficiency of the control (0.1% DMSO), error bars for mono-treatment with ^{223}Ra show ± SD of mean of three independent

experiments (n=3). **(D-E)** Drug interaction values of JQ1 **(D)**, AZD5153 **(E)** or ENZA**(F)** in combination with 1 kBq/ml or 2.5 kBq/ml ^{223}Ra are presented. An interaction value CI <1 is considered synergistic.

Table4.7. Summary of C4-2 SFs treated with BET or AR inhibitors alone or with ^{223}Ra Interaction values were calculated. The results are from three independent experiments. Degree of interaction; significant at p-value <0.05.

Drug/ study day	^{223}Ra activity (kBq/ml)	Drug concen-trations	Survival fraction normalized to control			Interaction value	p-value	Statistically significant synergy
			^{223}Ra	Drug	Drug & ^{223}Ra			
JQ1/	1	25 nM	0.83	1.04	0.90	1.04	0.286	NO
		50 nM	0.90	0.90	0.30	0.36	0.020	**YES**
		50 nM	0.84	1,00	1.00	0.91	0.117	NO
Day 14	2.5	25 nM	0.40	1.04	0.50	1.20	0.203	NO
		50 nM	1.00	1.00	0.31	0.49	0.050	**YES**
		50 nM	0.50	1.00	0.50	1.14	0.163	NO
AZD-5153/	1	6.25 nM	1.00	1.00	0.8	1.10	0.330	NO
		10 nM	1.00	0.32	0. 20	0.74	0.043	**YES**
		25 nM	1.00	1.02	0.20	0.20	0.003	**YES**
Day 14	2.5	6.25 nM	0.40	1.00	0.33	1.01	<0.001	NO
		10 nM	0.50	0.32	0.13	0.90	0.132	NO
		25 nM	0.70	1.00	0.20	0.30	0.028	**YES**
ENZA/	1	1.25 nM	1.00	1.00	0,50	1.11	0.301	NO
		10 µM	1.00	1.00	0.34	0.41	0.002	**YES**
		10 µM	1.00	0.30	0.20	0.75	0.003	**YES**
Day 14	2.5	1.25 nM	0.40	1.00	0.42	2.04	0.002	NO
		10 µM	1.00	1.00	0.13	0.23	0.003	**YES**
		10 µM	0.50	0.30	0.10	0.54	0.061	**YES**

4.2.2 Response of C4-2 spheroids to BET or AR inhibitors in combination with ^{223}Ra

Next, three independent experiments to examine the effect of BET or AR inhibitors in combination with ^{223}Ra on C4-2 spheroids were performed. Technical problems did not allow to analyze all days in all three independent experiments. Spheroid growth upon combination treatment was evaluated at day 7 and 14 in one independent experiment, at day 7 in the second experiment, and at day 12 in the third experiment (Appendix D). A summary of the obtained results and interaction values from all three experiments are presented below (Table 4.10).

4.2.2.1 Synergistic effect of JQ1 and ^{223}Ra in C4-2 spheroids

The combination treatment of C4-spheroids with 100 nM JQ1 and 1 or 2.5 kBq/ml ^{223}Ra, resulted in inhibition of spheroid growth and significantly smaller cross-sectional area of the spheroids compared to

mono treatment (JQ1 or ^{223}Ra alone) on day 7 and 14 after treatment (Fig. 4.8). The activity of 5 and 10 kBq/ml ^{223}Ra alone has prevented the growth of spheroids (Fig.4.8). Therefore, the combined effects of these activities with the BET or AR inhibitors were not studied. The combination of 100 nM JQ1 and 1 or 2.5 kBq/ml ^{223}Ra were statistically synergistic (CI<1, p< 0.05) compared to the expected theoretically calculated additive group at day 7 and 14 (Fig. 4.9 B-C, E-F, and Table 4.10), except for the results in one experiment (study day 12) in which additive effect (CI=1) upon treatment of 100 nM JQ1 and 1 kBq/ml with ^{223}Ra were observed (Table 4.10 and Appendix D1).

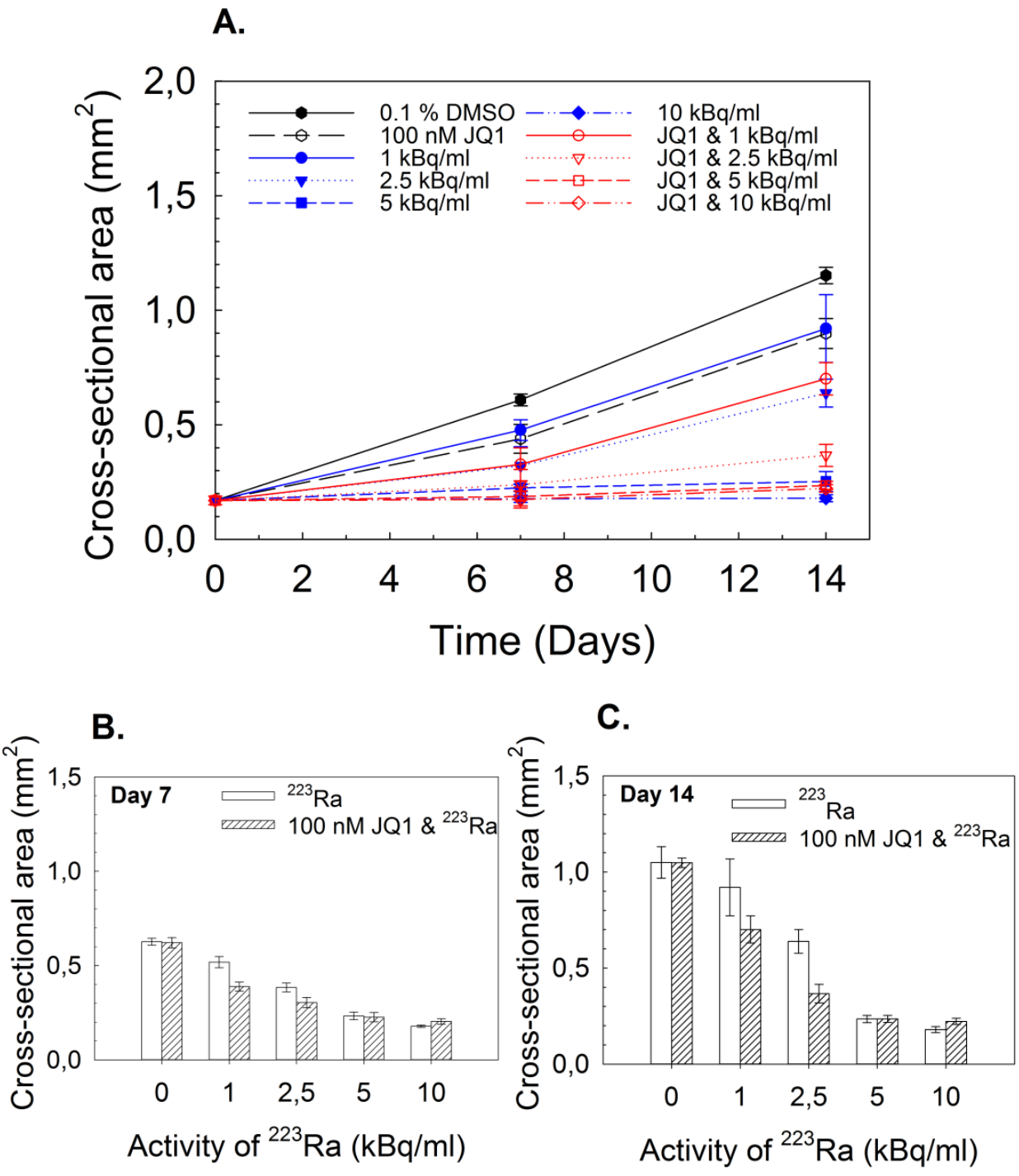

Figure 4.8. Spheroid growth upon combination treatment with JQ1 and ^{223}Ra. (A) Cross sectional area (mm^2) of C4-spheroids, day 7 and 14 after combination treatment with 100 nM JQ1 and various activity of ^{223}Ra. C4-2 cells (500 cells/well) were seeded in 96 well plates and incubated for 5 days to form spheroids. Before treatment microscopy images (4x objective) of spheroids were taken, and treated with the final concentration 100 nM JQ1 and incubated for 2-3 h. Further co-treated with 2.5, 5 or 10 kBq/ml of ^{223}Ra for 1 h. Afterwards the spheroids were washed 6 times and the media were replaced with fresh drug-containing media and incubated for 14 days. Seven days after treatment the media were replaced with fresh media twice a week. Six to eleven individual spheroids per treatment condition. Error bars show ± SD of the mean of two independent experiments (day 7). Day 14 are from one independent experiment and error bars present ±SD within the six to eleven spheroids per treatment condition. (**B and C)** Bar graphs of cross-sectional area (mm^2) measured at day 7 and day 14 after treatment as function of activity of ^{223}Ra (kBq/ml).

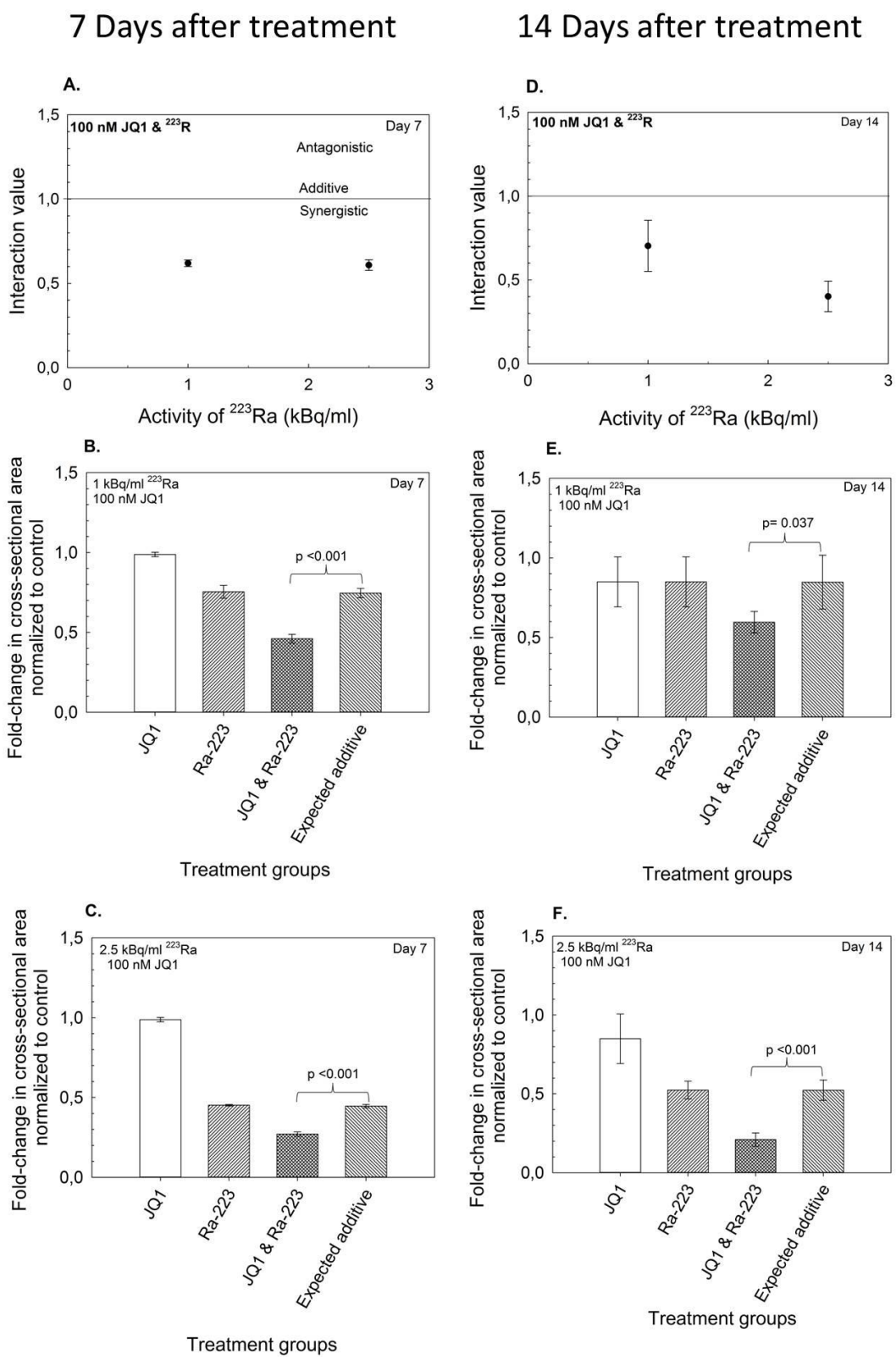

Figure 4.9. Drug interaction for testing synergy of 100 nM JQ1 and 1 or 2.5 kBq/ml ^{223}Ra in C4-2 spheroids). (A and D) Interaction values graphs (day 7 and 14 after treatment). **(B, C, E and F)** Bar graphs, fold change in C4-2 spheroids cross-sectional area after treatment relative to spheroid cross-sectional area at day 0 (before treatment) normalized to the control (0, 1% DMSO). Statistical differences were determined by statistical Welch's t-test and $p<0.05$ were considered statistically significant. Error bars show ±SD of the mean of two independent experiments (**A-C**). **(D-F)** n= one independent experiment at day 14, error bars present ±SD within the six to eleven per treatment condition.

Table 4.10 Summary of interaction values for treatment of C4-2 spheroids with 100 nM JQ1 alone or in combination with ^{223}Ra. Mean of two independent experiments (study day 7), one independent experiment (study day 12), and one independent experiment (study day 14). Degree of interaction; significant at p-value <0.05.

Study day	^{223}Ra activity (kBq/ml)	JQ1 concen-trations	Fold change from day 0 (pre-treatment)			Interaction value	p-value	Statistically significant synergy
			^{223}Ra	Drug	Drug & ^{223}Ra			
	1	100 nM	1.00	1.00	0.40	0.56	<0.001	**YES**
Day 7	2.5	100 nM	0.42	1.00	0.20	0.47	<0.001	**YES**
	1	100 nM	1.00	1.00	1.00	1.02	0.368	NO
Day 12	2.5	100 nM	1.00	1.00	0.31	0.71	0.01	**YES**
	1	100 nM	1.00	1.00	1.00	0.70	0.037	**YES**
Day 14	2.5	100 nM	1.00	1.00	0.21	0.40	<0.001	**YES**

4.2.2.2 Synergistic effect of AZD5153 and ^{223}Ra in C4-2 spheroids

The combination treatment of 25 nM AZD5153 and 1 or 2.5 kBq/ml ^{223}Ra reduced the growth rate and the cross-sectional area of C4-2 spheroids in comparison with AZD5153 or ^{223}Ra alone measured at on day 7 and 14 after treatment (Fig. 4.11 A-C). The combination of 25 nM AZD5153 and 1 or 2.5 kBq/ml ^{223}Ra were statistically synergistic (CI<1, p< 0.05) compared to mono-treatment (AZD5153 and ^{223}Ra alone) on day 7 or 14 after treatment (Fig. 4.12 B-C, E-F and Table 4.13), except for the results in one experiment (study day 12) in which additive effect (CI=1) upon treatment with 25 nM AZD5153 and 1 kBq/ml of ^{223}Ra were observed (Appendix D2 and Table 4.13). An enhanced synergistic response in C4-2 spheroids treated with 25 nM AZD5153 in combination with ^{223}Ra was observed at study day 7 and 14 experiments (Fig. 4.12 and Table 4.13).

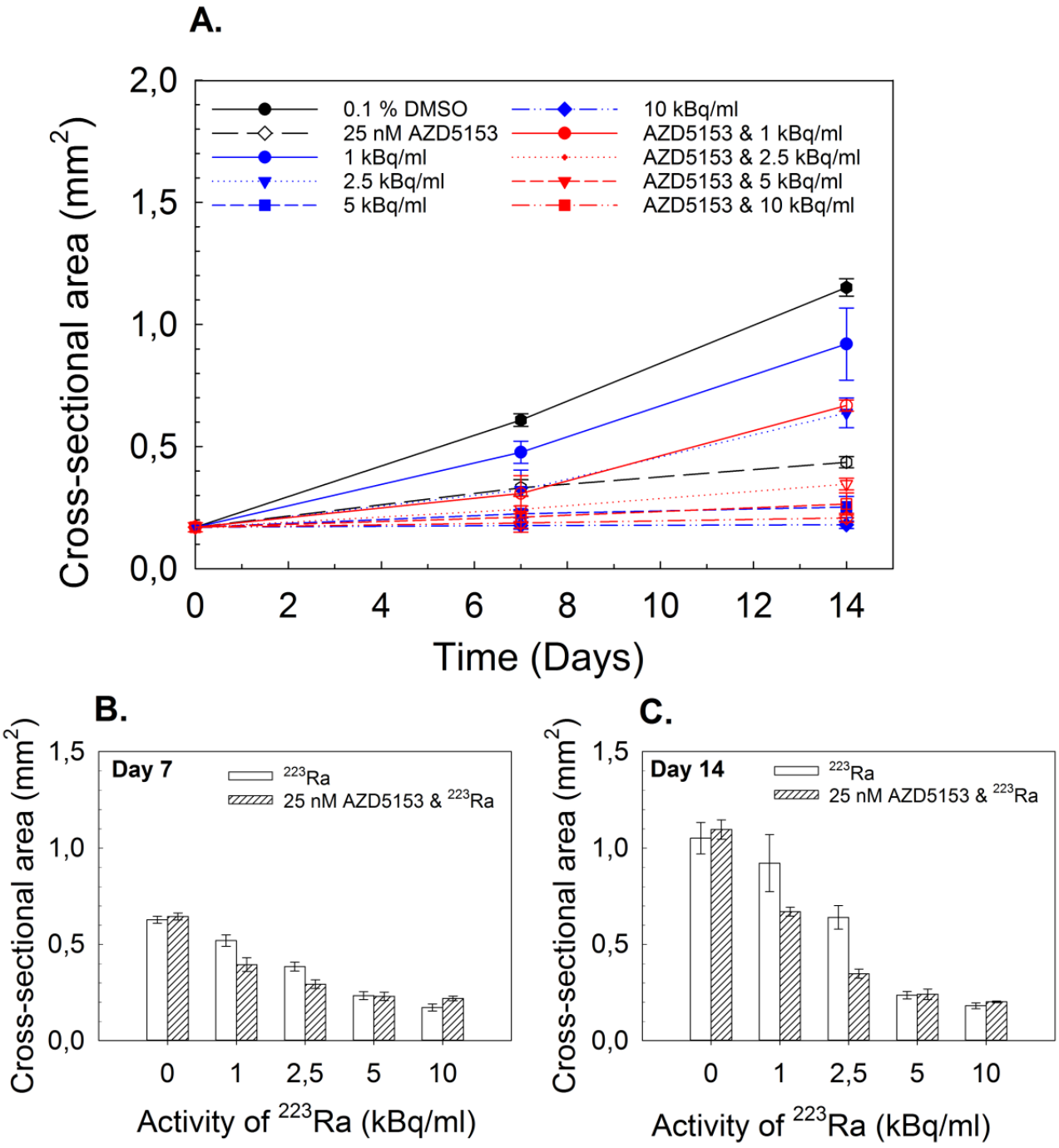

Figure 4.11: Spheroid growth upon combination treatment with AZD5153 and ^{223}Ra. (A) Cross sectional area (mm^2) of C4-spheroids, day 7 and 14 after combination treatment with 25 nM AZD5153 and various activity of ^{223}Ra. C4-2 cells (500 cells/well) were seeded in 96 well plates and incubated for 5 days to form spheroids. Before treatment microscopy images (4x objective) of spheroids were taken, and treated with the final concentration 25 nM AZD5153 and incubated for 2-3 h. Further co-treated with of 2.5, 5 or 10 kBq/ml of ^{223}Ra for 1 h. Afterwards the spheroids were washed 6 times and the media were replaced with fresh drug-containing media and incubated for 14 days. Seven days after treatment the media were replaced with fresh media twice a week. Six to eleven individual spheroids per treatment condition. Error bars show ± SD of the mean of two independent experiments (day 7). Day 14 are from one independent experiment and error bars present ±SD within the six to eleven spheroids per treatment condition. (**B and C)** Bar graphs of cross-sectional area (mm^2) measured at day 7 and day 14 after treatment as function of activity of ^{223}Ra (kBq/ml).

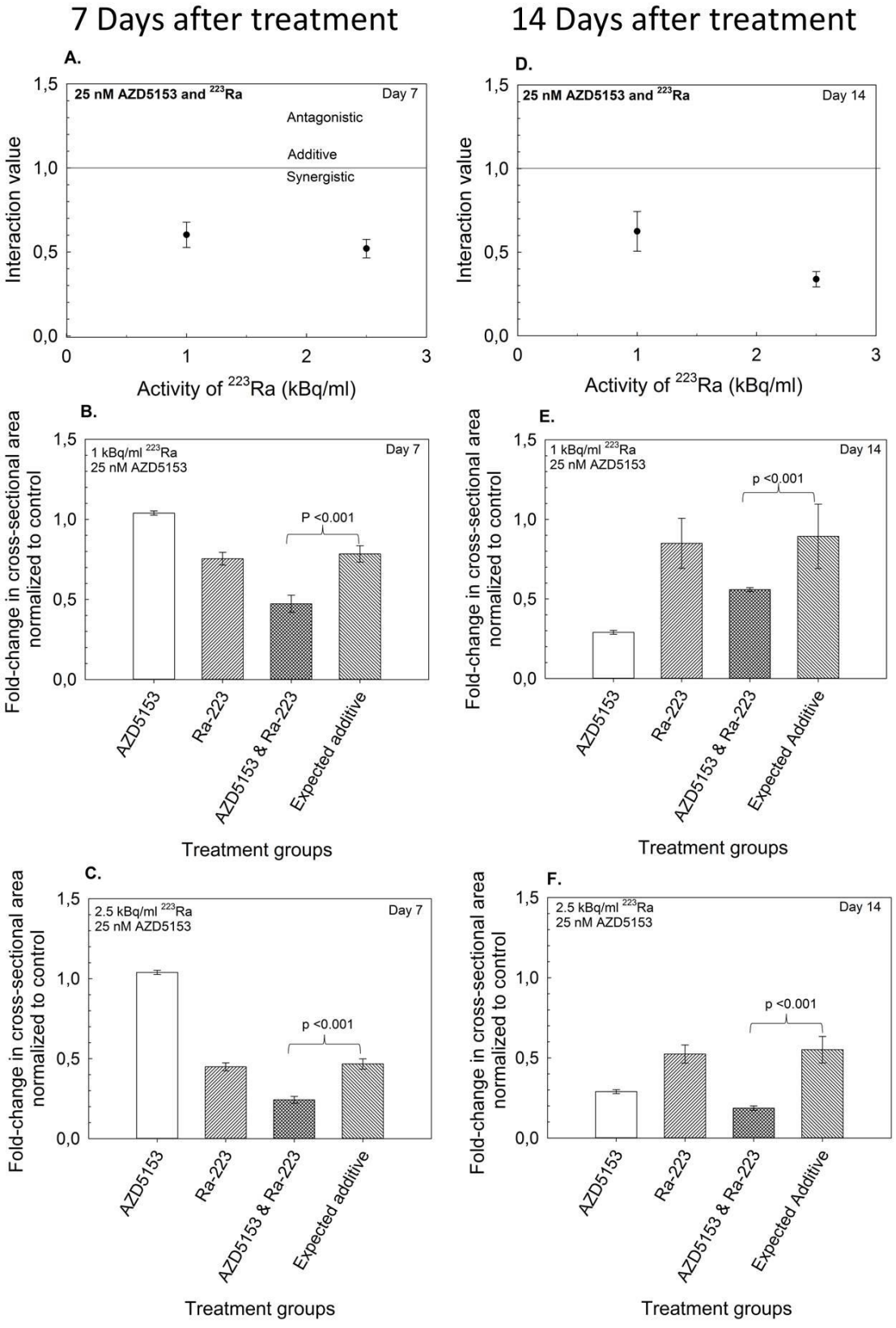

Figure 4.12. Drug interaction for testing synergy of 25 nM AZD5153 and 1 or 2.5 kBq/ml ^{223}Ra in C4-2 spheroids). (A and D) Interaction values graphs (day 7 and 14 after treatment). **(B, C, E, and F)** Bar graphs, fold change in C4-2 spheroids cross-sectional area after treatment relative to spheroid cross-sectional area at day 0 (before treatment) normalized to the control (0, 1% DMSO). Statistical differences were determined by statistical Welch's t-test and $p<0,05$ were considered statistically significant. Error bars show ±SD of the mean of two independent experiments (**A-C**). **(D-F)** n= one independent experiment at day 14, error bars present ±SD within the six to eleven spheroids per treatment condition.

Table 4.13. Summary of interaction values for treatment of C4-2 spheroids with 25 nM AZD5153 alone or in combination with ^{223}Ra. Mean of two independent experiment (study day 7), one independent experiment (study day 12), and one independent experiment (study day 14). Degree of interaction; significant at p-value <0.05.

Study day	^{223}Ra activity (kBq/ml)	AZD5153 concen-trations	Fold change from day 0 (pre-treatment)			Interaction value	p-value	Statistically significant synergy
			^{223}Ra	Drug	Drug & ^{223}Ra			
	1	25 nM	1.00	1.00	0.32	0.45	<0.001	**YES**
Day 7	2.5	25 nM	0.40	1.00	0.20	0.43	<0.001	**YES**
	1	25 nM	1.00	1.00	0.30	1.00	0.140	NO
Day 12	2.5	25 nM	1.00	1.00	0.13	0.42	<0.001	**YES**
	1	25 nM	1.00	1.10	1.00	0.62	<0.001	**YES**
Day 14	2.5	25 nM	1.00	1.10	0.20	0.34	<0.001	**YES**

4.2.2.3 Synergistic effect of ENZA and ^{223}Ra in C4-2 spheroids

Similarly, to the BET inhibitors, 10 µM ENZA in combination with 1 or 2.5 kBq/ml ^{223}Ra, reduced the growth and the cross-sectional area of the spheroids compared to mono-treatment (ENZA or ^{223}Ra alone) (Fig. 4.14). The combination of 10 µM ENZA and 1 or 2.5 kBq/ml ^{223}R ^{223}Ra were statistically synergistic (CI<1, p< 0.05) compared to the expected theoretically calculated additive group at all studied days (day 7, 12 and 14) (Fig. 4.15, Appendix D3 and Table 4.16).

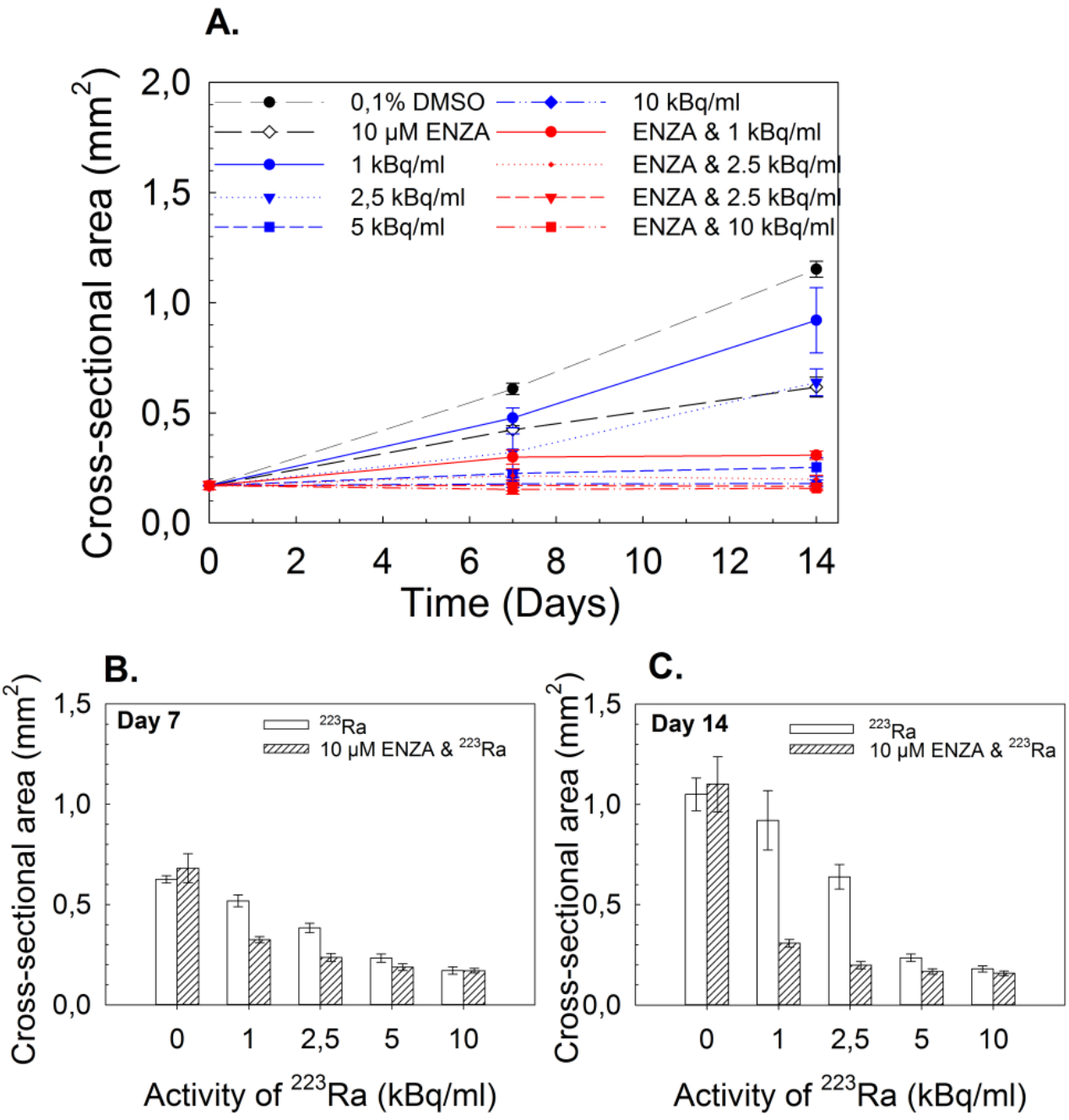

Figure 4.14. Spheroid growth upon combination treatment with ENZA and ^{223}Ra. (A) Cross sectional area (mm^2) of C4-spheroids, day 7 and 14 after combination treatment with 10 µM ENZA and various activity of ^{223}Ra. C4-2 cells (500 cells/well) were seeded in 96 well plates and incubated for 5 days to form spheroids. Before treatment microscopy images (4x objective) of spheroids were taken, and treated with the final concentration 10 µM ENZA and incubated for 2-3 h. Further, co-treated with 2.5, 5 or 10 kBq/ml of ^{223}Ra for 1 h. Afterwards the spheroids were washed 6 times and the media were replaced with fresh drug-containing media and incubated for 14 days. Seven days after treatment the media were replaced with fresh media twice a week. Six to eleven individual spheroids per treatment condition. Error bars show ± SD of the mean of two independent experiments (day 7). Day 14 are from one independent experiment and error bars present ±SD within the six to eleven spheroids per treatment condition. (**B and C)** Bar graphs of cross-sectional area (mm^2) measured at day 7 and day 14 after treatment as function of activity of ^{223}Ra (kBq/ml).

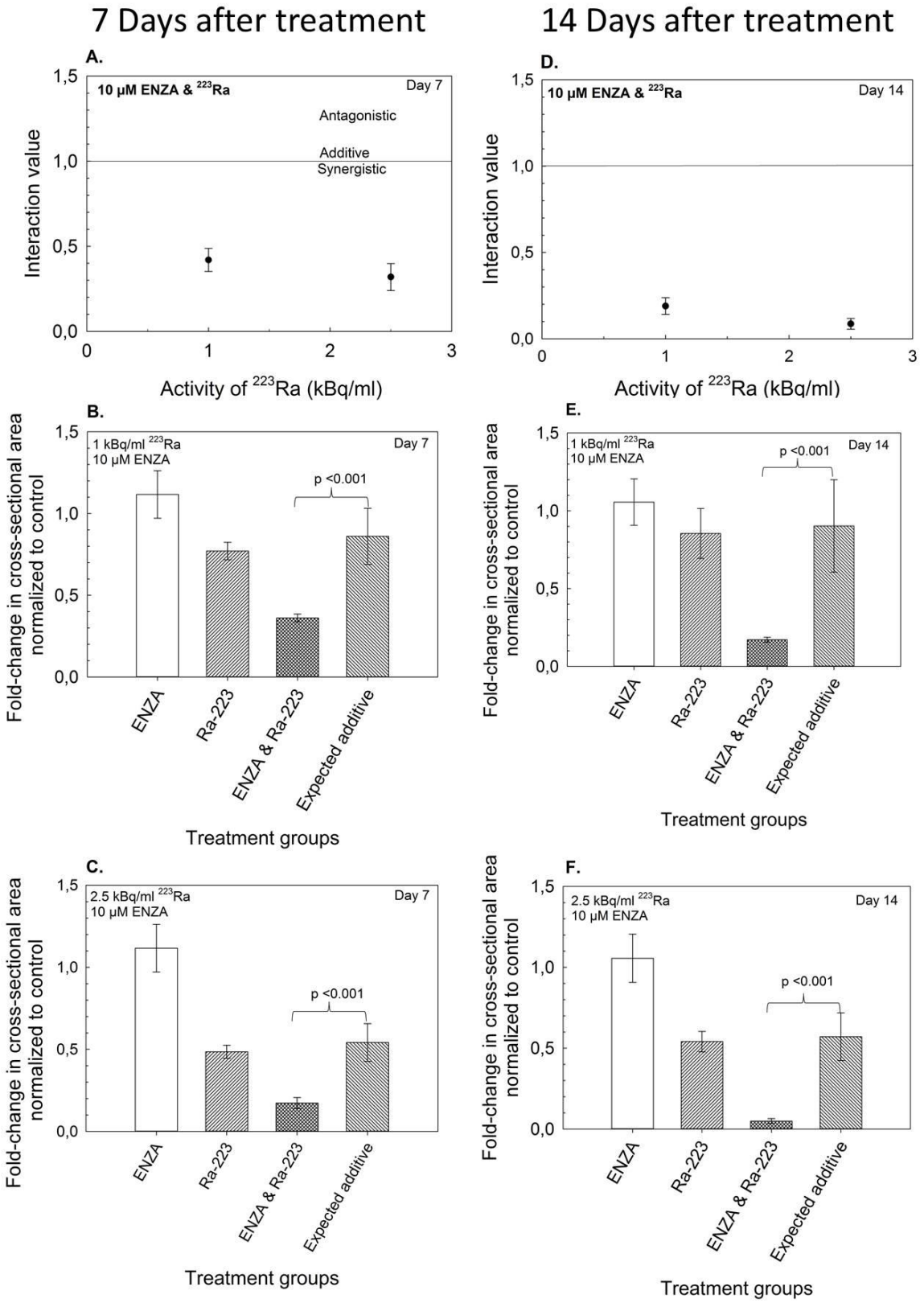

Figure 4.15. Drug interaction for testing synergy of 10 µM ENZA and 1 or 2.5 kBq/ml ^{223}Ra in C4-2 spheroids). (A and D) Interaction values graphs (day 7 and 14 after treatment). **(B, C, E, and F)** Bar graphs, fold change in C4-2 spheroids cross-sectional area after treatment relative to spheroid cross-sectional area at day 0 (before treatment) normalized to the control (0, 1% DMSO). Statistical differences were determined by statistical Welch's t-test and p<0. 05 were considered statistically significant. Error bars show ±SD of the mean of two independent experiments (**A-C**). **(D-F)** n= 1 independent experiment at day 14, error bars present ±SD within the six to eleven spheroids per treatment condition.

Table 4.16. Summary of interaction values for treatment of C4-2 spheroids with 10 µM ENZA alone or in combination with ^{223}Ra. Mean of two independent experiment (study day 7), one independent experiment (study day 12), and one independent experiment (study day 14). Degree of interaction; significant at p-value <0.05.

Study day	^{223}Ra activity (kBq/ml)	ENZA concen-trations	Fold change from day 0 (pre-treatment)			Interaction value	p-value	Statistically significant synergy
			^{223}Ra	Drug	Drug & ^{223}Ra			
	1	10 µM	1.00	1.12	0.40	0.42	<0.001	**YES**
Day 7	2.5	10 µM	0.50	1.12	0.40	0.32	<0.001	**YES**
	1	10 µM	1.00	0.50	0.30	0.22	<0.001	**YES**
Day 12	2.5	10 µM	1.00	0.50	0.13	0.13	<0.001	**YES**
	1	10 µM	1.00	1.10	0.20	0.20	<0.001	**YES**
Day 14	2.5	10 µM	1.00	1.10	0.05	0.10	<0.001	**YES**

4.3 Response of C4-2 spheroids to AZD5153 with ^{177}Lu-PSMA-617 treatment

AZD5153 was combined with ^{177}Lu-PSMA-617 in C4-2 spheroids (Fig. 4.17). The activities of 2.5 and 5 MBq/ml ^{177}Lu-PSMA- were toxic and resulted in inhibition of growth rate of spheroids and thus cross-sectional area were smaller (Fig 4.17 A). Therefore, no interaction value graphs for the combined effect of AZD5153 and ^{177}Lu-PSMA-617 at these activities were not presented.

4.3.1 Synergistic effect of AZD5153 and 177Lu-PSMA-617 in C4-2 spheroids

Combination of 25 nM AZD5153 and 0. 5 or 1 MBq/ml ^{177}Lu-PSMA-617 on C4-2-spheroids showed notably reduced cross-sectional area compared to mono-treatment (AZD5153 or ^{177}Lu-PSMA-617 alone) (Fig. 4.17 A). The combination effect of 25 nM AZD5153 and 0. 5 or 1 MBq/ml ^{177}Lu-PSMA-617 22 days after treatment were statistically synergistic (CI<1 and p< 0.05) compared to the expected theoretically calculated additive group (Fig. 4.17 B-D).

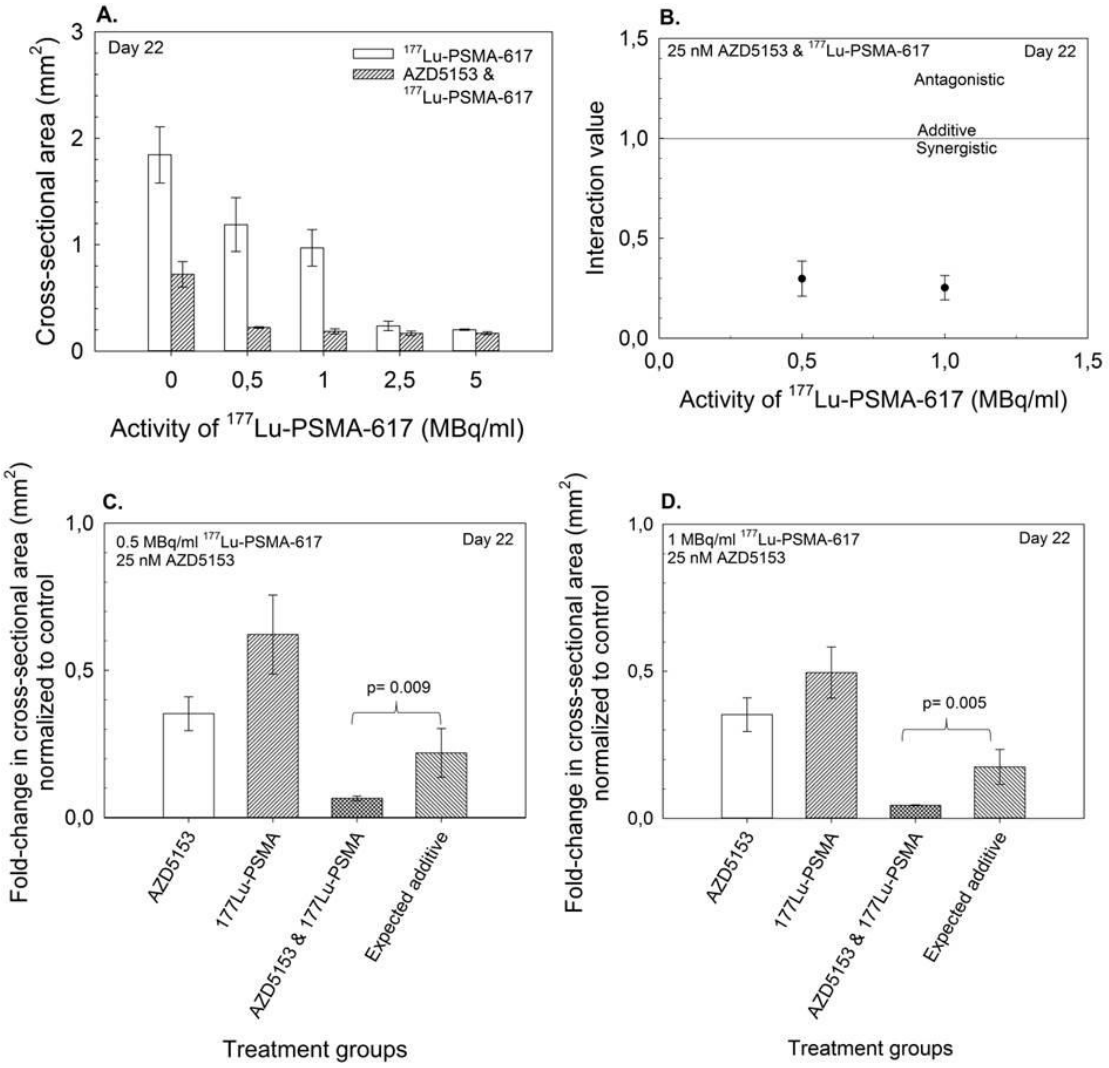

Figure 4.17. Spheroid growth upon combination treatment with AZD5153 and ^{177}Lu-PSMA-617 A) Measured cross-sectional area (mm^2) upon treatment with 25 nM AZD5153 and 0.5,1,2.5 or 5 MBq/ml of ^{177}Lu-PSMA-617at day 22 after treatment. Five hundred cells/well were seeded in 96 well plates and incubated for 5 days to form spheroids. Before treatment (day 0), microscopy images (4x objective) of spheroids were taken, and treated with final concentration 25 nM AZD5153 and incubated for 2-3 h, followed by co-treatment with 0.5,1,2.5 or 5 MBq/ml of ^{177}Lu-PSMA-617. Afterwards the spheroids were washed 6 times and the media were replaced with fresh drug-containing media and incubated for 22 days. The media from each well were replaced with fresh drug-containing media and incubated further. Seven days after treatment the media were replaced with fresh media twice a week. Error bars present ±SD within the two to three spheroids per treatment condition. **(B)** Drug interaction for testing synergy of 25 nM AZD5153 and 0.5 or 1 MBq/ml ^{177}Lu-PSMA-617. **(C and D)** Bar graphs, fold change in C4-2 spheroids cross-sectional area after treatment relative to spheroid cross-sectional area at day 0 (before treatment) normalized to the control (0. 1% DMSO). Statistical differences were determined by statistical Welch's t-test and p<0. 05 were considered statistically significant.

Table 4.18. Summary of interaction values for treatment of C4-2 spheroids with 25 nM AZD5153 alone or in combination with ^{177}Lu-PSMA-617. n=1 independent experiment (study day 22). Degree of interaction; significant at p-value <0.05.

Study day	^{177}Lu-PSMA activity (kBq/ml)	AZD5153 concen-trations	Fold change from day 0 (pre-treatment)			Interaction value	p-value	Statistically significant synergy
			^{177}Lu-PSMA	Drug	Drug & ^{177}Lu-PSMA			
	0.5	25 nM	0.60	0.40	0.10	0.30	0.009	**YES**
Day 22	1	25 nM	0.50	0 .40	0.04	0.25	0.005	**YES**

4.4 Survival of C4-2 cells treated with BET or AR inhibitors in combination with ^{223}Ra

To determine the ^{223}Ra activity to use further in flow cytometry experiments C4-2 cells were treated with 250 nM JQ1, 50 nM AZD5153 or 10 µM ENZA in combination with varying activities of ^{223}Ra and cell survival was assayed using MTT assay (Fig. 4.19). The treatment of C4-2 cells with increasing activities of ^{223}Ra alone or in combination with the various drugs led to decreased cell survival fraction (Fig. 4.19). Any significant effect was observed in this experiment. The following activities 2.5, 5 and 10 kBq/ml ^{223}Ra were selected for flow cytometry analysis, since 25 kBq/ml ^{223}Ra reduced cell survival by 75%, thus this activity was not selected (Fig.4.19)

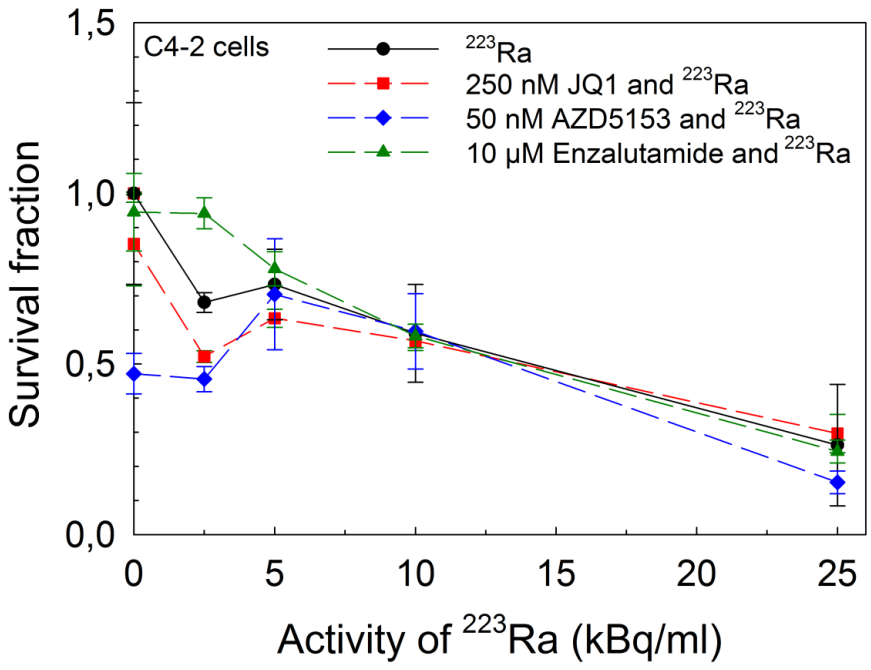

Figure 4.19. Cell survival curves measured by MTT assay for C4-2 cells treated with increasing activity of ^{223}Ra alone (black) or in combination with 250 nM JQ1 (red), 50 nM AZD5153 (blue) or 10 µM ENZA (green). Thousand cells per well were seeded in 96-well plates, after 24 h incubation, the medium in each well was replaced with drug-containing media, cells were treated with 250 nM JQ1, 50 nM AZD5153 or 10 µM ENZA for 2 h, followed by 1 h treatment with 0, 2.5, 5, 10 or 25 kBq/ml ^{223}Ra. Afterwards the media were replaced with fresh drug-containing media. Survival fraction is normalized to the control (0.1 % DMSO). Error bars show ±SD for three parallels used per treatment group, and n= one independent experiment.

4.5 Flow cytometry analysis of C4-2 cells growing in monolayer treated with BET or AR inhibitors and 223-Ra

Flow cytometry analysis was performed to detect apoptotic and necrotic cells, DNA damage and the cell cycle analysis distribution in C4-2 cells treated with BET or AR inhibitors alone or in combination with ^{223}Ra.The C4-2 cells were treated with 250 nM JQ1, 50 nM AZD5153 or 10 µM ENZA alone or with 2.5, 5 or 10 kBq/ml ^{223}Ra for 1 h, and then ^{223}Ra were removed and further incubated again with 250 nM JQ1, 50 nM AZD5153 or 10 µM ENZA for 72 h prior to flow cytometry analysis. This time point of 72 h was based on the results from MTT and CellTiter-Glo cell viability assays (Fig.4.1 I-K). Necrotic PI-stained and Annexin V-FITC stained cells were gated (Fig. 4.20 A). The treated groups did not differ from the control. Over 87 % of the cells were still viable in all groups.

.

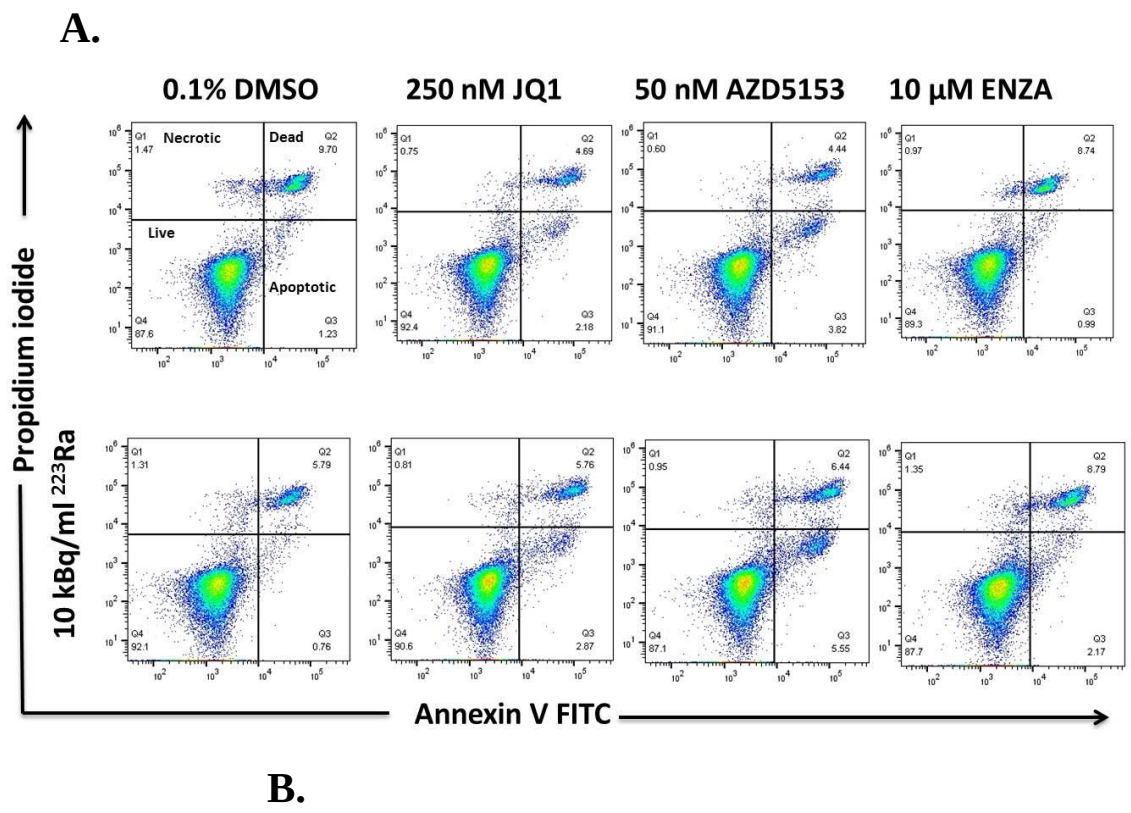

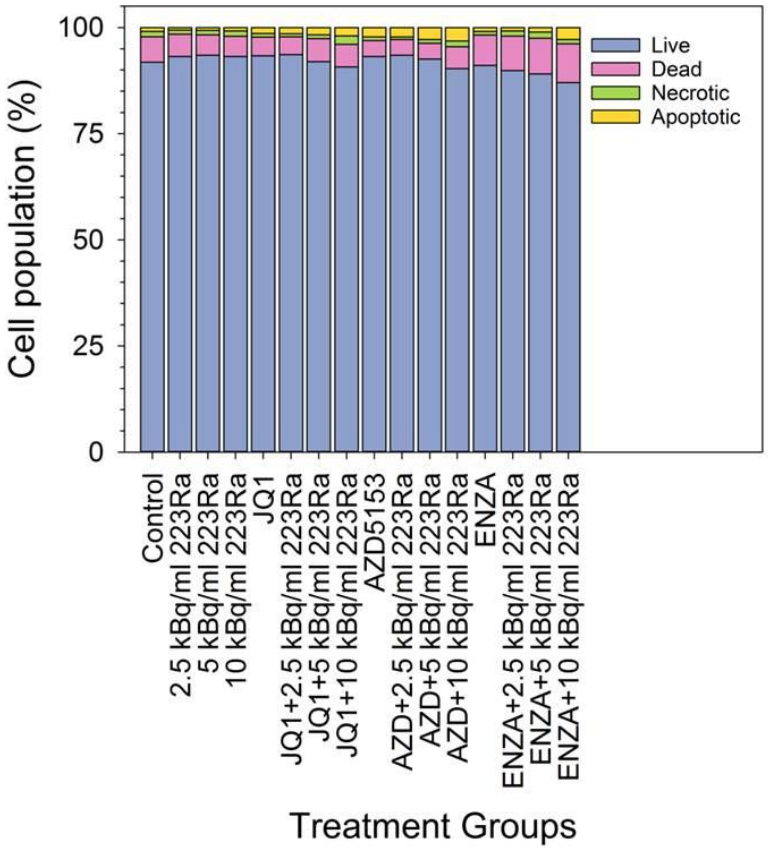

Figure 4.20. Flow cytometry analysis of apoptosis in C4-2 cells upon combination treatment between JQ1, AZD5153 or ENZA with different activities of ^{223}Ra. Cells were plated at a density of 0.5 $\times 10^6$ or 1 $\times 10^6$ in 25cm^2 flasks (1 flask per group), after 24 h incubation, the medium in each flask was replaced with drug-containing media, and cells were incubated for 2 h with 250 nM JQ1, 50 nM AZD5153 or 10 µM ENZA, followed by 1 h co-treatment with 2.5, 5 or 10 kBq/ml ^{223}Ra. Afterwards the media were replaced with fresh drug-containing media and incubated for 72 h. **(A)** the percentage of apoptotic and necrotic cells as analyzed by flow cytometry after treatment. The necrotic cells are shown in quadrant Q1, late apoptosis/dead cells are shown in upper right quadrant Q2, apoptotic cells is shown in lower right quadrant Q3 and viable cells is shown in lower left quadrant Q4. **(B)** The data are presented as the means of two independent experiments. A statistical ANOVA test run ($p>0.05$), except for combination of ENZA and 10 kBq/ml ^{223}Ra compared to the control group ($p<0.05$).

The cell cycle distribution (Fig. 4.21) under the same conditions was analyzed. The combination treatments altered the cell cycle status of the cells, in which the reduction of the population of cells in synthesis (S) was observed. However, statistical analysis ANOVA run, showed no statistically significant difference ($p>0.05$) between the cell cycle phases of the groups that were treated with a combination of 250 nM JQ1, 50 nM AZD5153 or 10 µM ENZA and 10 kBq/ml ^{223}Ra and the control groups. The percentage of cells in the M phase was reduced significantly in the combination of BET inhibitors and ^{223}Ra treated cell groups, but not for ENZA, compared to the control groups (drugs or ^{223}Ra alone) (Fig.4.21 B and C). The reduction of cells in the cell cycle phase, despite no significant increase of apoptotic cells detected, might indicate that the cells are not proliferating properly when treated with combination treatment.

A.

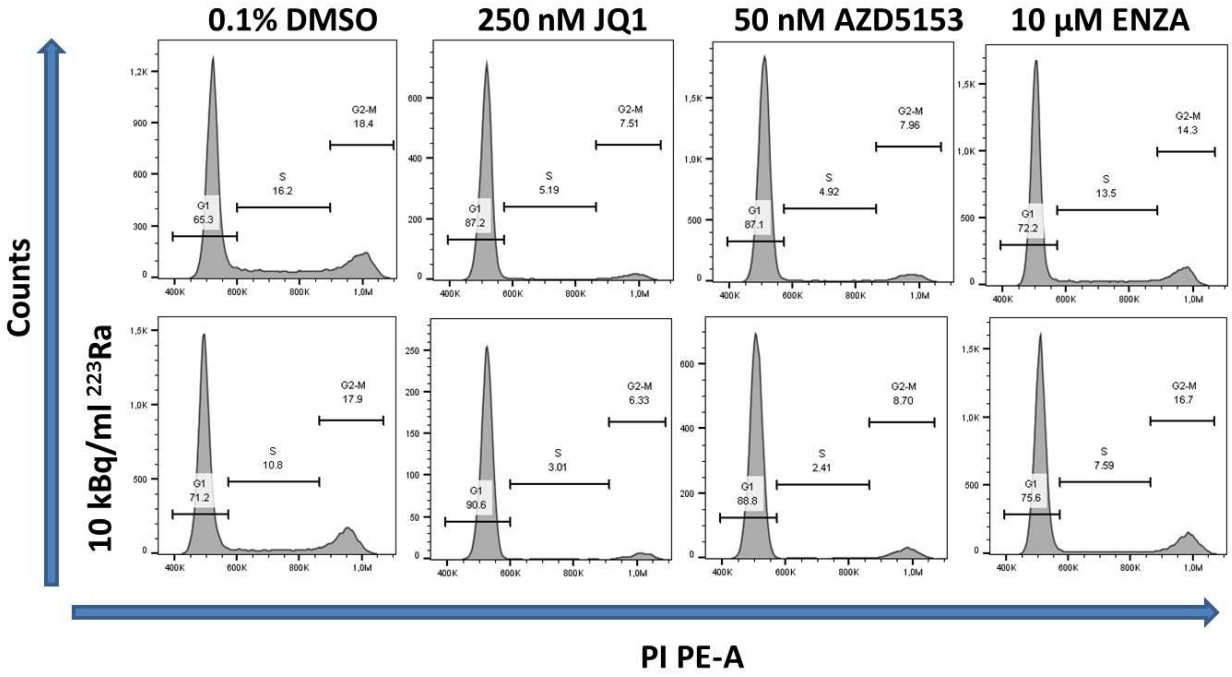
0.1% DMSO
250 nM JQ1
50 nM AZD5153
10 µM ENZA
Counts
10 kBq/ml 223Ra
PI PE-A
G1 65.3
S 16.2
G2-M 18.4
G1 87.2
S 5.19
G2-M 7.51
G1 87.1
S 4.92
G2-M 7.96
G1 72.2
S 13.5
G2-M 14.3
G1 71.2
S 10.8
G2-M 17.9
G1 90.6
S 3.01
G2-M 6.33
G1 88.8
S 2.41
G2-M 8.70
G1 75.6
S 7.59
G2-M 16.7

B.

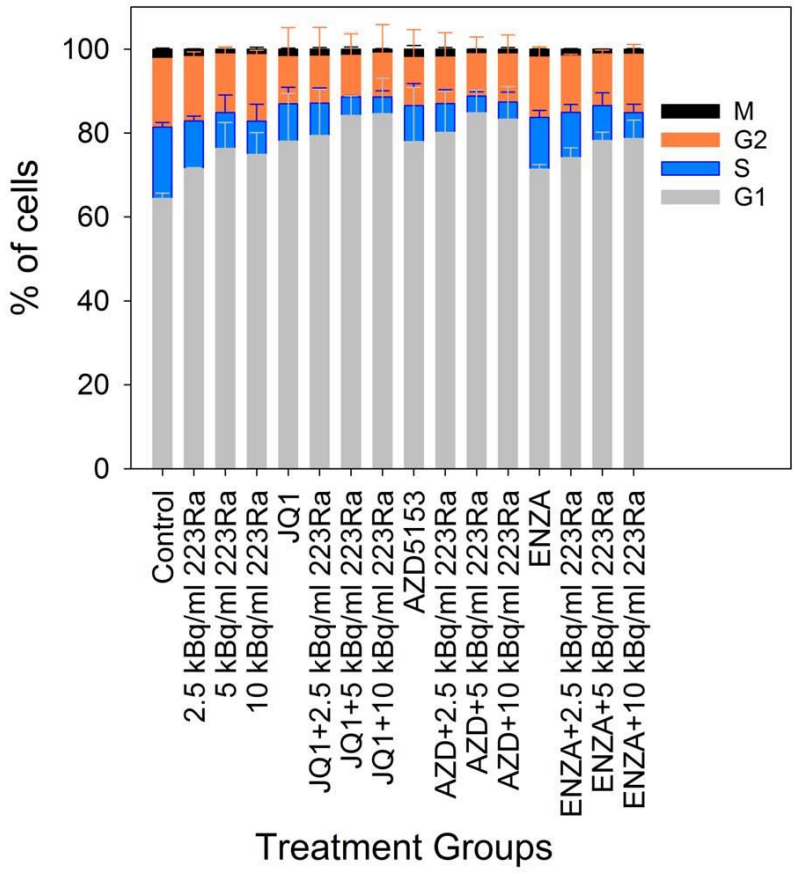
% of cells
M
G2
S
G1
Control
2.5 kBq/ml 223Ra
5 kBq/ml 223Ra
10 kBq/ml 223Ra
JQ1
JQ1+2.5 kBq/ml 223Ra
JQ1+5 kBq/ml 223Ra
JQ1+10 kBq/ml 223Ra
AZD5153
AZD+2.5 kBq/ml 223Ra
AZD+5 kBq/ml 223Ra
AZD+10 kBq/ml 223Ra
ENZA
ENZA+2.5 kBq/ml 223Ra
ENZA+5 kBq/ml 223Ra
ENZA+10 kBq/ml 223Ra
Treatment Groups

C.

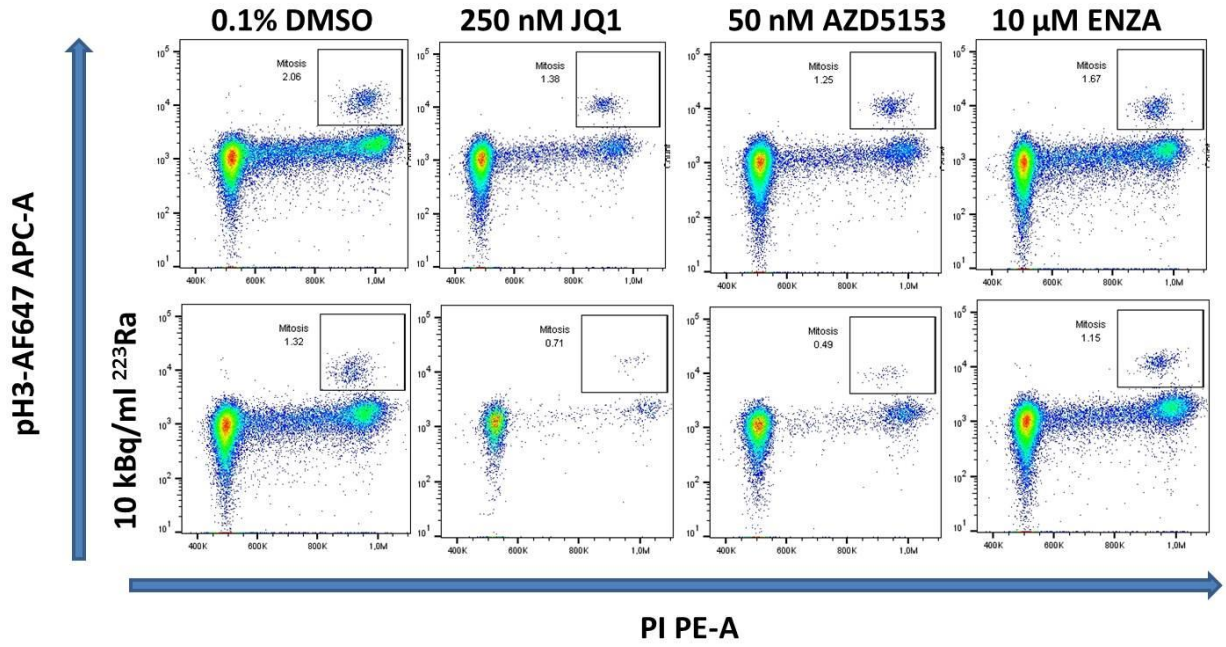

Figure 4.21. Cell cycle distribution of C4-2 cells 72 h after treatment with BET or AR inhibitors alone or in combination with ^{223}Ra. Cells were plated at a density of 0.5 ×10^6 or 1 ×10^6 in 25cm^2 flasks (1 flask each treatment group), after 24 h incubation, the media in each flask was replaced with drug-containing media, cells were treated with 250 nM JQ1, 50 nM AZD5153 or 10 µM ENZA for 2 h, followed by 1 h co-treatment with 2.5, or 10 kBq/ml of ^{223}Ra, then incubated for 72 h, followed by harvesting cells and incubated with eFluor 450 dye(staining dead cells) for 30 minutes, then fixed with 100% ice-cold methanol. Fixed cells were washed with PBST and centrifuged. Then cells were incubated with primary antibodies, rabbit anti-phospho Ser10 Histone H3 and anti-phospho-Histone γH2A.X (Ser139) for 60 minutes at room temperature. In addition, RNase enzyme was added. After washing with PBST and centrifugation, the cells were incubated with secondary antibodies Alexa Fluor™ 647 donkey anti-rabbit IgG (H+l) and polyclonal goat anti-mouse IgG for 30 minutes at room temperature. Finally, after washing with PBST, cells were stained with PI in PBST/BSA for 30 minutes and DNA damage content analysis using flow cytometry were performed. A statistical ANOVA test run (p>0, 05). **(A)** DNA content (PI stain) and cell cycle analysis frequency histogram. In the upper row the control sample (0.1% DMSO) is presented in the left panel and the samples for 250 nM JQ1, 50 nM AZD5153 and 10 µM ENZA alone are shown to the right. In the lower row the cell sample exposed to 10 kBq/ml ^{223}Ra only is presented in the left panel and the three samples subjected to the combination of 10 kBq/ml ^{223}Ra and the corresponding compounds are shown to the right. **(B)** Cell cycle profiles as the function of treatment groups,error bars show ±SD from two independent experiments each with two parallels. **(C)** Population of cell in the M phase. DNA content (PI stain) is plotted against pH3 (AF647 stain), In the upper row the control sample (0.1% DMSO) is presented in the left panel and the samples for 250 nM JQ1, 50 nM AZD5153 and 10 µM ENZA alone are shown to the right. In the lower row the cell sample exposed to 10 kBq/ml ^{223}Ra only is presented in the left panel and the three samples subjected to the combination of 10 kBq/ml ^{223}Ra and the corresponding drugs are shown to the right.

The treatments have not induced significant DNA damage (Fig.4.22). An increased percentage of DNA damage was observed in the samples treated with a combination of 250 nM JQ1, 50 nM AZD5153 or 10 µM ENZA in combination with 10 kBq/ml ^{223}Ra (Fig. 4.22).

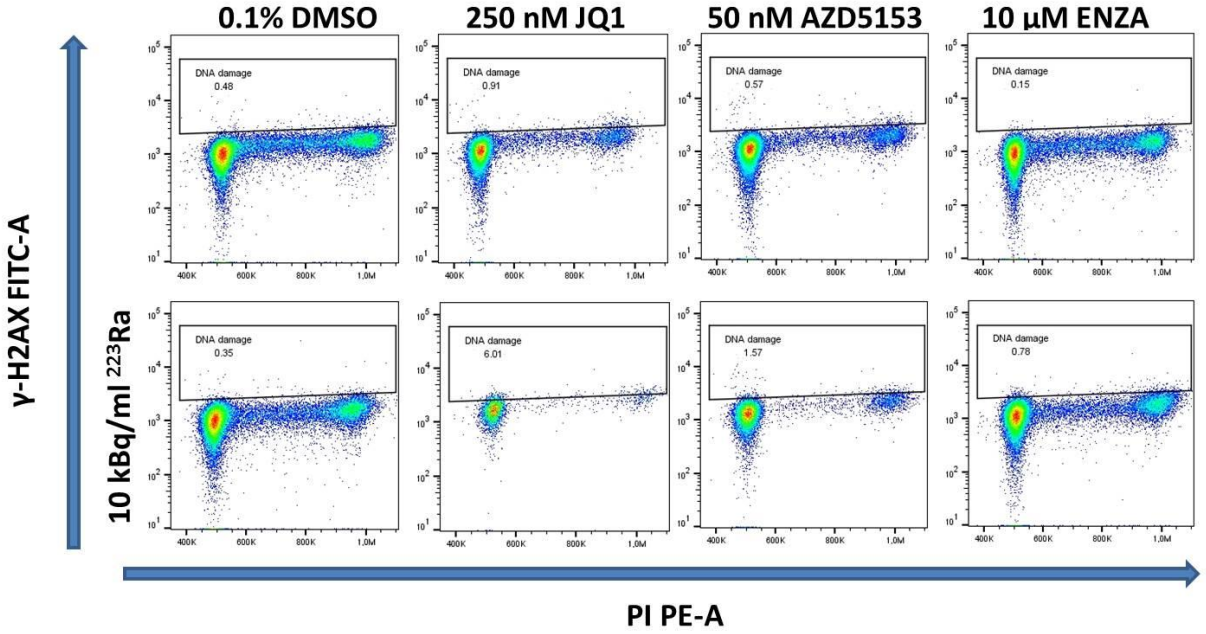

Figure 4.22. DNA damage detection of C4-2 cells 72 h after treatment with BET or androgen receptor inhibitors alone or in combination with ^{223}Ra. DNA content (PI stain) is plotted against γ -H2AX (FITC stain). The C4-2 cells were plated at a density of 0.5×10^6 or 1×10^6 in 25cm^2 flasks (1 flask per group), after 24 h incubation, the media in each flask was replaced with drug-containing media, cells were treated with 250 nM JQ1, 50 nM AZD5153 or 10 µM ENZA for 2 h, followed by 1 h co-treatment with 2.5, or 10 kBq/ml of ^{223}Ra, then incubated for 72 h, followed by harvesting cells and incubated with eFluor 450 dye(staining dead cells) for 30 minutes, then fixed with 100% ice-cold methanol. Fixed cells were washed with PBST and centrifuged. Then cells were incubated with primary antibodies, rabbit anti-phospho Ser10 Histone H3 and anti-phospho-Histone γH2A.X (Ser139) for 60 minutes at room temperature. In addition, RNase enzyme was added. After washing with PBST and centrifugation, the cells were incubated with secondary antibodies Alexa Fluor™ 647 donkey anti-rabbit IgG (H+l) and polyclonal goat anti-mouse IgG for 30 minutes at room temperature. Finally, after washing with PBST, cells were stained with PI in PBST/BSA for 30 minutes and DNA damage content analysis using flow cytometry were performed. In the upper row the control sample (0.1% DMSO) is presented in the left panel and the samples for 250 nM JQ1, 50 nM AZD5153 and 10 µM ENZA alone are shown to the right. In the lower row the cell sample exposed to 10 kBq/ml ^{223}Ra only is presented in the left panel and the three samples subjected to the combination of 10 kBq/ml ^{223}Ra and the corresponding drugs are shown to the right. Results presented are from one independent experiment.

5 DISCUSSION

This study was the first to assess the effects of combination therapy of BET, JQ1 or AZD5153 or AR ENZA inhibitor with α-emitting ^{223}Ra (Xofigo) targeting bone metastases or ß-emitting ^{177}Lu-PSMA-617 targeting PSMA in C4-2 cells growing in monolayers and multicellular spheroids. This chapter provides a detailed discussion based on the obtained results (Chapter 4).

The second-generation AR inhibitor ENZA is used for the treatment of both castrate sensitive and castrate resistant prostate cancer (160, 161). ENZA prolong patient survival for some time until resistance develops in nearly all patients (162, 163). Disease progression correlates with rising PSA levels, indicating continued AR signaling and highlighting the need for additional therapies. The epigenetic drugs JQ1 is a molecular test probe used as a research tool to investigate the inhibition of three important BET proteins (BRD4, BRD3, BRD2, and BRDT) (164). AZD5153 (BRD4 inhibitor) (134, 135) a lead compound from AstraZeneca, at the moment is in a phase 1 clinical trial for several solid tumors including prostate cancer (165).
Despite several novel therapeutic options, CRPC remains highly lethal (2, 166). CRPC is very heterogeneous diseases (2, 166),and the survival benefits of the available drugs account for roughly few months (Table 1.2), suggesting that monotherapies are not sufficient and that combinatory approaches for CRPC are urgently needed.
Bromodomain containing proteins have been explored as drug targets (126) and clinical trials (167, 168) are determining the efficacy of some BET inhibitors such as ZEN-3964 alone or in combination with ENZA in CRPC patients.
Clinical trials have already shown effects of use of radiopharmaceuticals ^{223}Ra or ^{177}Lu-PSMA-617 on mCRPC patients and trials combining ENZA with these radiopharmaceuticals are ongoing (169, 170). In depth molecular studies are not found in the literature. Therefore, the determination of the effects of BET and AR inhibitors in combination with radiopharmaceuticals against CRPC may be synergistic.

5.1 Targeting BET or AR decrease viability of C4-2 cells growing in monolayers and inhibits proliferation of C4-2 spheorids

Several studies have been investigating the potential of BET inhibitors, mostly utilizing JQ1(171). Various AR positive CRPC cell lines have shown to be sensitive to JQ1 (172). In this study, the effect of JQ1 and AZD5153 in C4-2 cells, which is an AR positive prostate cancer cell line, was investigated in 2D (Fig. 4.1) and 3D (Fig.4.3 and 4.4) models. In 2D monolayers, C4-2 cells treated for 3 days with JQ1 or AZD5153, but not with ENZA, showed a reduction in metabolic activity, as assessed by the MTT assay, and a reduction in ATP quantity, as assessed by the CellTiter assay (Fig.4.1). The clonogenic assay has demonstrated the decreased capacity of cells to proliferate and establish colonies, but under microscope many surviving single C4-2 cells were observed at the end of the experiment (data not shown). These results are in accordance with previous studies on the effect of JQ1 or AZD5153 on prostate cell growth *in vitro* and *in vivo* (135, 173). The obtained results show that the BET and AR inhibitors at used concentrations and incubations times have

reduced cell proliferation. However, the reliable data are missing regarding cytotoxicity. Zhao et al. have demonstrated that the cell viability of C4-2 cells treated with DMSO measured by MTS assay (measures metabolic activity and it is similar to the MTT assay) increased from day 1 to 5, but remained static when treated with 10 µM ENZA (174). They concluded that ENZA was not cytotoxic, but cytostatic, to C4-2 CRPC cells and that C4-2 CRPC cells are resistant to ENZA (174). Their results are in agreement with the results obtained in this study when the viability of C4-2 cells treated with ENZA was measured by the MTT and CellTiter assays (Fig.4.1).

Growth rate of the spheroids upon treatment were evaluated by following the morphological changes and size increase until day 21-24. The doubling times of the C4-2 spheroids treated with increased concentration of JQ1 and AZD5153 increased, while the doubling time of the spheroids treated with ENZA was around 10-12 days at increasing concentrations (Fig.4.4 G). The spheroids treated with the highest concentrations of BET or AR inhibitors had viable cells (Fig.4.3 F-H), as indicated by FDA stain, and necrotic, as indicated by PI staining. In a prostate cancer patient-derived, 3D spheroid culture model (tissue sample obtained from radical prostatectomy specimen of prostate cancer patients) study by Johannes Linxweiler et.al, a similar reduction of spheroids viability upon treatment with 200 µM ENZA were consistently observed compared to untreated controls(175). JQ1 has previously in breast cancer cell lines shown to reduce spheroid growth (176), however no studies on the effect of JQ1 or AZD5153 on prostate cancer spheroid *in vitro* model were found upon searching on databases, including PubMed, Google Scholar and Scopus.
The shrinkage or disintegration of spheroids treated with BET or AR inhibitors was not observed (Fig.4.3 B-D), while at day 21-24 the spheroids in the control group were so big, that they started to disintegrate (Fig. 4.3 B-D and F-H). The control group and ENZA group spheroids had viable layer and necrotic core in the spheroids at day 24 (Fig. 4.3 F-H).
The treatment with ENZA was not responsible for the necrotic core. The limitation of nutrition and oxygen are responsible for necrotic core in bigger spheroids. Based on the results (Fig. 4.3 D and H) a concentration of 10 µM ENZA, were selected for further combination experiments, since a higher concentration of the drug, do not inhibit spheroid growth significantly.

5.2 BET or AR inhibitors in combination with 223-Ra

ENZA in combination with other agents, such as ADT, docetaxel or ^{223}Ra, has been studied earlier (177-179). Several clinical trials have demonstrated that patients treated with concomitant ENZA and ^{223}Ra showed a survival benefit (179). However, no preclinical studies combining ENZA with ^{223}Ra or combination of the BET inhibitors with ^{223}Ra or 177Lu-PSMA-617 on C4-2 prostate cancer cells have been explored before this thesis to our knowledge.

The non-overlapping mechanisms of action between BET or AR inhibitors and ^{223}Ra against cancer cells, provides a rational for combination treatments (140, 180). The two different culture methods were chosen to determine the effect of combination treatment in both methods. The microenvironment of spheroids more

closely mimics that of tumors *in vivo*, making it superior to the monolayer culture model (2D) (181). Here, the response of spheroids (established from C4-2 PC cell line) showed additive or synergistic effect to combination treatment BET or AR inhibitors and radiopharmaceuticals as evaluated in terms of spheroid growth. It can be speculated that radiation-induced bystander effects or crossfire effects (allowing irradiation of non-targeted cells) is more likely to occur in spheroid model than in cells grown in monolayer, since in spheroids the cells are close and in gap junction communication with each other, explaining the stronger response upon exposure to the radionuclide. The combination of JQ1 with ^{223}Ra resulted in synergistic effect in C4-2 spheroids as assessed by slower growth in spheroids treated with a combination of JQ1 and ^{223}Ra compared to the compounds alone (Fig 4.8-4.9). A synergistic combined effect of AZD5153 and ^{223}Ra were also observed in C4-2 spheroids (4.11-4.12). Synergistic effect was observed when ENZA was used in combination with ^{223}Ra in C4-2 spheroids (4.14-4.15). As ^{223}Ra have shown to exhibit a dual targeting mode-of-action; inducing tumor growth suppression and inhibition of tumor-induced pathological bone alteration in preclinical prostate cancer models (182). The natural bone seeking radiopharmaceutical, ^{223}Ra have a half-life of 11.4 days, decay by predominantly emitting α-particles (high LET), causing localized cytotoxicity through DNA DSBs (140). Thus the combination of DNA double strand breaks caused by ^{223}Ra and the inhibition of AR signaling pathway through the AR inhibitor (ENZA) or the inhibition of BRD4 by JQ1 or AZD5153, which generally binds to acetylated histones, recruits RNA polymerase II (183), and have been implicated in participating in the DNA damage response(25) entails a stronger effect on C4-2 spheroids than that can be achieved by treatment of these compounds alone, as we observed in this study.

In monolayer cell survival experiments a consistent trend of additivity or synergy between the tested combinations treatments were observed (Fig.4). However, three experiments with different drug concentrations gave different results. The impact on the sublethal effect for the different compounds alone varied from combination experiment to experiment and did not behave as in mono-treatment experiments (Fig 4.1). In mono-treatments the C4-2 cells grew into colonies and C4-2 cells adhered nicely to the bottom of the 25cm^2 culture flasks, which indicate that there was not any adhesion issue when C4-2 cells were exposed to the drugs alone, as a study done by Andrew D.Woods et.al, has shown that AZD5153 has an anti-adhesion activity (184). The altered adhesion of C4-2 cells by AZD5153 treatment may be responsible for the high standard deviations observed in mono-treatment (Fig.4.6). A possible cause for this variation upon combination treatments may be also that the combination experiments consist of many removing of the media steps that might have caused removal of cells in the process as a result of their weak adherence to the bottom of the flasks.

Different drug concentrations were used in independent combinational experiments, as a result of the big variation of concentrations of the drugs to obtain the same SF on mono-treatment experiments (Fig. 4.1 and Table 4.2).

The cell viability assays used to select a final concentration for combination treatments, are based on various cellular measurements (described in detail in Chapter 3.3 Materials and Methods). MTT measuring formazan produced by viable cells only and CellTiter assay measuring ATP, while clonogenic assay are based on cells ability to grow into colonies which happens only if the DNA of the cells are not damaged or the cell had the ability to repair the damage, for this reason various drug concentrations among the cell viability assays were obtained to result in the same percentage of cell survival fractions. A higher concentration is needed to reduce the survival fraction detected by MTT and CellTiter assays, while a lower concentration is needed to demonstrate clonogenicty of the cells to treatment.

5.3 AZD5153 in combination with 177-Lu PSMA

When C4-2 spheroids were treated with a combination of AZD5153 and ^{177}Lu-PSMA-617, strong synergism was observed. The spheroid growth was slower in spheroids treated with a combination of AZD5153 and ^{177}Lu-PSMA-617 compared to AZD5153 or ^{177}Lu-PSMA-617 alone (Fig.4.17). Tumor targeting ^{177}Lu-PSMA-617, binds to PSMA receptors on targeted cells, is internalized and emits ß-particle with a maximum energy of 497 keV and a soft –tissue path length of 1, 5 mm, resulting in cell damage. This radiopharmaceutical is currently being tested in phase 3 trials for treating patients with mCRPC (92, 107). The enhanced response observed in C4-2 spheroids treated with a combination of AZD5153 and ^{177}Lu-PSMA-617, might be due to the inhibition of BRD4 that might result in sensitizing the cells to radiation. Since, BRD4 has shown to maintain chromatin in an open and accessible state (126), the inhibition of BRD4 by AZD5153 might result in sensitizing the cells to radiation. Additionally, overexpression of AR has been shown to drive genome-wide chromatin relaxation (126), which might contribute to the counteracting effect of AZD5153 with radiation from ^{177}Lu-PSMA-617. The spheroids were evaluated at day 7, 14 and 21, however due to technical problems, involving damaged hard disk and microscopy computer not responding, I was only able to present the data from day 22.

5.4 Combination treatment effect on apoptosis, DNA damage and cell cycle distribution

Although strong significant synergistic effect was observed upon combination treatment of C4-2 spheroids with JQ1, AZD5153 or ENZA and ^{223}Ra, the combination of these treatment had no impact on DNA damage and the number of apoptotic cells as measured by flow after 72 hours after treatment (Figs. 4.20 and 4.21). The treated cells had the same viability as untreated cells (Fig. 4.20). Previous studies have addressed that the BET inhibitors alone reduce proliferation, induce apoptosis and cell cycle arrest, hamper DNA damage repair through several distinct mechanisms in prostate cancer cells (135, 185) (164, 186-188). In the present study no treatment was able to induce apoptosis (87-95% of the total cells were viable in all groups) or DNA damage. However, the reduced number of mitotic cells and cell number in S and G2 phases were observed in combination groups (Fig. 4.21 A-C), which show that proliferation of the C4-2 cells were reduced. Flow cytometry analysis was performed 3 days (72 h) based on MTT and CellTiter assays (Fig. 4.2), which might be indeed too early to assess such alterations in cell cycle distribution or increase in apoptosis after treatment. If this analysis would be done after 7 days with higher activities and incubation times of

radiopharmaceuticals and higher concentrations of BET or AR inhibitors an even stronger effects could be obtained. The results from the apoptosis analyses align with that of the spheroid growth or cell proliferation, as the cells within the spheroids treated with even high concentrations of the same compounds are still viable (Fig. 4.7), suggesting that the combined effect of these compounds is rather cytostatic than cytotoxic at these concentrations.

Limitations of this study:

I have shown here that BET or AR inhibition synergizes with radiopharmaceuticals to reduce growth of multicellular C4-2 spheroids, but the obtained results in C4-2 cells growing in monolayers were conflicting and no conclusion can be drawn.

The mechanisms underlying this synergistic effect in multicellular spheroids and discrepancy between 2D and 3D results have not been studied, understood and explained properly. The C4-2 cells growing in monolayer culture and the same cells growing in spheroids behave differently. Proliferation studies of the cells treated with BET or AR inhibitors and radiopharmaceuticals were not performed due to radiation safety requirements for radionuclide laboratories. A type C laboratory is intended for the handling of low activities (maximum 1 MBq ^{223}Ra and 100 MBq ^{177}Lu). The cell proliferation can be measured in 96 well plates using IncuCyte® Systems for live-cell imaging and analysis. Unfortunately, these plates with radioactive cells cannot be moved to other laboratories. The effects of combinational therapies on cell migration capability (Scratch assay) or apoptosis (cleaved-PARP by Western blot) at studied concentrations and activities drugs have not been observed due to absence of the synergistic effects in 2D models (MTT assay, flow cytometry assay).

6 CONCLUSIONS

The overall aim of this thesis was to study the combined effect of BET, JQ1 and AZD5153, or AR, ENZA, inhibitors with radiopharmaceuticals, ^{223}Ra and ^{177}Lu-PSMA-617 in CRPC C4-2 cell line. Cell monolayer and multicellular spheroids culture models in C4-2 cells were used to study. The combination of 0-25 kBq/ml ^{223}Ra with 0-250 nM JQ1, 0- 50 nM AZD51653 or 0- 10 µM ENZA.JQ1, AZD5153 and ENZA resulted in synergistic interactions in multicellular spheroids with ^{223}Ra. AZD5153 combined synergistically with ^{177}Lu-PSMA-617 in in C4-2 spheroids.

The survival fractions obtained in cells growing in monolayer, although showed a similar trend toward synergism, remain controversial ue to conflicting results obtained in different experiments. This is possibly caused by technical issues and needs further investigations. The use of 3D culture method, despite being time consuming, are a reliable and representative *in vitro* culture model for experiments in drugs combinations with radionuclides. The potentially enhanced effects of the treatment combinations investigated here are possibly due to increased chance of radiation-induced bystander or cross-fire effect, which, in turn, enhances the effect of radiation induced cell damage while mimicking the scenario within the tumor.

In conclusion, it has been demonstrated that the combination treatment of JQ1, AZD5153 or ENZA and ^{223}Ra or AZD5153 and^{177}Lu-PSMA-617 induced synergistic inhibition of C4-2 spheroids growth rate. These preclinical results can help in optimizing future preclinical studies in mice. These results show that the combination treatment of BET or AR inhibitors and radiopharmaceuticals is a potential treatment for mCRPC patients.

7 FUTURE PERSPECTIVES

The combination of ^{223}Ra and ENZA is already in randomized phase III trial in mCRPC but the molecular rational for such combination in the clinic is still elusive. Combination of ^{223}Ra and ENZA showed significant synergy in the work done in this master's thesis in 3D culture model. Therefore additional mechanistic studies using these models and methods are granted.

In addition, our study was the first one to combine radiopharmaceutical agents with BET inhibitors. This preclinical *in vitro* study reveals the potential of combining radiopharmaceuticals with BET or AR inhibitors to enhance the therapeutic effect of the drugs for PC treatment.

Additional experiments will be performed to understand the enhancing effect on prostate cancer cell line in 3D model. A natural continuation of this work in animal studies to validate the results from this study might be worth pursuing. Investigation using these radiopharmaceuticals in combination with BET or AR inhibitors in clonogenic assay (2D model) should be repeated also using other prostate cancer cell line models, and completed using higher concentrations of the drugs, since I found conflicting results at the tested doses with the clonogenic assay. Because of the limited time and unavailability of ^{177}Lu-PSMA-617, the experiment with such compound was performed only once, therefore this should also be repeated at least two more times to be more reliable . In addition, the results of the treatment combinations were much clearer in the spheroids than in cell monolayer (2D), which should also be repeated. Flow cytometry analysis for detection of apoptosis and DNA damage experiments should be performed also with spheroids and the analyses performed at multiple time points.

Further, mechanistic studies should be performed to elucidate the consequences of the treatment combinations at the molecular level, for instance by performing chromatin immunoprecipitation analysis with the inhibited BET proteins, or determining DNA damage markers such as ɣH2AX foci upon treatment.

REFERENCES

1. Datta D, Aftabuddin M, Gupta DK, Raha S, Sen P. Human Prostate Cancer Hallmarks Map. Scientific Reports. 2016;6(1):30691.
2. Haffner MC, Zwart W, Roudier MP, True LD, Nelson WG, Epstein JI, et al. Genomic and phenotypic heterogeneity in prostate cancer. Nature reviews Urology. 2021;18(2):79-92.
3. Rawla P. Epidemiology of Prostate Cancer. World journal of oncology. 2019;10(2):63-89.
4. Norway. CRo. Cancer in Norway 2019 - Cancer incidence, mortality, survival and prevalence in Norway Oslo2019 [April 2021]. Available from: https://www.kreftregisteret.no/globalassets/cancer-in-norway/2019/cin_report.pdf.
5. Sung H, Ferlay J, Siegel RL, Laversanne M, Soerjomataram I, Jemal A, et al. Global cancer statistics 2020: GLOBOCAN estimates of incidence and mortality worldwide for 36 cancers in 185 countries. CA: a cancer journal for clinicians. 2021;n/a(n/a).
6. Crawford ED. Epidemiology of prostate cancer. Urology. 2003;62(6, Supplement 1):3-12.
7. Oczkowski M, Dziendzikowska K, Pasternak-Winiarska A, Włodarek D, Gromadzka-Ostrowska J. Dietary Factors and Prostate Cancer Development, Progression, and Reduction. Nutrients. 2021;13(2).
8. Vietri MT, D'Elia G, Caliendo G, Resse M, Casamassimi A, Passariello L, et al. Hereditary Prostate Cancer: Genes Related, Target Therapy and Prevention. Int J Mol Sci. 2021;22(7).
9. Sarkar S, Das S. A Review of Imaging Methods for Prostate Cancer Detection. Biomed Eng Comput Biol. 2016;7(Suppl 1):1-15.
10. Dan Sperling M. Prostate Zone Anatomy, Prostate Cancer and Imaging [Available from: https://sperlingprostatecenter.com/prostate-zone-anatomy-prostate-cancer-and-imaging/.
11. Lamb AD, Warren AY, Neal DE. Pre-malignant Disease in the Prostate. Pre-Invasive Disease: Pathogenesis and Clinical Management2011. p. 467-91.
12. Karthaus WR, Hofree M, Choi D, Linton EL, Turkekul M, Bejnood A, et al. Regenerative potential of prostate luminal cells revealed by single-cell analysis. Science. 2020;368(6490):497.
13. Brawer MK. Prostatic intraepithelial neoplasia: an overview. Reviews in urology. 2005;7 Suppl 3(Suppl 3):S11-8.
14. Wang G, Zhao D, Spring DJ, DePinho RA. Genetics and biology of prostate cancer. Genes & development. 2018;32(17-18):1105-40.
15. Bubendorf L, Schöpfer A, Wagner U, Sauter G, Moch H, Willi N, et al. Metastatic patterns of prostate cancer: An autopsy study of 1,589 patients. Human Pathology. 2000;31(5):578-83.
16. Davey RA, Grossmann M. Androgen Receptor Structure, Function and Biology: From Bench to Bedside. Clin Biochem Rev. 2016;37(1):3-15.
17. Dehm SM, Tindall DJ. Regulation of androgen receptor signaling in prostate cancer. Expert review of anticancer therapy. 2005;5(1):63-74.
18. Imamoto T, Suzuki H, Yano M, Kawamura K, Kamiya N, Araki K, et al. The role of testosterone in the pathogenesis of prostate cancer. International journal of urology : official journal of the Japanese Urological Association. 2008;15(6):472-80.
19. Heinlein CA, Chang C. Androgen receptor in prostate cancer. Endocr Rev. 2004;25(2):276-308.
20. Grossmann ME, Huang H, Tindall DJ. Androgen Receptor Signaling in Androgen-Refractory Prostate Cancer. JNCI: Journal of the National Cancer Institute. 2001;93(22):1687-97.
21. Koochekpour S. Androgen receptor signaling and mutations in prostate cancer. Asian J Androl. 2010;12(5):639-57.
22. Culig Z, Comuzzi B, Steiner H, Bartsch G, Hobisch A. Expression and function of androgen receptor coactivators in prostate cancer. The Journal of steroid biochemistry and molecular biology. 2004;92(4):265-71.
23. Wade CA, Kyprianou N. Profiling Prostate Cancer Therapeutic Resistance. Int J Mol Sci. 2018;19(3).
24. Braadland PR, Urbanucci A. Chromatin reprogramming as an adaptation mechanism in advanced prostate cancer. Endocrine-related cancer. 2019;26(4):R211-r35.
25. Chiu L-Y, Gong F, Miller KM. Bromodomain proteins: repairing DNA damage within chromatin. Philosophical Transactions of the Royal Society B: Biological Sciences. 2017;372(1731):20160286.
26. Ichikawa T, Suzuki H, Ueda T, Komiya A, Imamoto T, Kojima S. Hormone treatment for prostate cancer: current issues and future directions. Cancer Chemotherapy and Pharmacology. 2005;56(1):58-63.

27. Sherbet GV. 17 - The Androgens and Androgen Receptors in Development, Differentiation and Neoplasia. In: Sherbet GV, editor. Growth Factors and Their Receptors in Cell Differentiation, Cancer and Cancer Therapy. London: Elsevier; 2011. p. 213-8.
28. Waltering KK, Porkka KP, Jalava SE, Urbanucci A, Kohonen PJ, Latonen LM, et al. Androgen regulation of micro-RNAs in prostate cancer. The Prostate. 2011;71(6):604-14.
29. Shore ND, Abrahamsson PA, Anderson J, Crawford ED, Lange P. New considerations for ADT in advanced prostate cancer and the emerging role of GnRH antagonists. Prostate cancer and prostatic diseases. 2013;16(1):7-15.
30. Tan MH, Li J, Xu HE, Melcher K, Yong EL. Androgen receptor: structure, role in prostate cancer and drug discovery. Acta pharmacologica Sinica. 2015;36(1):3-23.
31. Descotes JL. Diagnosis of prostate cancer. Asian journal of urology. 2019;6(2):129-36.
32. Fleshner K, Assel M, Benfante N, Lee J, Vickers A, Fine S, et al. Clinical Findings and Treatment Outcomes in Patients with Extraprostatic Extension Identified on Prostate Biopsy. The Journal of urology. 2016;196(3):703-8.
33. Kader A, Brangsch J, Kaufmann JO, Zhao J, Mangarova DB, Moeckel J, et al. Molecular MR Imaging of Prostate Cancer. Biomedicines. 2020;9(1).
34. Short E, Warren AY, Varma M. Gleason grading of prostate cancer: a pragmatic approach. Diagnostic Histopathology. 2019;25(10):371-8.
35. Epstein JI, Egevad L, Amin MB, Delahunt B, Srigley JR, Humphrey PA. The 2014 International Society of Urological Pathology (ISUP) Consensus Conference on Gleason Grading of Prostatic Carcinoma: Definition of Grading Patterns and Proposal for a New Grading System. The American journal of surgical pathology. 2016;40(2):244-52.
36. Tolkach Y, Kristiansen G. The heterogeneity of prostate cancer: a practical approach. Pathobiology : journal of immunopathology, molecular and cellular biology. 2018;85(1-2):108-16.
37. Humphrey PA. Gleason grading and prognostic factors in carcinoma of the prostate. Modern pathology : an official journal of the United States and Canadian Academy of Pathology, Inc. 2004;17(3):292-306.
38. Penney K, Schumacher F, Kraft P, Mucci L, Sesso H, Niu Y, et al. Association of KLK3 (PSA) genetic variants with prostate cancer risk and PSA levels. Carcinogenesis. 2011;32:853-9.
39. Nogueira L, Corradi R, Eastham JA. Prostatic specific antigen for prostate cancer detection. International braz j urol. 2009;35(5):521-31.
40. David MK, Leslie SW. Prostate Specific Antigen. StatPearls. Treasure Island (FL): StatPearls Publishing
Copyright © 2021, StatPearls Publishing LLC.; 2021.
41. Chen FZ, Zhao XK. Prostate cancer: current treatment and prevention strategies. Iranian Red Crescent medical journal. 2013;15(4):279-84.
42. N. Mottet (Chair) PCV-c, R.C.N. van den Bergh, , E. Briers (Patient Representative) MDS, S. Fanti, , S. Gillessen JG, A.M. Henry, T.B. Lam, M.D. Mason, , T.H. van der Kwast HGvdP, O. Rouvière, , I.G. Schoots. D. Tilki TW, Guidelines Associates: T. Van den Broeck MC, et al. EAU - EANM -
ESTRO - ESUR - SIOG
Guidelines on Prostate Cancer: European Association of Urology; 2020 [Available from: https://uroweb.org/guideline/prostate-cancer/.
43. Litwin MS, Tan HJ. The Diagnosis and Treatment of Prostate Cancer: A Review. Jama. 2017;317(24):2532-42.
44. O'Donnell H, Parker C. What is low-risk prostate cancer and what is its natural history? World journal of urology. 2008;26(5):415-22.
45. Mottet N, Bellmunt J, Bolla M, Briers E, Cumberbatch MG, De Santis M, et al. EAU-ESTRO-SIOG Guidelines on Prostate Cancer. Part 1: Screening, Diagnosis, and Local Treatment with Curative Intent. European Urology. 2017;71(4):618-29.
46. Cornford P, Bellmunt J, Bolla M, Briers E, De Santis M, Gross T, et al. EAU-ESTRO-SIOG Guidelines on Prostate Cancer. Part II: Treatment of Relapsing, Metastatic, and Castration-Resistant Prostate Cancer. Eur Urol. 2017;71(4):630-42.
47. Artibani W, Porcaro AB, De Marco V, Cerruto MA, Siracusano S. Management of Biochemical Recurrence after Primary Curative Treatment for Prostate Cancer: A Review. Urologia internationalis. 2018;100(3):251-62.

48. Pisansky TM, Thompson IM, Valicenti RK, D'Amico AV, Selvarajah S. Adjuvant and Salvage Radiation Therapy After Prostatectomy: ASTRO/AUA Guideline Amendment, Executive Summary 2018. Practical Radiation Oncology. 2019;9(4):208-13.
49. Martin NE, D'Amico AV. Progress and controversies: Radiation therapy for prostate cancer. CA: a cancer journal for clinicians. 2014;64(6):389-407.
50. Wilkins A, Parker C. Treating prostate cancer with radiotherapy. Nature reviews Clinical oncology. 2010;7(10):583-9.
51. Vanneste BGL, Limbergen EJV, Lin ENv, Roermund JGHv, Lambin P. Prostate Cancer Radiation Therapy: What Do Clinicians Have to Know? biomed research international. 2016;2016.
52. Greco C, Vazirani AA, Pares O, Pimentel N, Louro V, Morales J, et al. The evolving role of external beam radiotherapy in localized prostate cancer. Seminars in Oncology. 2019;46(3):246-53.
53. Liauw S, Connell P, Weichselbaum R. New Paradigms and Future Challenges in Radiation Oncology: An Update of Biological Targets and Technology. Science translational medicine. 2013;5:173sr2.
54. Mottet N, Bellmunt J, Bolla M, Briers E, Cumberbatch MG, Santis MD, et al. EAU–ESTRO–SIOG Guidelines on Prostate Cancer. Part 1: Screening, Diagnosis, and Local Treatment with Curative Intent. european urology. 2017;71(4):618-29.
55. Palermo G, Foschi N, D'Agostino D, Sacco E, Bassi P, Pinto F. Local relapse of prostate cancer after primary definitive treatment: the management. Minerva urologica e nefrologica = The Italian journal of urology and nephrology. 2016;68(3):282-92.
56. Corral DA, Pisters LL, von Eschenbach AC. Treatment options for localized recurrence of prostate cancer following radiation therapy. The Urologic clinics of North America. 1996;23(4):677-84.
57. Chang AJ, Autio KA, Roach M, 3rd, Scher HI. High-risk prostate cancer-classification and therapy. Nature reviews Clinical oncology. 2014;11(6):308-23.
58. Albala D. Imaging and treatment recommendations in patients with castrate-resistant prostate cancer. Reviews in urology. 2017;19:200-2.
59. Katzenwadel A, Wolf P. Androgen deprivation of prostate cancer: Leading to a therapeutic dead end. Cancer letters. 2015;367(1):12-7.
60. Chandrasekar T, Yang JC, Gao AC, Evans CP. Mechanisms of resistance in castration-resistant prostate cancer (CRPC). Transl Androl Urol. 2015;4(3):365-80.
61. Katzenwadel A, Wolf P. Androgen deprivation of prostate cancer: Leading to a therapeutic dead end. Cancer letters. 2015;367(1):12-7.
62. Gerritsen WR, Sharma P. Current and emerging treatment options for castration-resistant prostate cancer: a focus on immunotherapy. Journal of clinical immunology. 2012;32(1):25-35.
63. Vellky JE, Ricke WA. Development and prevalence of castration-resistant prostate cancer subtypes. Neoplasia. 2020;22(11):566-75.
64. Huang Y, Jiang X, Liang X, Jiang G. Molecular and cellular mechanisms of castration resistant prostate cancer. Oncology letters. 2018;15(5):6063-76.
65. Edwards J, Krishna NS, Grigor KM, Bartlett JM. Androgen receptor gene amplification and protein expression in hormone refractory prostate cancer. British journal of cancer. 2003;89(3):552-6.
66. Visakorpi T, Hyytinen E, Koivisto P, Tanner M, Keinänen R, Palmberg C, et al. In vivo amplification of the androgen receptor gene and progression of human prostate cancer. Nat Genet. 1995;9(4):401-6.
67. Steketee K, Timmerman L, Ziel-van der Made AC, Doesburg P, Brinkmann AO, Trapman J. Broadened ligand responsiveness of androgen receptor mutants obtained by random amino acid substitution of H874 and mutation hot spot T877 in prostate cancer. Int J Cancer. 2002;100(3):309-17.
68. Stashi E, York B, O'Malley BW. Steroid receptor coactivators: servants and masters for control of systems metabolism. Trends in Endocrinology & Metabolism. 2014;25(7):337-47.
69. Cai C, Chen S, Ng P, Bubley GJ, Nelson PS, Mostaghel EA, et al. Intratumoral de novo steroid synthesis activates androgen receptor in castration-resistant prostate cancer and is upregulated by treatment with CYP17A1 inhibitors. Cancer Res. 2011;71(20):6503-13.
70. Lubik AA, Gunter JH, Hendy SC, Locke JA, Adomat HH, Thompson V, et al. Insulin increases de novo steroidogenesis in prostate cancer cells. Cancer Res. 2011;71(17):5754-64.
71. Shtivelman E, Beer TM, Evans CP. Molecular pathways and targets in prostate cancer. oncotarget. 2014;5(17):7217-59.
72. Feng Z, Graff JN. Next-Generation Androgen Receptor-Signaling Inhibitors for Prostate Cancer: Considerations for Older Patients. Drugs & Aging. 2021;38(2):111-23.

73. Rice MA, Malhotra SV, Stoyanova T. Second-Generation Antiandrogens: From Discovery to Standard of Care in Castration Resistant Prostate Cancer. Frontiers in oncology. 2019;9:801.
74. Crona DJ, Whang YE. Androgen receptor-dependent and-independent mechanisms involved in prostate cancer therapy resistance. Cancers. 2017;9(6):67.
75. Scott L. Enzalutamide: A Review in Castration-Resistant Prostate Cancer. Drugs. 2018;78.
76. Menon MP, Higano CS. Enzalutamide, a second generation androgen receptor antagonist: development and clinical applications in prostate cancer. Current oncology reports. 2013;15(2):69-75.
77. Schalken J, Fitzpatrick JM. Enzalutamide: targeting the androgen signalling pathway in metastatic castration-resistant prostate cancer. BJU international. 2016;117(2):215-25.
78. Teo MY, Rathkopf DE, Kantoff P. Treatment of Advanced Prostate Cancer. Annual review of medicine. 2019;70:479-99.
79. Tucci M, Zichi C, Buttigliero C, Vignani F, Scagliotti GV, Di Maio M. Enzalutamide-resistant castration-resistant prostate cancer: challenges and solutions. OncoTargets and therapy. 2018;11:7353.
80. Bungaro M, Buttigliero C, Tucci M. Overcoming the mechanisms of primary and acquired resistance to new generation hormonal therapies in advanced prostate cancer: focus on androgen receptor independent pathways. Cancer Drug Resistance. 2020;3(4):726-41.
81. de Bono JS, Oudard S, Ozguroglu M, Hansen S, Machiels J-P, Kocak I, et al. Prednisone plus cabazitaxel or mitoxantrone for metastatic castration-resistant prostate cancer progressing after docetaxel treatment: a randomised open-label trial. The Lancet. 2010;376(9747):1147-54.
82. Tannock IF, de Wit R, Berry WR, Horti J, Pluzanska A, Chi KN, et al. Docetaxel plus prednisone or mitoxantrone plus prednisone for advanced prostate cancer. The New England journal of medicine. 2004;351(15):1502-12.
83. Kantoff PW, Higano CS, Shore ND, Berger ER, Small EJ, Penson DF, et al. Sipuleucel-T Immunotherapy for Castration-Resistant Prostate Cancer. New England Journal of Medicine. 2010;363(5):411-22.
84. Fizazi K, Scher HI, Molina A, Logothetis CJ, Chi KN, Jones RJ, et al. Abiraterone acetate for treatment of metastatic castration-resistant prostate cancer: final overall survival analysis of the COU-AA-301 randomised, double-blind, placebo-controlled phase 3 study. The Lancet Oncology. 2012;13(10):983-92.
85. Scher HI, Fizazi K, Saad F, Taplin ME, Sternberg CN, Miller K, et al. Increased survival with enzalutamide in prostate cancer after chemotherapy. The New England journal of medicine. 2012;367(13):1187-97.
86. de Bono J, Mateo J, Fizazi K, Saad F, Shore N, Sandhu S, et al. Olaparib for Metastatic Castration-Resistant Prostate Cancer. New England Journal of Medicine. 2020;382(22):2091-102.
87. Parker C, Nilsson S, Heinrich D, Helle SI, O'Sullivan JM, Fosså SD, et al. Alpha emitter radium-223 and survival in metastatic prostate cancer. The New England journal of medicine. 2013;369(3):213-23.
88. Zhao S, Yu EY. Castrate-resistant prostate cancer: postdocetaxel management. Curr Opin Urol. 2013;23(3):201-7.
89. Serpa Neto A, Tobias-Machado M, Kaliks R, Wroclawski ML, Pompeo ACL, Del Giglio A. Ten Years of Docetaxel-Based Therapies in Prostate Adenocarcinoma: A Systematic Review and Meta-Analysis of 2244 Patients in 12 Randomized Clinical Trials. Clinical genitourinary cancer. 2011;9(2):115-23.
90. Ogura T, Tanaka Y, Tamaki H, Harada M. Docetaxel induces Bcl-2- and pro-apoptotic caspase-independent death of human prostate cancer DU145 cells. Int J Oncol. 2016;48(6):2330-8.
91. Zhao S, Yu EY. Castrate-resistant prostate cancer: postdocetaxel management. Curr Opin Urol. 2013;23(3):201-7.
92. Juzeniene A, Stenberg VY, Bruland Ø S, Larsen RH. Preclinical and Clinical Status of PSMA-Targeted Alpha Therapy for Metastatic Castration-Resistant Prostate Cancer. Cancers (Basel). 2021;13(4).
93. Pouget JP, Navarro-Teulon I, Bardiès M, Chouin N, Cartron G, Pèlegrin A, et al. Clinical radioimmunotherapy--the role of radiobiology. Nature reviews Clinical oncology. 2011;8(12):720-34.
94. Amato J. Giaccia Eric J. Hall AJG. Radiobiology for the Radiologist, by Eric J. Hall and Amato J. Giaccia: Lippincott Williams & Wilkins; 2006.
95. Torgny Stigbrand JC, Gregory P. Adams Targeted Radionuclide Tumor Therapy; Biological Aspects 8th Edition ed: Springer Dordrecht.
96. Cox MM. Proteins pinpoint double strand breaks. eLife. 2013;2:e01561.
97. Donya M, Radford M, ElGuindy A, Firmin D, Yacoub MH. Radiation in medicine: Origins, risks and aspirations. global cardiology science and practice. 2014;2014(4):437-48.
98. Saha GB. Fundamentals of Nuclear Pharmacy. fifth ed. New York, NY: Springer; 2004.

99. DeNardo GL. Concepts in radioimmunotherapy and immunotherapy: Radioimmunotherapy from a Lym-1 perspective. Seminars in oncology. 2005;32(1 Suppl 1):S27-35.
100. Karagiannis TC. Comparison of different classes of radionuclides for potential use in radioimmunotherapy. Hellenic journal of nuclear medicine. 2007;10(2):82-8.
101. Najafi M, Fardid R, Hadadi G, Fardid M. The mechanisms of radiation-induced bystander effect. Journal of biomedical physics & engineering. 2014;4(4):163-72.
102. Pouget J-P, Navarro-Teulon I, Bardiès M, Chouin N, Cartron G, Pèlegrin A, et al. Clinical radioimmunotherapy—the role of radiobiology. Nature reviews Clinical oncology. 2011;8(12):720-34.
103. Gallicchio R, Mastrangelo PA, Nardelli A, Mainenti PP, Colasurdo AP, Landriscina M, et al. Radium-223 for the treatment of bone metastases in castration-resistant prostate cancer: when and why. Tumori. 2019;105(5):367-77.
104. Ruigrok EAM, van Weerden WM, Nonnekens J, de Jong M. The Future of PSMA-Targeted Radionuclide Therapy: An Overview of Recent Preclinical Research. Pharmaceutics. 2019;11(11).
105. Ferdinandus J, Violet J, Sandhu S, Hofman M. Prostate-specific membrane antigen theranostics: Therapy with lutetium-177. Current Opinion in Urology. 2017;28:1.
106. Dash A, Pillai MR, Knapp FF, Jr. Production of (177)Lu for Targeted Radionuclide Therapy: Available Options. Nuclear medicine and molecular imaging. 2015;49(2):85-107.
107. von Eyben FE, Roviello G, Kiljunen T, Uprimny C, Virgolini I, Kairemo K, et al. Third-line treatment and (177)Lu-PSMA radioligand therapy of metastatic castration-resistant prostate cancer: a systematic review. European journal of nuclear medicine and molecular imaging. 2018;45(3):496-508.
108. Rasul S, Hartenbach M, Wollenweber T, Kretschmer-Chott E, Grubmüller B, Kramer G, et al. Prediction of response and survival after standardized treatment with 7400 MBq 177Lu-PSMA-617 every 4 weeks in patients with metastatic castration-resistant prostate cancer. European journal of nuclear medicine and molecular imaging. 2020.
109. Corn PG, Agarwal N, Araujo JC, Sonpavde G. Taxane-based Combination Therapies for Metastatic Prostate Cancer. European Urology Focus. 2019;5(3):369-80.
110. Beltran H, Beer TM, Carducci MA, de Bono J, Gleave M, Hussain M, et al. New Therapies for Castration-Resistant Prostate Cancer: Efficacy and Safety. European Urology. 2011;60(2):279-90.
111. U.S. National Library of Medicine N. Abiraterone Acetate in Combination With Docetaxel After Disease Progression to Abiraterone Acetate in Metastatic Castration Resistant Prostate Cancer. (ABIDO) 2020 [updated November 16, 2020; cited 2021 May 17]. Available from: https://clinicaltrials.gov/ct2/show/NCT02036060?term=abiraterone%2C+docetaxel&cond=Metastatic+Castration-resistant+Prostate+Cancer&draw=2&rank=2.
112. U.S. National Library of Medicine N. Sequencing of Radium-223 and Docetaxel in Symptomatic Bone-only Metastatic Castration-resistant Prostate Cancer (RAPSON [updated April 22, 2020; cited 2021 May 17]. Available from: https://clinicaltrials.gov/ct2/show/NCT03230734?term=Docetaxel&cond=Metastatic+Castration-resistant+Prostate+Cancer&draw=2&rank=1.
113. Shore N, Higano CS, George DJ, Sternberg CN, Saad F, Tombal B, et al. Concurrent or layered treatment with radium-223 and enzalutamide or abiraterone/prednisone: real-world clinical outcomes in patients with metastatic castration-resistant prostate cancer. Prostate cancer and prostatic diseases. 2020;23(4):680-8.
114. Urbanucci A, Mills IG. Bromodomain-containing proteins in prostate cancer. Molecular and Cellular Endocrinology. 2018;462:31-40.
115. Miranda Furtado CL, Dos Santos Luciano MC, Silva Santos RD, Furtado GP, Moraes MO, Pessoa C. Epidrugs: targeting epigenetic marks in cancer treatment. Epigenetics. 2019;14(12):1164-76.
116. Marrocco-Tallarigo DL, Centenera MM, Scher HI, Tilley WD, Butler LM. Finding the place of histone deacetylase inhibitors in prostate cancer therapy. Expert Review of Clinical Pharmacology. 2009;2(6):619-30.
117. Syeda SS, Jakkaraj S, Georg GI. Scalable syntheses of the BET bromodomain inhibitor JQ1. Tetrahedron letters. 2015;56(23):3354-457.
118. Shi J, Vakoc Christopher R. The Mechanisms behind the Therapeutic Activity of BET Bromodomain Inhibition. Molecular Cell. 2014;54(5):728-36.
119. Suarez-Alvarez B, Rodriguez RM, Ruiz-Ortega M, Lopez-Larrea C. BET Proteins: An Approach to Future Therapies in Transplantation. American journal of transplantation : official journal of the American Society of Transplantation and the American Society of Transplant Surgeons. 2017;17(9):2254-62.

120. Alqahtani A, Choucair K, Ashraf M, Hammouda DM, Alloghbi A, Khan T, et al. Bromodomain and extra-terminal motif inhibitors: a review of preclinical and clinical advances in cancer therapy. Future science OA. 2019;5(3):Fso372.
121. Bennett RL, Licht JD. Targeting epigenetics in cancer. Annual review of pharmacology and toxicology. 2018;58:187-207.
122. Doroshow DB, Eder JP, LoRusso PM. BET inhibitors: a novel epigenetic approach. Annals of oncology : official journal of the European Society for Medical Oncology. 2017;28(8):1776-87.
123. French CA, Miyoshi I, Kubonishi I, Grier HE, Perez-Atayde AR, Fletcher JA. BRD4-NUT fusion oncogene: a novel mechanism in aggressive carcinoma. Cancer Res. 2003;63(2):304-7.
124. Stathis A, Bertoni F. BET Proteins as Targets for Anticancer Treatment. Cancer discovery. 2018;8(1):24-36.
125. Baratta MG, Schinzel AC, Zwang Y, Bandopadhayay P, Bowman-Colin C, Kutt J, et al. An in-tumor genetic screen reveals that the BET bromodomain protein, BRD4, is a potential therapeutic target in ovarian carcinoma. Proceedings of the National Academy of Sciences of the United States of America. 2015;112(1):232-7.
126. Urbanucci A, Barfeld SJ, Kytölä V, Itkonen HM, Coleman IM, Vodák D, et al. Androgen receptor deregulation drives bromodomain-mediated chromatin alterations in prostate cancer. Cell reports. 2017;19(10):2045-59.
127. Ameratunga M, Braña I, Bono P, Postel-Vinay S, Plummer R, Aspegren J, et al. First-in-human Phase 1 open label study of the BET inhibitor ODM-207 in patients with selected solid tumours. British journal of cancer. 2020;123(12):1730-6.
128. Lewin J, Soria J-C, Stathis A, Delord J-P, Peters S, Awada A, et al. Phase Ib Trial With Birabresib, a Small-Molecule Inhibitor of Bromodomain and Extraterminal Proteins, in Patients With Selected Advanced Solid Tumors. Journal of Clinical Oncology. 2018;36(30):3007-14.
129. Park IH, Yang HN, Jeon SY, Hwang J-A, Kim MK, Kong S-Y, et al. Anti-tumor activity of BET inhibitors in androgen-receptor-expressing triple-negative breast cancer. Scientific Reports. 2019;9(1):13305.
130. Lochrin SE, Price DK, Figg WD. BET bromodomain inhibitors--a novel epigenetic approach in castration-resistant prostate cancer. Cancer biology & therapy. 2014;15(12):1583-5.
131. Asangani IA, Dommeti VL, Wang X, Malik R, Cieslik M, Yang R, et al. Therapeutic targeting of BET bromodomain proteins in castration-resistant prostate cancer. Nature. 2014;510(7504):278-82.
132. Asangani IA, Wilder-Romans K, Dommeti VL, Krishnamurthy PM, Apel IJ, Escara-Wilke J, et al. BET Bromodomain Inhibitors Enhance Efficacy and Disrupt Resistance to AR Antagonists in the Treatment of Prostate Cancer. Molecular cancer research : MCR. 2016;14(4):324-31.
133. Yang CY, Qin C, Bai L, Wang S. Small-molecule PROTAC degraders of the Bromodomain and Extra Terminal (BET) proteins - A review. Drug discovery today Technologies. 2019;31:43-51.
134. Rhyasen GW, Hattersley MM, Yao Y, Dulak A, Wang W, Petteruti P, et al. AZD5153: A Novel Bivalent BET Bromodomain Inhibitor Highly Active against Hematologic Malignancies. Molecular cancer therapeutics. 2016;15(11):2563-74.
135. Shen G, Chen J, Zhou Y, Wang Z, Ma Z, Xu C, et al. AZD5153 Inhibits Prostate Cancer Cell Growth in Vitro and in Vivo. Cellular physiology and biochemistry : international journal of experimental cellular physiology, biochemistry, and pharmacology. 2018;50(2):798-809.
136. De Vincentis G, Gerritsen W, Gschwend JE, Hacker M, Lewington V, O'Sullivan JM, et al. Advances in targeted alpha therapy for prostate cancer. Annals of oncology : official journal of the European Society for Medical Oncology. 2019;30(11):1728-39.
137. Ngollo M, Dagdemir A, Karsli-Ceppioglu S, Judes G, Pajon A, Penault-Llorca F, et al. Epigenetic modifications in prostate cancer. Epigenomics. 2014;6(4):415-26.
138. Markowski MC, De Marzo AM, Antonarakis ES. BET inhibitors in metastatic prostate cancer: therapeutic implications and rational drug combinations. Expert opinion on investigational drugs. 2017;26(12):1391-7.
139. Urbanucci A, Mills IG. Bromodomain-containing proteins in prostate cancer. Molecular and cellular endocrinology. 2018;462(Pt A):31-40.
140. Morris MJ, Corey E, Guise TA, Gulley JL, Kevin Kelly W, Quinn DI, et al. Radium-223 mechanism of action: implications for use in treatment combinations. Nature reviews Urology. 2019;16(12):745-56.
141. Pfitzenmaier J, Quinn JE, Odman AM, Zhang J, Keller ET, Vessella RL, et al. Characterization of C4–2 Prostate Cancer Bone Metastases and Their Response to Castration. Journal of Bone and Mineral Research. 2003;18(10):1882-8.

142. Namekawa T, Ikeda K, Horie-Inoue K, Inoue S. Application of Prostate Cancer Models for Preclinical Study: Advantages and Limitations of Cell Lines, Patient-Derived Xenografts, and Three-Dimensional Culture of Patient-Derived Cells. Cells. 2019;8(1).
143. Xie BX, Zhang H, Yu L, Wang J, Pang B, Wu RQ, et al. The radiation response of androgen-refractory prostate cancer cell line C4-2 derived from androgen-sensitive cell line LNCaP. Asian journal of andrology. 2010;12(3):405-14.
144. Wu HC, Hsieh JT, Gleave ME, Brown NM, Pathak S, Chung LW. Derivation of androgen-independent human LNCaP prostatic cancer cell sublines: role of bone stromal cells. Int J Cancer. 1994;57(3):406-12.
145. Ryan S-L, Baird A-M, Vaz G, Urquhart AJ, Senge h, Richard DJ, et al. Drug discovery approaches utilizing three-dimensional cell culture. Assay and drug development technologies. 2016;14(1):19-28.
146. Kapałczyńska M, Kolenda T, Przybyła W, Zajączkowska M, Teresiak A, Filas V, et al. 2D and 3D cell cultures–a comparison of different types of cancer cell cultures. Archives of medical science: AMS. 2018;14(4):910.
147. Edmondson R, Broglie JJ, Adcock AF, Yang L. Three-dimensional cell culture systems and their applications in drug discovery and cell-based biosensors. Assay Drug Dev Technol. 2014;12(4):207-18.
148. Friedrich J, Ebner R, Kunz-Schughart LA. Experimental anti-tumor therapy in 3-D: spheroids–old hat or new challenge? International journal of radiation biology. 2007;83(11-12):849-71.
149. Leek R, Grimes DR, Harris AL, McIntyre A, editors. Methods: Using Three-Dimensional Culture (Spheroids) as an In Vitro Model of Tumour Hypoxia2016; Cham: Springer International Publishing.
150. Cui X, Hartanto Y, Zhang H. Advances in multicellular spheroids formation. Journal of The Royal Society Interface. 2017;14(127):20160877.
151. Sant S, Johnston PA. The production of 3D tumor spheroids for cancer drug discovery. Drug discovery today Technologies. 2017;23:27-36.
152. Kamatar A, Gunay G, Acar H. Natural and Synthetic Biomaterials for Engineering Multicellular Tumor Spheroids. Polymers. 2020;12(11):2506.
153. Pieters R, Loonen A, Huismans D, Broekema G, Dirven M, Heyenbrok M, et al. In vitro drug sensitivity of cells from children with leukemia using the MTT assay with improved culture conditions. 1990.
154. DAVID L. SMITH PD, AND WILLIAM A. RICKETTS, PH.D., ONCOTECH, INC. CELLTITER-GLO® LUMINESCENT CELL VIABILITY ASSAY:
APPLICATION FOR VIABILITY STUDIES OF CELLS GROWN IN AGAROSE 2007 [cited 2021. Available from: https://www.promega.in/-/media/files/resources/cell-notes/cn017/celltiter-glo-luminescent-cell-viability-assay-application-for-viability-studies-of-cells-grown.pdf?la=en.
155. CellTiter-Glo® 2.0 Assay TECHNICAL MANUAL [cited 2021 January]. Available from: https://www.promega.com/-/media/files/resources/protocols/technical-manuals/101/celltiterglo-2-0-assay-protocol.pdf?la=en.
156. Jones K, Kim D, Park J, Khang CH. Live-cell fluorescence imaging to investigate the dynamics of plant cell death during infection by the rice blast fungus Magnaporthe oryzae. BMC Plant Biology. 2016;16.
157. Boyd V, Cholewa OM, Papas KK. Limitations in the use of fluorescein diacetate/propidium iodide (FDA/PI) and cell permeable nucleic acid stains for viability measurements of isolated islets of Langerhans. Current trends in biotechnology and pharmacy. 2008;2(2):66.
158. McKinnon KM. Flow Cytometry: An Overview. Current Protocols in Immunology. 2018;120(1):5.1.-5.1.11.
159. Demidenko E, Miller TW. Statistical determination of synergy based on Bliss definition of drugs independence. PLoS One. 2019;14(11):e0224137.
160. Sternberg CN. Enzalutamide, an oral androgen receptor inhibitor for treatment of castration-resistant prostate cancer. Future oncology (London, England). 2019;15(13):1437-57.
161. Kessel A, Kohli M, Swami U. Current management of metastatic castration-sensitive prostate cancer. Cancer treatment and research communications. 2021;28:100384.
162. McKay RR, Kwak L, Crowdis J, Sperger JM, Zhao SG, Xie W, et al. Phase 2 multicenter study of enzalutamide in metastatic castration resistant prostate cancer to identify mechanisms driving resistance. Clinical cancer research : an official journal of the American Association for Cancer Research. 2021.
163. Wang Y, Chen J, Wu Z, Ding W, Gao S, Gao Y, et al. Mechanisms of enzalutamide resistance in castration-resistant prostate cancer and therapeutic strategies to overcome it. British journal of pharmacology. 2021;178(2):239-61.
164. Shi X, Liu C, Liu B, Chen J, Wu X, Gong W. JQ1: a novel potential therapeutic target. Die Pharmazie. 2018;73(9):491-3.

165. (NLM) USNLoM. A Phase I, Multicenter Dose-Escalation Study to Assess the Tolerability, Pharmacokinetics and Preliminary Anti-tumor Activity of AZD5153 in Patients With Relapsed/Refractory Malignant Solid Tumors, Including Lymphomas [updated May 6, 2021; cited 2021 May 14th]. Available from: https://clinicaltrials.gov/ct2/show/NCT03205176?term=AZD5153&draw=2&rank=1.
166. Staniszewska M, Iking J, Lückerath K, Hadaschik B, Herrmann K, Ferdinandus J, et al. Drug and molecular radiotherapy combinations for metastatic castration resistant prostate cancer. Nuclear medicine and biology. 2021;96-97:101-11.
167. (NLH) USNLoM. A Phase 1b/2a Safety and Tolerability Study of ZEN003694 in Combination With Enzalutamide in Patients With Metastatic Castration-Resistant Prostate Cancer 2020 [updated October 5, 2020; cited 2021 May 14th]. Available from: https://clinicaltrials.gov/ct2/show/NCT02711956
168. (NLM) USNLoM. ZEN-3694, Enzalutamide, and Pembrolizumab for the Treatment of Metastatic Castration-Resistant Prostate Cancer 2020 [updated December 22, 2020; cited 2021 May 14th]. Available from: https://clinicaltrials.gov/ct2/show/NCT04471974.
169. Van den Wyngaert T, Tombal B. The changing role of radium-223 in metastatic castrate-resistant prostate cancer: has the EMA missed the mark with revising the label? The quarterly journal of nuclear medicine and molecular imaging : official publication of the Italian Association of Nuclear Medicine (AIMN) [and] the International Association of Radiopharmacology (IAR), [and] Section of the So. 2019;63(2):170-82.
170. Satapathy S, Das CK, Parihar AS, Sood A, Mittal BR. Response to Concomitant Enzalutamide and 177Lu-PSMA-617 Radioligand Therapy in ATM-Mutated Metastatic Castration Resistant Prostate Cancer. Clinical nuclear medicine. 2021.
171. Ghoshal A, Yugandhar D, Srivastava AK. BET inhibitors in cancer therapeutics: a patent review. Expert Opinion on Therapeutic Patents. 2016;26(4):505-22.
172. Asangani IA, Dommeti VL, Wang X, Malik R, Cieslik M, Yang R, et al. Therapeutic targeting of BET bromodomain proteins in castration-resistant prostate cancer. Nature. 2014;510(7504):278-82.
173. Wang L, Xu M, Kao CY, Tsai SY, Tsai MJ. Small molecule JQ1 promotes prostate cancer invasion via BET-independent inactivation of FOXA1. The Journal of clinical investigation. 2020;130(4):1782-92.
174. Zhao J, Zhao Y, Wang L, Zhang J, Karnes RJ, Kohli M, et al. Alterations of androgen receptor-regulated enhancer RNAs (eRNAs) contribute to enzalutamide resistance in castration-resistant prostate cancer. Oncotarget. 2016;7(25):38551-65.
175. Linxweiler J, Hammer M, Muhs S, Kohn M, Pryalukhin A, Veith C, et al. Patient-derived, three-dimensional spheroid cultures provide a versatile translational model for the study of organ-confined prostate cancer. Journal of Cancer Research and Clinical Oncology. 2019;145(3):551-9.
176. da Motta LL, Ledaki I, Purshouse K, Haider S, De Bastiani MA, Baban D, et al. The BET inhibitor JQ1 selectively impairs tumour response to hypoxia and downregulates CA9 and angiogenesis in triple negative breast cancer. Oncogene. 2017;36(1):122-32.
177. Triggiani L, Colosini A, Buglione M, Pasinetti N, Orizio F, Bardoscia L, et al. Exploring the Role of Enzalutamide in Combination with Radiation Therapy: An In Vitro Study. Anticancer research. 2018;38(6):3487-92.
178. Adashek JJ, Reed JP, Tandon A, Freedland SJ, Posadas E, Bhowmick N, et al. Combination Androgen Receptor Inhibition and Docetaxel in Metastatic Castration-sensitive Prostate Cancer: The Next Step in First-line Treatment? Clinical genitourinary cancer. 2020;18(6):425-8.
179. Cursano MC, Iuliani M, Casadei C, Stellato M, Tonini G, Paganelli G, et al. Combination radium-223 therapies in patients with bone metastases from castration-resistant prostate cancer: A review. Critical reviews in oncology/hematology. 2020;146:102864.
180. Jiang G, Deng W, Liu Y, Wang C. General mechanism of JQ1 in inhibiting various types of cancer. Mol Med Rep. 2020;21(3):1021-34.
181. Brüningk SC, Rivens I, Box C, Oelfke U, ter Haar G. 3D tumour spheroids for the prediction of the effects of radiation and hyperthermia treatments. Scientific Reports. 2020;10(1):1653.
182. Suominen MI, Fagerlund KM, Rissanen JP, Konkol YM, Morko JP, Peng Z, et al. Radium-223 Inhibits Osseous Prostate Cancer Growth by Dual Targeting of Cancer Cells and Bone Microenvironment in Mouse Models. Clinical cancer research : an official journal of the American Association for Cancer Research. 2017;23(15):4335-46.
183. Yang Z, He N, Zhou Q. Brd4 Recruits P-TEFb to Chromosomes at Late Mitosis To Promote G₁ Gene Expression and Cell Cycle Progression. Molecular and Cellular Biology. 2008;28(3):967-76.

184. Woods AD, Keller C, Berlow NE, Michalek JE, Royer-Pokora B, Purohit R, et al. Bromodomain 4 inhibition leads to MYCN downregulation in Wilms' tumor cells. bioRxiv. 2021.
185. Tan Y, Wang L, Du Y, Liu X, Chen Z, Weng X, et al. Inhibition of BRD4 suppresses tumor growth in prostate cancer via the enhancement of FOXO1 expression. Int J Oncol. 2018;53(6):2503-17.
186. Li X, Baek G, Ramanand SG, Sharp A, Gao Y, Yuan W, et al. BRD4 Promotes DNA Repair and Mediates the Formation of TMPRSS2-ERG Gene Rearrangements in Prostate Cancer. Cell Rep. 2018;22(3):796-808.
187. Sun C, Yin J, Fang Y, Chen J, Jeong KJ, Chen X, et al. BRD4 Inhibition Is Synthetic Lethal with PARP Inhibitors through the Induction of Homologous Recombination Deficiency. Cancer Cell. 2018;33(3):401-16.e8.
188. Wang L, Xie L, Ramachandran S, Lee Y, Yan Z, Zhou L, et al. Non-canonical Bromodomain within DNA-PKcs Promotes DNA Damage Response and Radioresistance through Recognizing an IR-Induced Acetyl-Lysine on H2AX. Chemistry & biology. 2015;22(7):849-61.

APPENDIX

Appendix A: Materials

Reagents

Reagents	Company	Catalog number/ID
0.4% methylene	Thermo Fisher	15250061
$^{177}Lu\ Cl_3$ dissolved in diluted	ITG,Garching, Germany	
95% ethanol	Antibac As	
Agarose, type I	Sigma Aldrich	A6013-250G
Alexa Fluor 647 donkey anti-rabbit IgG (H+L)	Thermo Fisher	A-31573
Annexin V-FITC	ImmunoTools	31490013
Anti-phosfo Histone H3 (Ser10), Mitosis Marker	Merck	06-570
Anti-phospho-Histone H2A.X (Ser139), clone JBW301	Merck	05-636
BET inhibitor AZD5153	Cayman Chemical	20864
BET inhibitor JQ1	Sigma Aldrich	SML0974
Bovine Serum Albumin (BSA)	Sigma Aldrich	A6003
CellTiter-Glo reagent	Promega	G7570
Dimethyl sulfoxide (DMSO)	Sigma Aldrich	D5879-500ML
DPBS without Ca&Mg	Sigma Aldrich	D8537-500ML
Dulbecco's Phosphate Buffered Saline (DPBS) with Ca&Mg	Sigma Aldrich	D8662-500ML
eFluor 450	Thermo Fisher	65-0863
Enzalutamide	Cayman Chemical	1159
Fluorescein Diacetate (FDA)	Sigma Aldrich	F7378
Heat Inactivated Fetal Bovine Serum (FBS)	Thermo Fisher	10500-056
Instant thin layer chromatography strips	Tec-control, Biodex	Instant thin layer chromatography strips
MTT powder	Sigma Aldrich	135038-500MG
NaCl 0.9%	B Braun	10258674
Penicillin streptomycin (PS)	Thermo Fisher	15140-122
Polyclonal Goat Anti-Mouse Immunoglobulin/FTC Goat F $(ab')_2$	Dako	F0479
Propidium iodide (PI)	Sigma Aldrich	P4170
PSMA-617 ligand	MedKoo	

PureLink™ RNase A	Thermo Fisher	1209102
RPMI medium 1640	Sigma Aldrich	R8758
Trypsin EDTA-solution	Sigma Aldrich	T3924
Tween-20 PBST	Sigma Aldrich	P5927

Cell line

Name	Origin	Culturing medium
C4-2	Human prostate cancer LNCaP cells grown in xenograft tumor of castrated nude mice	RPMI-1640

Equipments

Equipment/instrument type	Manufacturer	Catalog number/REF
0.22µm Filter	MILLEX-GV	SLGV004SL
96 white well plate	COSTAR	
Corning®cell culture Flask, 175 ml	Thermo Fisher	159910
Corning®cell culture Flask, 25ml	Thermo Fisher	156367
Corning®cell culture Flask, 75 ml	Thermo Fisher	156499
Eppendorf tubes	Eppendorf AG	E164255R
Needles	BD Microlance	
Serological pipette 10 ml	SARSTEDT	86.1254.001
Serological pipette 25 ml	SARSTEDT	86.1685.001
Serological pipette 5 ml	SARSTEDT	86.1253.001
Syringe 1 ml	Terumo	SS+01T1
Test Tube Soda Glass	VWR	212-0013
Transparent 96-well flat-bottomed plate	(Nunclon™ Delta Surface, Thermo Scientific	167008
Tube 15 ml	SARSTEDT	62.553.542
Tube 50 ml	SARSTEDT	62.559.001

Instruments

Name	Company
Axiovert 200m Inverted Fluorescence Motorized Microscope	Carl Zeiss
Centrifuge	Eppendorf AG
COBRA™ II AUTO-GAMMA	Packard
Cooking plate with stirring magnet	IKA
CountessTM II Automated cell Counter	Thermo Fisher
CytoFlex	Beckman Colulter Life Sciences
Ice machine	PORKA
Incubator	Forma Scientific
Olympus Ck-40 Inverted microscope	OLYMPUS OPTICAL CO.LTD
RADEYE B20	Thermo Fisher
Spark multimode reader	Tecan
Water bath	Grant

Appendix B: Microscopy images of spheroids after treatment with various concentrations of BET or AR inhibitors.

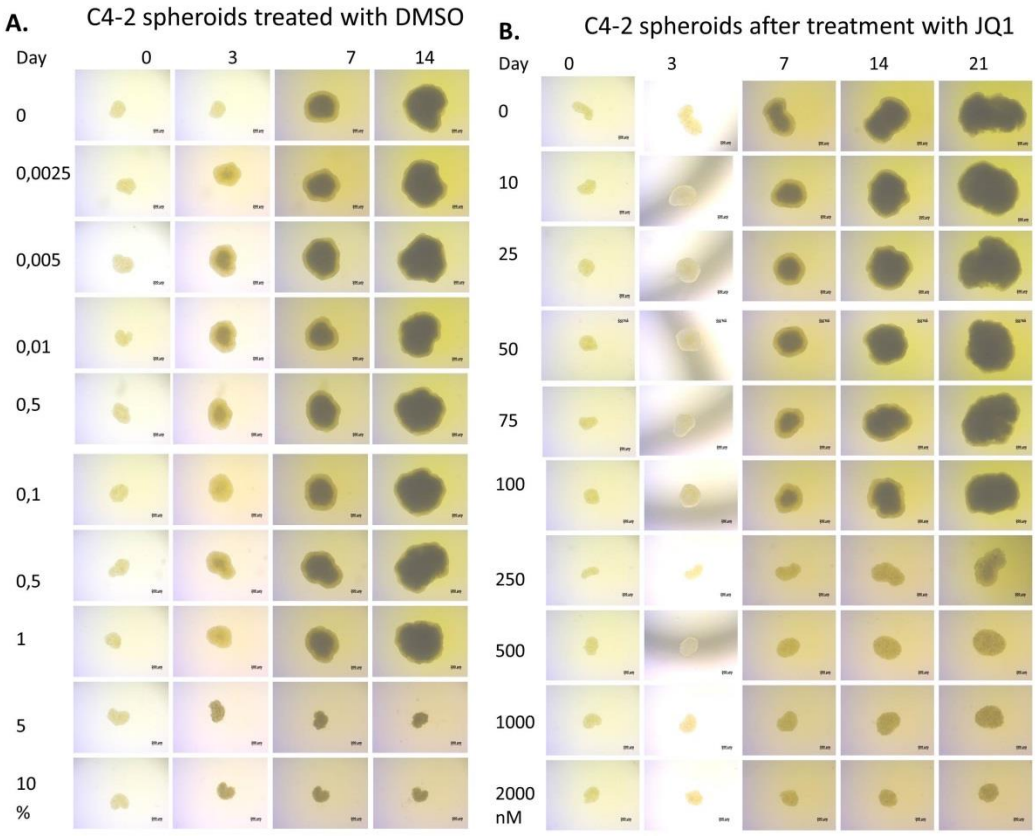

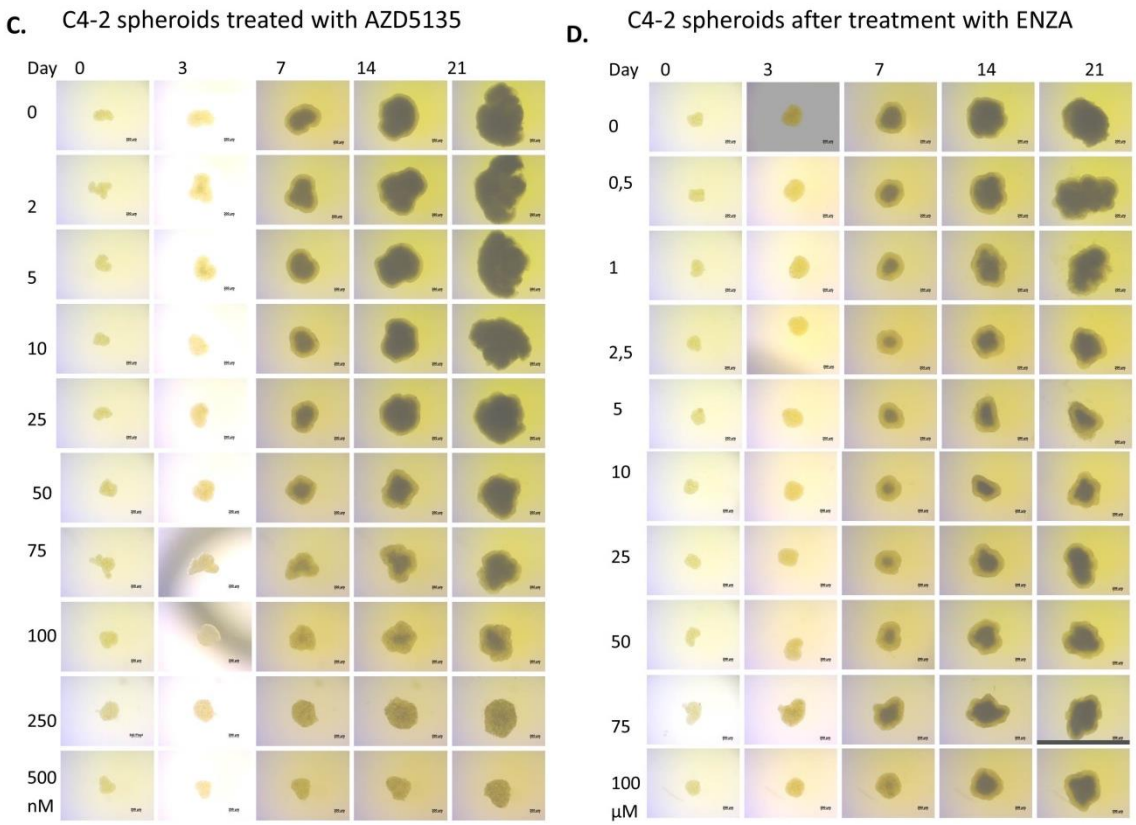

Figure B1. Growth of C4-2 spheroids after the treatment with DMSO, BET or AR inhibitors. Time-lapse representative bright-field microscopy images of C4-2 spheroids day 3, 7,14 and 21after treated with of DMSO **(A)**, JQ1 **(B)**, AZD5153 **(C)** or ENZA **(D)** in increasing concentrations. Five hundred cells per well were seeded in 96 well plates and incubated for 5 days for spheroids to form. Further images (objective 4x) of spheroids were taken before treatment (day 0), and spheroids were incubated with varying concentrations of DMSO, JQ1, AZD5153 or ENZA and incubated for 21-24 days. Seven days after treatment the media were replaced twice per week. Followed treatment spheroid images were taken of the same spheroid at day 3, 7, 14 and 21. The scale bar is 200 µm. N is one independent experiment.

Appendix C: C4-2 cells growing in monolayer treated with BET or AR inhibitors in combination with ^{223}Ra.

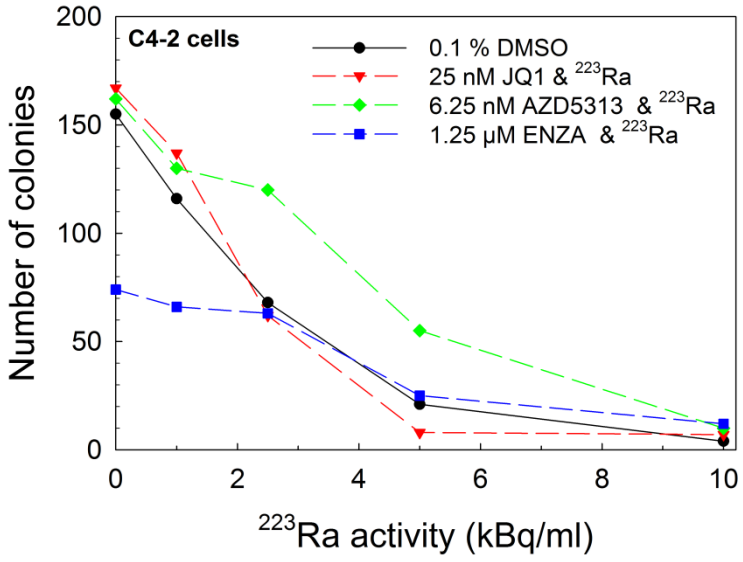

Figure C1. Number of colonies counted of C4-2 cells after treatment with BET or AR inhibitors in combination with various activities (kBq/ml) of ^{223}Ra. Thousand cells per 5 ml were subcultered in 25cm^2 flasks (2 technical replicates per treatment group). After 24 h incubation, the media in each flask was

replaced with 5 ml drug-containing media. The cells were treated with 25 nM JQ1, 6.25 nM AZD5153, or 1.25 µM ENZA, for 2 h, followed by 1 h co-treatment with 1,2.5, 5 or 10 kBq/ml ^{223}Ra. Further the media were replaced with fresh drug-containing media and incubated for cells to grow into colonies. N= one independent experiment.

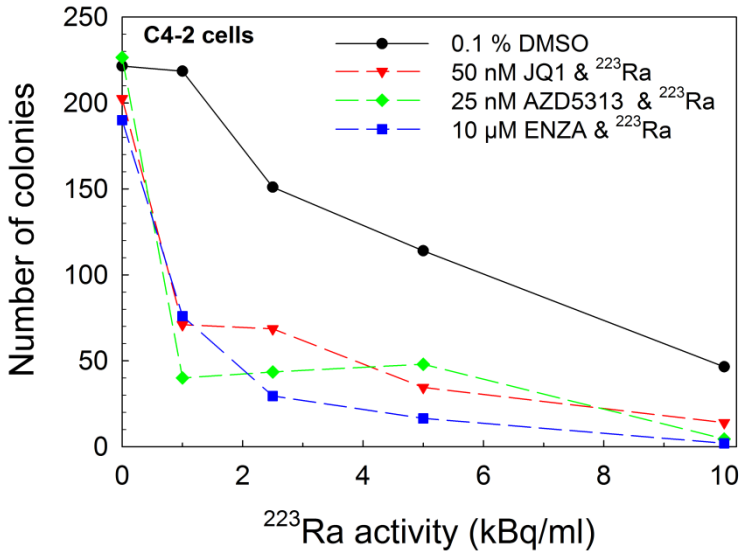

Figure C2. Number of colonies counted after exposure of C4-2 cells with BET or AR inhibitors in combination with various activities (kBq/ml) of ^{223}Ra. Thousand cells per 5 ml were subcultered in 25cm^2 flasks (2 technical replicates per treatment group). After 24 h incubation, the media in each flask was replaced with 5 ml drug-containing media. The cells were treated with 50 nM JQ1, 25 nM AZD5153, or 10 µM ENZA, for 2 h, followed by 1 h co-treatment with 1,2.5, 5 or 10 kBq/ml ^{223}Ra. Further the media were replaced with fresh drug-containing media and incubated for 10-14 days cells to grow into colonies. N= one independent experiment.

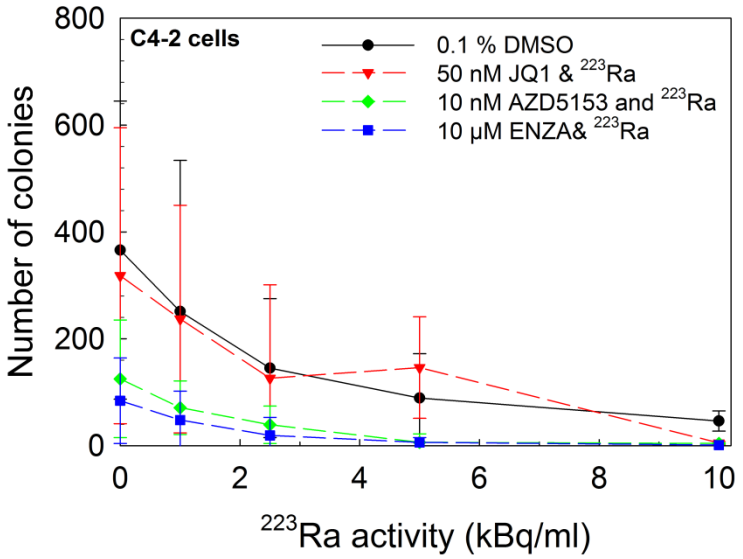

Figure C3. Number of colonies counted after exposure of C4-2 cells with BET or AR inhibitors in combination with various activities (kBq/ml) of ^{223}Ra. Thousand cells per 5 ml were subcultered in 25cm^2 flasks (3 tecknical replicates per treatment group). After 24 h incubation, the media in each flask was replaced with 5 ml drug-containing media. The cells were treated with 50 nM JQ1, 10 nM AZD5153, or 10 µM ENZA, for 2 h, followed by 1 h co-treatment with 1,2.5, 5 or 10 kBq/ml ^{223}Ra. Further the media were replaced with fresh drug-containing media and incubated for 10-14 days cells to grow into colonies. Error bars show ±SD of the three replicates per treamtent-N= one independent experiment.

Appendix D: Response of C4-2 spheroids to BET or AR inhibitors in combination with ^{223}Ra

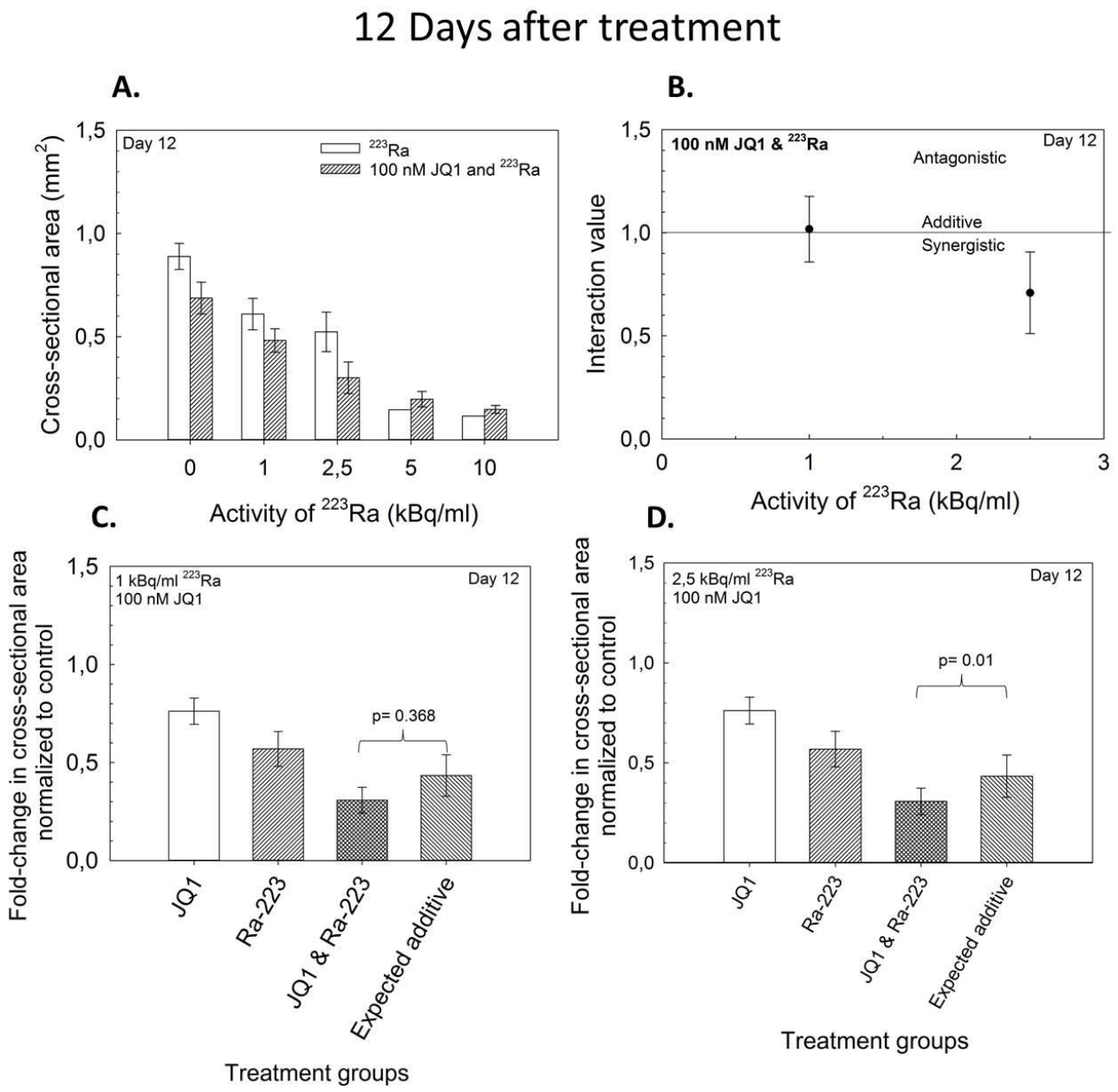

Figure D1: Spheroid growth upon combination treatment with JQ1 and ^{223}Ra. (A) Cross sectional area (mm^2) of C4-spheroids, day 12 after combination treatment with 100 nM JQ1 and various activities of ^{223}Ra. C4-2 cells (500 cells/well) were seeded in 96 well plates and incubated for 5 days to form spheroids. Before treatment microscopy images (4x objective) of spheroids were taken, and treated with the final concentration 100 nM JQ1 and incubated for 2-3 h. Further co-treated with 2.5, 5 or 10 kBq/ml of ^{223}Ra for 1 h. Afterwards the spheroids were washed 6 times and the media were replaced with fresh drug-containing media and incubated. Seven days after treatment the media were replaced with fresh media twice a week. Six to eleven individual spheroids per treatment condition. **(B)** Drug interaction for testing synergy of 100 nM JQ1 and 1 or 2.5 kBq/ml ^{223}Ra in C4-2 spheroids. **(C and D)** Fold change in C4-2 spheroids cross-sectional area, after treatment relative to spheroid cross-sectional area at day 0 normalized to control (0, 1% DMSO). $p<0.05$ (Welch's t test) for combination of 100 nM JQ1 and 2.5 kBq/ml ^{223}Ra. Error bars present ±SD for the 6-11 spheroids per treatment condition and n= one independent experiment. Statistical differences were determined by statistical Welch's t-test and $p<0.05$ were considered statistically significant

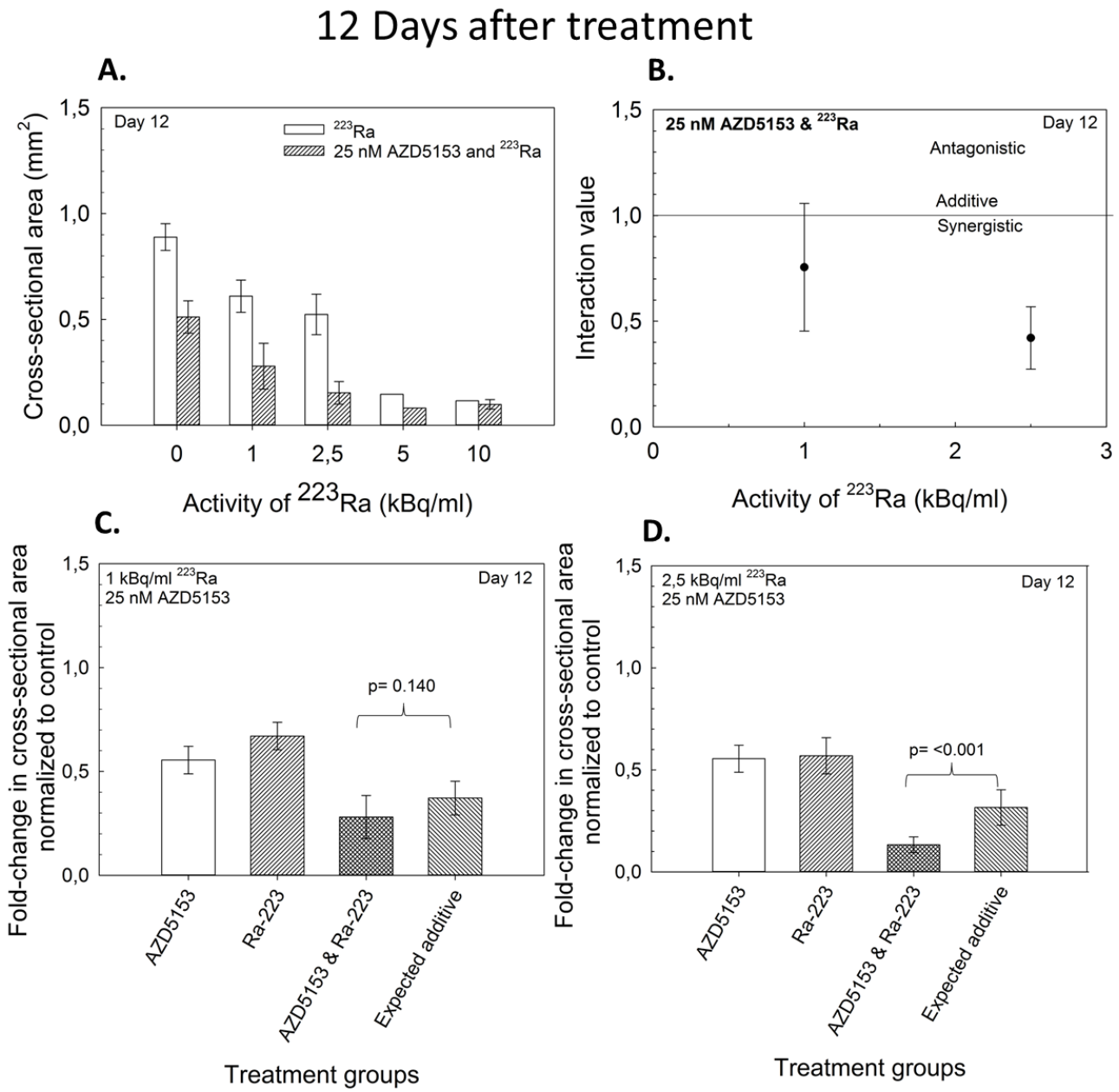

Figure D2: Spheroid growth upon combination treatment with AZD5153 and ^{223}Ra. (A) Cross sectional area (mm^2) of C4-spheroids, day 12 after combination treatment with 25 nM AZD5153 and various activities of ^{223}Ra. C4-2 cells (500 cells/well) were seeded in 96 well plates and incubated for 5 days to form spheroids. Before treatment microscopy images (4x objective) of spheroids were taken, and treated with the final concentration 25 nM AZD5153 and incubated for 2-3 h. Further co-treated with 2.5, 5 or 10 kBq/ml of ^{223}Ra for 1 h. Afterwards the spheroids were washed 6 times and the media were replaced with fresh drug-containing media and incubated. Seven days after treatment the media were replaced with fresh media twice a week. Six to eleven individual spheroids per treatment condition. **(B)** Drug interaction for testing synergy of 25 nM AZD5153 and 1 or 2.5 kBq/ml ^{223}Ra in C4-2 spheroids. **(C and D)** Fold change in C4-2 spheroids cross-sectional area, after treatment relative to spheroid cross-sectional area at day 0 normalized to control (0, 1% DMSO). $p<0.05$ (Welch's t test) for combination of 25 nM AZD5153 and 2.5 kBq/ml ^{223}Ra. Error bars present ±SD for the 6-11 spheroids per treatment condition and n= one independent experiment. Statistical differences were determined by statistical Welch's t-test and $p<0.05$ were considered statistically significant

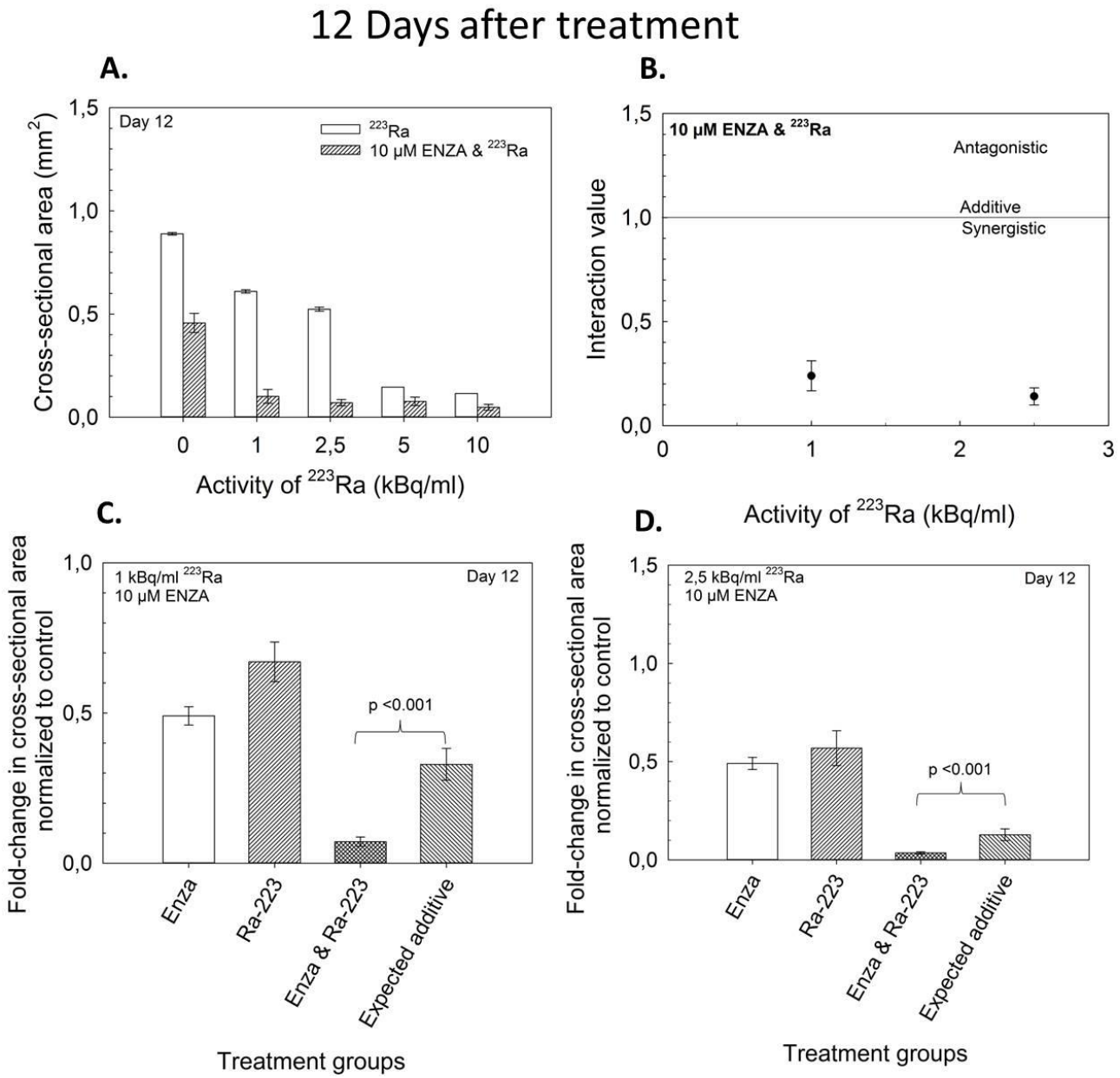

Figure D3: Spheroid growth upon combination treatment with ENZA and ^{223}Ra. (A) Cross sectional area (mm^2) of C4-spheroids, day 12 after combination treatment with 10 µM ENZA and various activities of ^{223}Ra. C4-2 cells (500 cells/well) were seeded in 96 well plates and incubated for 5 days to form spheroids. Before treatment microscopy images (4x objective) of spheroids were taken, and treated with the final concentration 10 µM ENZA and incubated for 2-3 h. Further co-treated with 2.5, 5 or 10 kBq/ml of ^{223}Ra for 1 h. Afterwards the spheroids were washed 6 times and the media were replaced with fresh drug-containing media and incubated. Seven days after treatment the media were replaced with fresh media twice a week. Six to eleven individual spheroids per treatment condition. **(B)** Drug interaction for testing synergy of 10 µM and 1 or 2.5 kBq/ml ^{223}Ra in C4-2 spheroids. **(C and D)** Fold change in C4-2 spheroids cross-sectional area, after treatment relative to spheroid cross-sectional area at day 0 normalized to control (0, 1% DMSO). $p<0.05$ (Welch's t test) for combination of 10 µM ENZA and 2.5 kBq/ml ^{223}Ra. Error bars present ±SD for the 6-11 spheroids per treatment condition and n= one independent experiment. Statistical differences were determined by statistical Welch's t-test and $p<0.05$ were considered statistically significant

OSLO METROPOLITAN UNIVERSITY
STORBYUNIVERSITETET